Modelling blood flow in large arteries using the finite volume method

by

AM de Villiers
20286805

A dissertation submitted in partial fulfillment
of the requirements for the degree

Master of Engineering in **Mechanical Engineering**

at the

North-West University
Potchefstroom

Supervisor: Prof CG du Toit
Co-supervisor: Dr O Ubbink

September 2012

Abstract

The purpose of this research is the development of a one-dimensional (1D) computer code that models blood flow through large arteries. There are many of these models in literature, the majority is solved with the finite element method. The problem is analogous to a compressible liquid in a pipe network. Methods to solve the pipe network flow problem have evolved over the years. One of these methods, which can handle discontinuities and branching naturally to solve the blood flow problem, was used in this research.

The blood flow problem can be modelled by solving mass flow, momentum conservation and the interaction between the blood flow and the arterial wall. In essence we are looking at two problems in two time scales, namely mass flow and the propagation of the pressure pulse. The mass flow rate of the blood is not very fast - it takes a blood particle approximately one minute to travel to the organs and back. Everytime the heart beats, it sends a 'shockwave' through the system. These waves or pulses propagate at speeds at least three orders higher than the blood flow. When these pressure waves reach a discontinuity or branch in the arterial network, part of the wave is reflected.

The method used for this study discretises the partial differential equations by using a staggered grid and the finite volume method. An iterative method similar to the Semi Implicit Method for Pressure Linked Equations (SIMPLE) was used to solve the discretised equations. By using the characteristic system, characteristic variables that are constant along characteristic lines can be derived. These variables represent forward and backward travelling wave fronts. By expressing the boundary conditions in terms of these variables, rather than in terms of flow, area and pressure, we can prescribe non-reflecting boundary conditions. This way pressure waves can travel out of the computational domain unhindered. Discontinuities and branching are handled naturally because of the staggered grid discretisation.

A computer code was written in Octave to solve the discretised equations for a number of test cases. The results show that when a small input pressure wave is prescribed, the solution behaves linearly. When a large input pressure wave is prescribed the solution behaves non-linearly. The non-reflecting boundary conditions work perfectly for the linear test case, but a small portion of the outgoing wave is reflected for the non-linear test case. Discontinuities and branching were handled satisfactorily with the code for a number of test cases.

Key words: finite volume method; blood flow; 1D; staggered grid; characteristic system

Opsomming

Modellering van bloedvloei in groot arteries deur gebruik te maak van die eindige volume metode.

Die doel van hierdie navorsing is om ‘n een dimensionele (1D) rekenaarkode te ontwikkel wat bloedvloei deur groot arteries modelleer. Daar is baie van hierdie modelle beskikbaar in die literatuur; die meerderheid daarvan word opgelos deur die eindige element metode te gebruik. Die probleem is analoog aan ‘n samedrukbare vloeistof in ‘n pyp netwerk. Metodes om die pyp netwerk probleem op te los het deur die jare ontwikkel. Een van hierdie metodes, wat diskontinuïteite en vertakkings op ‘n natuurlike manier kan hanteer om die bloedvloei probleem op te los, is in hierdie navorsing gebruik.

Die bloedvloei probleem kan gemodelleer word deur die massa- en momentumbehoud asook die interaksie tussen die bloedvloei en die bloedwand op te los. In essensie kyk ons na twee probleme in twee tydskale, naamlik die massavloei en die propagering van die drukpols. Die tempo van die massavloei van die bloed is nie baie vinnig nie – dit neem ‘n bloed deeltjie ongeveer een minuut om na al die organe en daarna terug na die hart te beweeg. Elke keer wat die hart klop stuur dit ‘n skokgolf deur die stelsel. Hierdie golwe of polse propageer teen snelhede van ten minste drie ordes groter as die van die bloedvloei. Wanneer die drukgolwe ‘n diskontinuïteit of vertakking in die arteriële netwerk bereik, word ‘n deel van die golf gereflekteer.

Die metode wat vir hierdie studie gebruik is, diskretiseer die parsiëel differensiaal vergelykings deur van ‘n verspringende rooster en die eindige volume metode gebruik te maak. ‘n Iteratiewe metode wat soortgelyk aan die Semi Implisiete Metode vir Druk Gekoppelde Vergelykings (SIMPLE) is, is gebruik om die gediskretiseerde vergelykings op te los. Deur gebruik te maak van die karakteristieke stelsel, kan karakteristieke veranderlikes afgelei word. Hierdie veranderlikes verteenwoordig die voorwaartse- en terugwaartse golffronte. Deur die randvoorwaardes in terme van hierdie veranderlikes uit te druk, eerder as in terme van die vloei, area en druk, kan ons nie-reflekterende randvoorwaardes voorskryf. Op hierdie manier kan drukgolwe ongehinderd uit die rekenaarmatige terrein beweeg. Diskontinuïteite en vertakkings

word natuurlik hanteer omdat ‘n uitgespreide rooster gebuik is vir diskretisasie. ‘n Rekenaar kode in Octave is geskryf om die gediskretiseerde vergelykings vir ‘n aantal toetsgevalle op te los. Die resultate wys dat wanneer ‘n klein inlaat drukgolf voorgeskryf word, die oplossing lineêr optree. Wanneer ‘n groot inlaat drukgolf voorgeskryf word, tree die oplossing nie-lineêr op. Die nie-reflekterende randvoorwaardes werk perfek vir die lineêre geval, maar ‘n klein deel van die uitgaande golf word reflekteer in die nie-lineêre toets gevalle. Diskontinuïteite en vertakkings in die toetsgevalle is bevredigend deur die kode hanteer.

Kern woorde: eindige volume metode; bloedvloei; groot arteries; 1D; verspringende rooster; karakteristieke stelsel

Acknowledgements

God has graciously blessed me during this study.

I would like to express my deepest gratitude to both my supervisors Professor C.G. du Toit and Dr. O. Ubbink. I appreciate their generous and steadfast encouragement and advice throughout my research. Professor du Toit guided me patiently, always many steps ahead in thinking. Dr. Ubbink's help was indispensable; not only did he help me with all academical matters, he was a magnificent pillar of strength during a challenging year.

I would like to thank the members of our competency unit Advanced Mathematical Modelling for many fruitful discussions, especially Dr. S. Kok and Mr. A. Bogaers. Furthermore I owe many thanks to Mr. G. Wessels and Mr. J. Jansen van Rensburg for their help with numerous software and other technical challenges.

I am grateful for the financial support from the CSIR competency unit Advanced Mathematical Modelling.

Lastly I want to thank my husband Willem, mother Annamie and the rest of my family for all the love, emotional support and encouragement throughout the year.

Contents

Nomenclature

A	Area of vessel
A_0	Relaxed area of artery
$\boldsymbol{A_f}$	Area vector
c_0	Intrinsic wave speed
Cr	Courant number
c	Wave speed
d	Deviatoric stresses due to the viscosity of the fluid
∂p	Pressure drop over control volume with length L
dS	Face of control volume
E	Young's modulus
f_b	Body forces
h	Thickness of vessel wall
K_R	Resistance term
l_i	Left eigenvector
L	Length of vessel
$\boldsymbol{n}$	Normal vector
p_0	Total pressure
p_{ext}	External pressure
p	Pressure

P_t Transmural pressure

Q Flow through vessel

r_0 Unstressed radius

R Reflective coefficient

r Radius

R_t Terminal reflection coefficient

S_i End section of artery

s_k Variable to indicate the direction of flow

S Generic axial section

s Velocity profile

T Circumferential tension

t Time

u_x X-component of velocity

u_b Velocity of boundary

u Axial velocity

$\boldsymbol{u_w}$ Velocity of the vessel wall

u_{wf} Velocity of the foot of the wave

u_{wfc} Computed velocity of the foot of the wave

V_t Arbitrary control volume

W Womersley parameter

w Angular frequency

x_1, x_2 X-coordinates at the end cross sections

x Axial direction

Y_0 Characteristic admittance

y Axis in radial direction

Z_0 Characteristic impedance

ϵ_{speed} Error in the speed of the wave

α Coriolis coefficient

β Mechanical properties

$\partial V_{t,w}$ Arterial wall

∂V_t Boundary of control volume

$\dot{\gamma}$ Shear rate

γ Length of control volume

$\lambda_{1,2}$ Eigenvalues

μ Dynamic viscosity

ω Relative velocity between fluid at lumen and arterial wall

ω_1 Characteristic variables associated with the forward travelling wavefront

ω_2 Characteristic variable associated with the backward travelling wavefront

ρ Density

σ Area of control volume

σ Poisson's ratio

τ Shear stress

θ Weighting parameter for time integration

τ_0 Yield stress

ϑ Description parameter of velocity profile

$\triangle x$ Length of increment

Abbreviations

1D	One Dimensional
3D	Three Dimensional
AMM	Advanced Mathematical Modelling
Ca	Calcium
CFD	Computational Fluid Dynamics
CO_2	Carbon Dioxide
CSIR	Council for Scientific and Industrial Research
CT	Computed Tomographic
EES	Engineering Equation Solver
K	Potassium
LDL	Low Density Lipids
MR	Magnetic Resonance
N	Nitrogen
Na	Sodium
O_2	Oxygen
SIMA	SIMulation in Anaesthesia
SIMPLE	Semi Implicit Method for Pressure Linked Equations

List of Figures

List of Tables

Chapter 1

Introduction

The CSIR Competency Area Advanced Mathematical Modelling (AMM) requires a skill base in the modelling of the human cardiovascular system to support its "Patient Specific Modelling" program. This study looks at the one dimensional (1D) modelling of blood flow.

Cardiovascular diseases represent the major cause of death and disability world wide. They are responsible for more than half of the deaths in the developed countries [10]. Many of the diagnostic decisions and intervention plans regarding cardiovascular diseases are made based on rough estimates of outcomes as well as previous experience. These estimates are often derived from generalised anatomic observations and measurements and do not necessarily take into account all available data. Often these methods do not reflect the sophistication of our current knowledge regarding vascular disease [19, 34]. More light may be shed on the diagnosis of a patient with a simple engineering tool. This tool would typically combine the results of various physiological and anatomical measurements (such as cardiac stress tests, duplex ultrasound, computed tomographic (CT) angiography and magnetic resonance (MR) angiography) and process the results based on geometry and flow theory using mathematical models. It can also assist in surgical planning and prediction of the outcomes of procedures.

Arteries can be viewed as pipes with elastic walls and blood flow can be modelled as a continuous flow problem(mass flow) with a pulse(pressure wave) superimposed on it. Blood takes approximately one minute to circulate through the body. Because blood is an incompressible fluid, each pump action of the heart induces a pressure wave that travels through the body at the speed of sound. When you listen with a stethoscope to the systolic heart beat you can almost simultaneously feel the pulse at the wrist. This makes the problem truly multiscale as the pressure waves travel at speeds more than three orders higher than the normal blood flow.

Engineers have developed a variety of methods and techniques to solve flow problems in pipe networks. The bulk of these programs solve flow for pipes with rigid walls. Some computer codes also include the effect of water hammer in the solution, which provide to some extent for the stretching of the wall. Water hammer is a pressure wave or surge that occurs when a fluid in motion is suddenly forced to stop or change direction.

The walls of larger arteries can expand by a much larger percentage than can be found in the water hammer phenomena. In the aorta, for example, the diameter may vary up to 10% between diastole and systole [28]. This fluid-structure interaction is responsible for the propagation of pulse pressure waves. The material properties for the arterial walls are quite difficult to obtain. This is due to the fact that it is living tissue, the properties change when it dies and it can not be assessed while the patient is alive. Although blood is an incompressible liquid, the expandability of the walls adds an effect that resembles that of compressible flow. This effect is the increased mass throughput per unit length of tube. The fluid-structure equation that relates area to pressure, resembles the equation of state of compressible flow. Altered blood flow conditions such as separation and flow reversal are important factors in the development of arterial disease. A new model that includes these characteristics should be developed to provide insight into the cause of problems and possible treatment options for different cardiovascular diseases. This computer code should zoom in on specific flow features, such as turbulence and separation and their effects [50].

The cardiovascular system can be divided into many parts that can be modelled separately and then combined to form a closed network. These parts include the heart chambers and valves and the systemic, coronary and pulmonary vessels. The vessels can be subdivided into arteries, carrying the blood away from the heart, and veins, carrying the blood towards the heart. Arteries can be divided into three groups: large arteries, medium arteries and capillaries.

In an ideal world where resources are unlimited we would model the entire cardiovascular system using three dimensional models (3D) based on the solution of the Navier-Stokes equations. It provides detailed descriptions of local flow features [50]. However, using 3D models are resource- and time intensive, making it unsuitable for large-scale simulation or for quick evaluation of alternate surgical options [36, 50]. Furthermore, precise information regarding 3D geometry and material properties are difficult to obtain [20]. Multiscale models (Figure 1.1) couple models of different physical dimensions to find the optimal balance between detail and computational cost [9].

When attempting to create a new model in fluid dynamics it is common practice to start with a simple model and then add complexities. This is also applicable to the cardiovascular model. It would be ideal to start with a 1D model. When the model is expanded to 3D in some areas,

the 1D model can be used to supply boundary conditions. Although 1D network models do not give results to the same level of flow detail as 3D models [50], they give reliable numerical results at a computational cost of several orders lower than those for 3D models [8] and thus generate results in a fraction of the time.

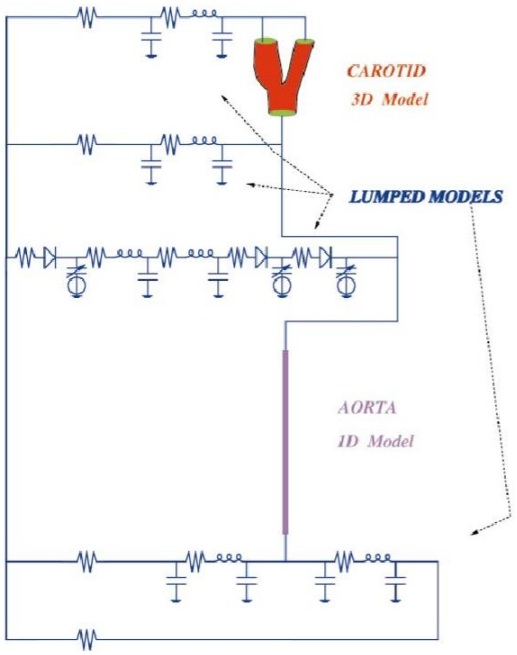

Figure 1.1: Multiscale model of the human cardiovascular system [9]

Currently there are two main approaches used to model large arteries in 1D: modelling in the frequency domain or modelling in the time domain. Most models found in literature function in the time domain [20, 28, 39, 40, 45] and are based on the nonlinear Navier-Stokes equations where the problem is approximated to obtain a numerical solution. The governing equations can be solved using different discretisation schemes. Most researchers used the finite element method [8, 39, 50]. However the method of characteristics [3] and the finite difference method [13, 24, 40] have also been used.

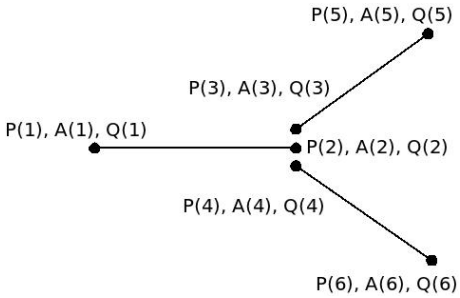

Figure 1.2: Discretisation at a branch using a co-located grid [20]

The discretisation shown in Figure 1.2 is done on a co-located grid. P represents pressure, A the area of the artery and Q the flow through the area. On a co-located grid all variables are defined at the same position in the control volume. Most of these methods create an extra node or nodes to handle discontinuities and branching (Figure 1.2), which in turn create additional equations to be solved. These increase the time needed to compute the solution. If a staggered grid can be used, where pressure and flow are calculated at different positions in the control volume, these nodes and equations could be eliminated (Figure 1.3). Staggered grids are used in several engineering applications such as the solution of flow in pipe networks [11, 12]. No 1D model that uses the finite volume or difference disretisation on a staggered grid to model blood flow has been encountered so far.

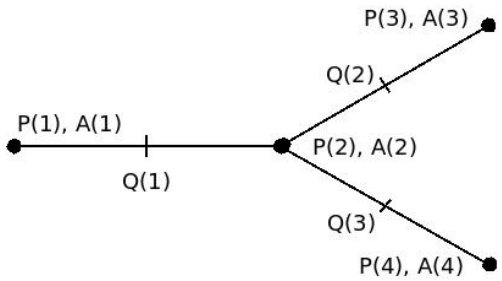

Figure 1.3: Discretisation at a branch using a staggered grid

In the analysis of a pipe network it is possible to isolate a part of the system and to study the flow features in that specific section as they would be found in the system. This is done by prescribing boundary conditions at the inlet and outlet. Most of the time this is done by prescribing either pressure or velocity values. It is more complex to isolate a part of the arteries. Pressure waves in the cardiovascular system are reflected at branches and other discontinuities. Thus, forward and backward pressure waves can be found at any place in the arterial network. The boundary conditions should not reflect these waves but rather let them pass through the boundary unchanged. To make this possible, non-reflecting boundary conditions should be prescribed.

1.1 Problem definition

In medicine, computational fluid dynamics is more of a push technology than a pull technology therefore currently although much research has been done on 1D models, the understanding that it provides is still more explanatory than predictive. The models that have been developed focus on the arteries that are close to the heart. Furthermore, very little research has been done on venous haemodynamics [52]. This results in an incomplete network with inadequate feedback to verify results. Hence, there is still a lot of room for improvement in the 1D model.

The techniques used by engineers to model 1D flow in pipe networks have evolved through the years. These techniques might also improve the modelling of blood flow through arteries. One of these methods is based on the finite volume method on a staggered grid, solved with an iterative procedure [11].

The aim of the study was to develop a 1D computer code that can model the blood flow in large arteries using a finite volume approach.

1.1.1 Scope

The research focused on the development of a transient 1D network code:

- The investigation was limited to the large arteries in the systemic circulation.
- Non-reflecting boundary conditions from existing research were used, with a prescribed pressure at the inlet.
- Discretisation was done using a finite volume approach on a staggered grid.
- The study investigated the effects of branching and discontinuities on wave reflection.
- Results from this model have been compared with results from a finite element model (where the results were available).

1.2 Group's objectives

This study contributes to the Council of Scientific and Industrial Research (CSIR) patient specific modelling group's aim to investigate different alterations and anomalies in the arterial network as well as ways to treat it. These alterations are sometimes induced by procedures, such as dialysis and heart bypasses. Sometimes these anomalies, such as the vein of Galen anomaly, are due to congenital defects. A 1D computer code can help to plan procedures in order to prevent or treat these shunts. It can also be used to provide better boundary conditions for 3D models of a specific area.

1.3 Overview of the dissertation

1.3.1 Chapter 2 - Literature survey

The literature survey covers two themes. Firstly it looks at the biology of the cardiovascular system and secondly it gives an overview of the different cardiovascular models found in literature.

The section on the physiology and pathology of the cardiovascular system takes a look at the heart, blood and the vascular system. The section also gives attention to the interaction between the blood and arterial walls as well as the attributes of the blood's viscosity. Disease can limit and alter the function of the cardiovascular system. The literature survey discusses the pathology of some of these diseases as well as the surgical procedures that exist to correct these vascular problems.

The second section of the literature survey gives attention to the uses of mathematical cardiovascular models. It also gives an overview of different types of models found in literature. A subsection focuses on different 1D models and the discretisation methods used in them.

1.3.2 Chapter 3 - The mathematical model

This chapter discusses the mathematical model which describes blood flow in large expandable arteries. The first section describes and shows the derivation of the Navier-Stokes equations for this application. The Navier-Stokes equations contains three variables, A, p and Q, as well as mass and momentum conservation equations. A third equation relates area to pressure and closes the system of equations. This equation is analogous to the constitutive equation for compressible flow.

A following section describes the staggered grid used to discretise the equations. In this grid pressure and area are defined at the wall of the control volume while the volume flow rate is defined at the centre of the control volume.

Next the iterative method that was used to solve the system of equations is discussed. This method is similar to the SIMPLE algorithm. A guessed field for the variables is calculated based on momentum conservation, the constitutive equation and the values of the previous time-step or iteration. A pressure correction equation solves for continuity after which the other variables are corrected. This process is repeated until convergence has been achieved.

The next section formulates the non-reflecting boundary conditions that were used in the model. These boundary conditions accomodate the forward and backward moving waves

that are found in the cardiovascular system. The boundary conditions are derived from the characteristic system and variables.

The way in which discontinuities and branching were handled is also explained in this chapter. The staggered grid allows for a more natural approach to both discontinuities and branching and no extra nodes are needed for a continuous solution.

1.3.3 Chapter 4 - Implementation

The chapter on the implementation of the model discusses the computer code that was developed. A section is dedicated to the general layout of the program. The iterative procedure is the core of this program. The pseudo code for the steady state solution and the non-reflecting boundary conditions are included in this chapter. Attention is also given to post-processing of the results.

1.3.4 Chapter 5 - Simulations

This chapter shows the results of the test cases that were run to demonstrate the ability of the computer coding to solve problems. First we look at the steady state solution, then at different transient solutions for a single artery and lastly at more complex cases where there is branching.

The steady state solution is important as it will be used as the initial condition for the transient cases. A section shows the results of numerical experiments on different discretisation schemes and on different primary variables that were used. This section also illustrates the effect that viscosity has on the flow.

The next section shows the results of different transient test cases for a single artery. It demonstrates the effect that numerical influences such as the size of the increment and time-step as well as the time integration schemes have on the solution. There are also results that show the damping effect of viscosity. A subsection shows the difference in the behaviour of the pulse when a smaller or larger input pulse is prescribed. The smaller input pulse shows linear behaviour and the larger input pulse non-linear behaviour as will be explained in Section 5.2.1.3. The peak of the larger pulse propagtes at a higher speed than its trough. The effect that material properties and relaxed initial area of the artery have on the propagation speed of the pulse is also discussed in this chapter. A subsection also demonstrates the reflection of the waves when different discontinuities are present. The boundary conditions can be prescribed as non-reflecting, positive reflecting or negative reflecting. This chapter shows results for all the possibilities.

At a branch in the artery part of the pressure wave gets reflected. This reflection depends on the relaxed area and material properties of the branches. The results for a test case of a parent vessel and two different branches are displayed in the following section.

This chapter is closed with the results of a more complex case that includes more than one branching point and a few discontinuities.

1.3.5 Chapter 6 - Conclusions and recommendations

This chapter presents the conclusions and recommendations for further research.

Chapter 2

Literature survey

As mentioned in the previous chapter, the aim of this study is the development of a 1D cardiovascular model. This chapter, divided into two sections, presents a broad overview, linking the biological aspects and modelling together. The first section gives detail on the biology of the cardiovascular system. The second section gives an overview of the cardiovascular models that have been developed.

2.1 Physiology and pathology of the cardiovascular system

In medicine, the field of physiology is concerned with the body's normal vital processes. Pathology describes diseases with special reference to the causes, essential nature and development of abnormal conditions, as well as the functional and structural changes that result from the disease processes [41]. This section will look at the physiology and pathology of some of the parts in the circulatory system.

The circulatory system acts as a transport system for the body. It consists of the heart, blood, blood vessels, lymphatic vessels and lymph. The cardiovascular system is a closed network. The heart rhythmically pumps deoxygenated blood through the pulmonary arteries to the lungs. The lungs oxygenate the blood and remove the carbon dioxide and then the pulmonary vein transports this blood back to the heart. The heart pumps the blood through the arteries to the organs, where the oxygen is extracted through the small capillaries to the tissue and carbon dioxide is added. From there it is collected by the veins and flows back to the heart and the cycle repeats.

Several diseases of the vessel walls, most commonly atherosclerosis and aneurysms, prevent the optimal functioning of the circulatory system. This section gives information to the causes and effects of these diseases.

The information communicated in this section is common knowledge in the medical field. Therefore, with a few exceptions, individual citations will not be made. I have used [18] and [33] for information about the physiology of the cardiovascular system. The pathology of the blood, vascular system and heart is covered in [47]. Information about the rheology of blood is communicated in [21] and [10]. Some additional insights on the mechanical influence of the physiology and pathology and the surgical procedures are also given in the latter.

2.1.1 The heart

The most important role of the heart is to maintain an adequate flow of blood throughout the cardiovascular system. Anatomically there is only one heart; however, physiologically there are two independent pumps, one associated with pulmonary and one with systemic circulation. In practice they are interdependent, both mechanically and electrically. The following section will consider the anatomy of the heart and the manner in which it contracts to generate pressure and flow.

2.1.1.1 Heart chambers and other components

The heart is a cone-shaped, hollow organ containing four chambers comprised mostly of myocardium (Figure 2.1). Myocardium consists of specialised muscle cells that have lower contractility and higher resistance to fatigue than other muscle cells. The heart weighs only 300 g in adults and has the size of a clenched fist. From an engineering perspective the heart looks like a thin balloon that is twisted in the middle to form two chambers, folded at the twist so that the chambers are next to each other and twisted again to form four chambers. There are two chambers on each side of the heart: an atrium and a ventricle. The atria, at the top, have thin walls and receive blood returning to the heart from the systemic network (right heart) or the lungs (left heart). Blood is pumped from the atria to the ventricle. The ventricles, especially the left ventricle, have thicker muscular walls. The ventricles can pump blood out of the heart at high pressures. An opening on each side in the atrioventricular septum allows the atria to communicate to the ventricles. One-way valves guard the openings in the atrioventricular septum. The valves that separate the ventricles from the systemic and pulmonary arteries are called semilunar valves. These valves are much thicker and stronger than the atrioventricular valves. The opening and closing of valves occurs in response to the blood pressure gradient across the valve.

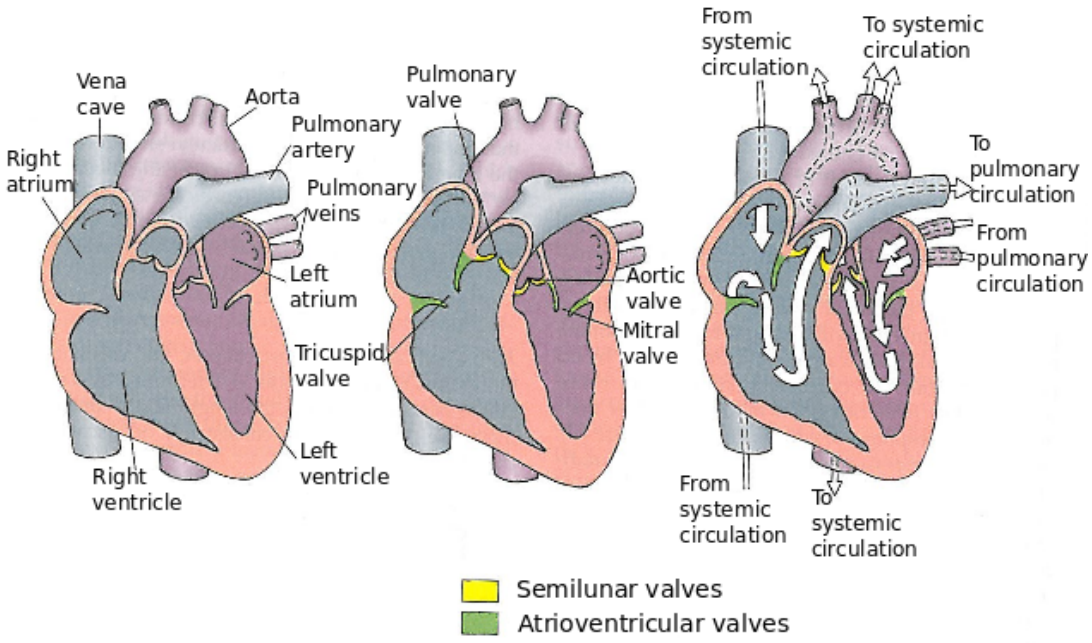

Figure 2.1: Overview of the heart, major arteries and veins leading into and out of the heart and heart valves [33].

The inner surface of the inner layer of the myocardium, the endocardium, is lined with a thin layer of endothelial cells. The endothelial layer covers the inner surfaces of the heart, the heart valves and also the entire vascular network and prevents clotting. Turbulent flow can damage this endothelial layer and cause clots to form.

There are specialised muscle cells that form the conducting system of the heart. These cells have the special ability to initiate impulses spontaneously. These impulses are conducted through the myocardium and cause the beating of the heart.

Blood supply to the heart itself is through the right and left coronary arteries and their branches, originating from small holes or sinuses just above the semilunar valve entering the aorta. The larger coronary arterial network lies on the outer layer of the heart wall. Smaller arteries form the microcirculation to the myocardium and are found in the wall. The constant supply of oxygen to the heart by the coronary vessel is crucial for regular functioning of the heart. This is because the myocardium can not contract anaerobically (without oxygen).

2.1.1.2 The cardiac cycle

The cardiac cycle is the series of events occurring during one complete heartbeat over a period of about 1 s (Figure 2.2). Systole is the period during which the atrial and ventricular

myocardium contracts and blood is ejected from the ventricle. Systole can be defined as the period between the closing of the mitral valve and the subsequent closing of the aortic valve. Diastole is defined as the period between the closing of the aortic and mitral valves or as the period when the myocardium relaxes. Diastole occupies approximately two thirds of the cardiac period during rest. As the heart rate increases, during exercise for example, the duration of systole remain almost the same while diastole is shortened, resulting in a faster heart rate.

The pulsatile nature of blood flow is caused by the events occurring during a cardiac cycle. At the beginning of a cardiac cycle both the ventricle and atria are relaxed. The atrioventricular valves are open and the semilunar valves closed. Blood flows from the vena cava and pulmonary veins into the right and left atria respectively. Blood flows because of the negative pressure that was imparted to it by the heart pump in the previous cycle. The atrioventricular valves are open and this allows almost 70% of the blood that enters the atria to flow to the ventricles. Next the sinu-atrial node discharges an impulse which depolarises the atria and after that the ventricles, causing the contractions of atria and ventricles. When the atria contracts the pressure increases to about 9 mmHg and causes the blood that is still present to flow into the ventricles. When the ventricles begin to contract, the atrioventricular valves close preventing blood to flow back into the atria. Once the atrioventricular valves are closed, the volume of the ventricles remains the same until the pressure inside the ventricle exceeds that in the arteries.

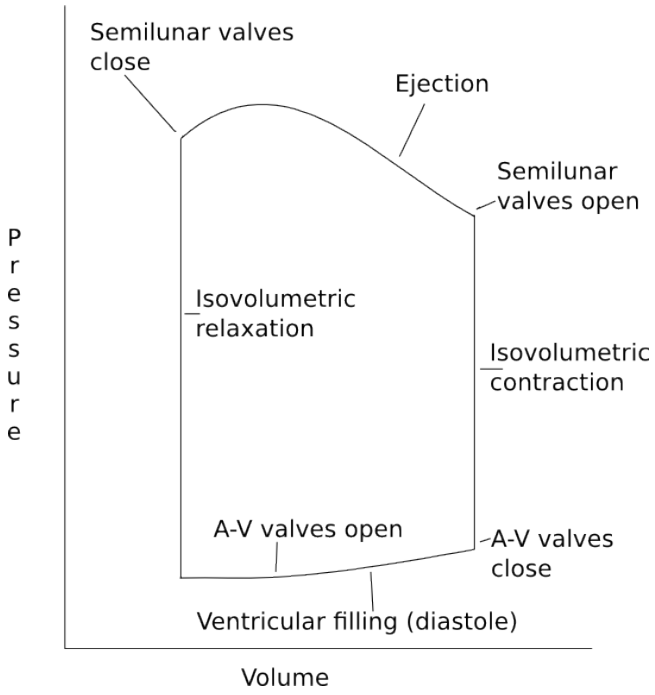

Figure 2.2: Pressure-volume loop of the cardiac cycle based on [18]

Then the semilunar valves are forced open and ventricular ejection begins. Almost two thirds

of the stroke volume (the volume ejected per beat) is ejected during the first third of systole. When the blood leaves the ventricle, the intraventricular pressure decreases and the rate of ejection decreases accordingly. Towards the end of the systole, blood flow at the root of the pulmonary artery and aorta is reversed for a short period, closing the semilunar valves. In the period that follows, the ventricles are closed chambers again and the muscle relaxes. When the intraventricular pressure falls below the intra-atrial pressure, the atrioventricular valves are pushed open by the blood and the cycle starts again. Many modellers approximate the effect of the cycle with a pressure sine wave, but more complexities should be added at a later stage.

2.1.2 Blood

Blood cells are suspended in plasma, making it a very complex fluid. The following sub-sections will look at the functions, composition and rheological aspects of blood. Furthermore, it will give attention to the causes and inhibitors of coagulation (clotting) and the problems that can arise if these are not in balance with each other.

Blood flow is determined by the pressure created by the heart and the resistance to the flow. Blood flow in the vascular network is laminar under normal circumstances. In the aortic valves and carotid sinus or restricted areas in vessels where the velocity is above a critical velocity, flow is turbulent. It is believed that turbulence can create separation and recirculation causing flow forces to erode vessel walls.

2.1.2.1 Function

The functions of blood centre primarily on transportation and homeostasis. Blood transports oxygen (O_2) from the lungs to the tissue, carbon dioxide (CO_2) from the tissue to the lungs, the absorbed nutrients and other substances from the digestive tract to the tissues, the products of metabolism to the kidneys and heat to the skin. It also provides buffers required for pH homeostasis and protects the body against haemorrhage (bleeding) and infection, by carrying blood platelets and white blood cells respectively to target areas.

2.1.2.2 Composition

The liquid component of blood is called plasma. The cells are suspended in this liquid and it makes up between 52-63% of total blood volume. Water is the main component ($90 - 92\%$) of the plasma. Organic solids, such as protein, glucose and lipids, constitute almost 9% of the

plasma volume. Inorganic proteins, including sodium (Na), Potassium (K) and Calcium (Ca) provide the remaining percentage of the composition. The plasma also contains very small amounts of gases namely, oxygen, carbon dioxide and nitrogen (N). The proteins don't affect the Newtonian behaviour of the plasma, and its viscosity is approximately 1.2×10^{-3} Pa.s. The plasma's density is approximately $1030\,\mathrm{kg/m^3}$.

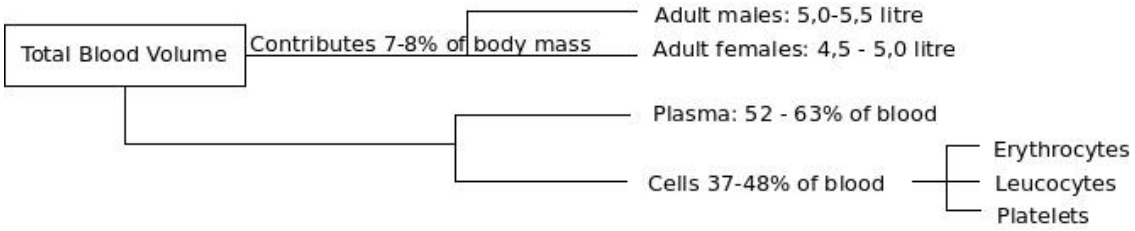

Figure 2.3: Composition of Blood based on [18]

There are three types of cells that are suspended in this plasma: Red blood cells (erythrocytes), white blood cells (leucocytes) and platelets (thrombocytes). The haematocrit is the ratio between the volume occupied by the cells and the volume of the total sample. This is in the range of $42 - 52\,\%$ for males and $37 - 47\,\%$ for females. The red blood cells constitute 97% of the cell volume of blood. The contribution of the white blood cells and platelets to the haematocrit is very small. In normal amounts, leukocytes don't have a big influence on the rheology of the blood.

Red blood cells have a biconcave discoid shape with a diameter between 6.5 and $8.8\,\mu$m and a thickness of $1 - 3\,\mu$m. The normal red cell count is $4.2 - 5.4 \times 10^{12}/l$ in females and $4.6 - 6.2 \times 10^{12}/l$ in males. Erythrocytes don't have a nucleus or mitochondria, making it flexible to squeeze through the capillaries (which has a diameter of about $6\,\mu$m). Erythrocytes have membranes covered with albumin on the outside and spectrin on the inside. On the inside is a liquid called haemoglobin which binds with O_2 and CO_2. The red blood cells play an important role in the rheological properties of blood, as will be seen in a next section.

A platelet is a non-nucleated particle of $2 - 4\,\mu$m. Normal blood contains $150 - 400 \times 10^9$ platelets per litre blood. The platelets play a big role in haemostasis by adhering to the vessel wall in damaged areas and to each other to plug the leaks. The platelets are responsible for coagulation (clotting), which can create serious health problems if the mechanism that inhibits clotting is not functioning well.

2.1.2.3 Clotting

The term haemostasis refers to mechanisms that minimise blood loss through interruptions in the vascular system. Haemostasis is very important because uncontrolled haemorrhage

(bleeding) eventually leads to cardiovascular collapse. Platelets can rapidly clump together at an injured blood vessel, and together with fibrin can cause a clot that plugs the defect. When there is no interruption in the vessel walls, clotting is undesirable. The body has several anti-clotting mechanisms (among other the smooth endothelial layer and the continued circulation of blood) that prevent platelets to aggregate and form a clot.

Normally the procoagulant and anticoagulant influences are finely balanced and allow normal haemostatic responses whilst preventing pathological thrombosis. When blood flow is low however, the balance between self-activation and inhibition of coagulation is overthrown and can lead to thrombi formulation. This can block vessel lumen inducing ischemia to the vessels it irrigates and cause tissue death. Thrombi can also detach to form an embolus which can lodge in a smaller vessel and cause infarction. When this happens in the brain, it is called a stroke; in the heart or coronary vessels, a heart attack and in the lungs, a pulmonary embolism. The interplay between rheological and haemostatic changes in thrombotic disease is not yet fully understood.

2.1.3 The vascular system

The vessels act as ducts for the blood to flow through. The arteries transport oxygen rich blood to the organs and can be divided into four groups:

- The large elastic arteries, including the aorta and its branches;
- The medium-sized muscular arteries;
- The small muscular arteries or arterioles;
- And the metarterioles or capillaries, that are responsible for the delivery of the oxygen and nutrients to the organs and tissues.

Blood vessels react dynamically when the flow or pressure in the arteries changes. These changes are sensed at a cellular level and initiate a series of biochemical signals that lead to a multi-scale reorganization ranging through the molecular, cellular, tissue and system scales. These changes includes the dilatation or constriction of vessels due to the minute to minute increase or decrease in blood flow and the thickening or thinning of the vessel walls in response to increased or decreased chronic pressure [43].

Blood vessels consist of three layers namely the tunica intima, tunica media and tunica adventitia (Figure 2.4). In the larger arteries the internal elastic lamina or basement membrane separates the inner endothelium layer and the media. The media and adventitia is separated

by the external elastic lamina. The adventitia is loose connective tissue with some smooth muscle cells and attaches the artery to the surrounding tissue. A single layer of squamous endothelial cells lines the surface of the blood vessels. This layer is continuous with the squamous endothelium forming the capillaries and ensures that effective transfer between the blood and tissue can occur. The arterioles represent the major resistance of the vascular system.

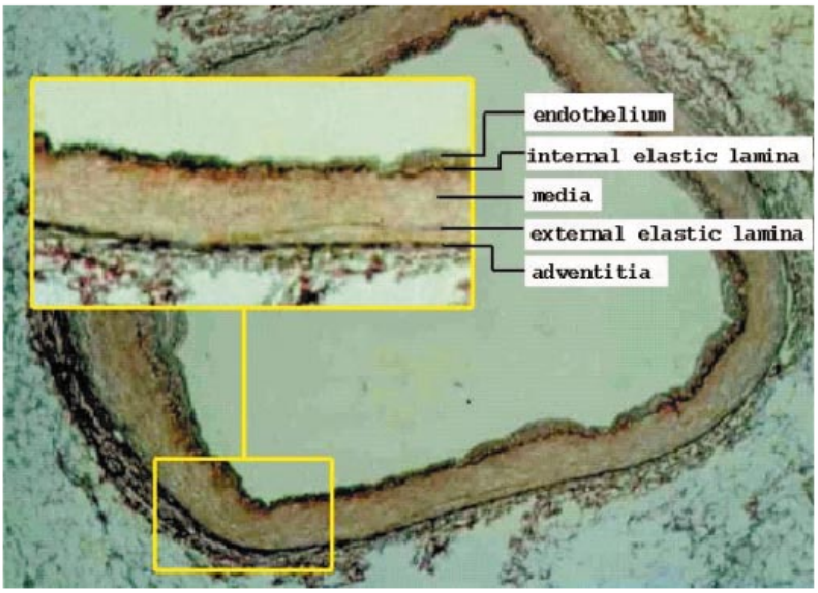

Figure 2.4: Cross-section of arterial wall shows the concentric arrangement of tunica intima, media and adventitia [29]

The media consists of a smooth muscle, interspersed with elastic lamellae (multi-unit smooth muscle fibres) with a thickness of about 5 μm. The larger arteries are much more elastic simply because they have more lamellae. There are subtle structural and property differences in large arteries at different locations in the arterial tree. The arteries that are proximal (or closer) to the heart are more elastic and have thinner walls.

During systole the vascular system is 'overfilled' with blood. This large volume of blood creates an outward force, know as blood pressure. Although this force can be found everywhere in the vascular system, blood pressure usually refers to the systemic arterial pressure. Blood pressure is conventionally written as the mean systolic pressure over the mean diastolic pressure and the unit is mmHg. Normal blood pressure is between 100/60 mmHg and 140/90 mmHg.

In the larger arteries, such as the pulmonary artery and aorta, the elastic tissue in the media dominates, while in all the other arteries the smooth muscle tissue dominates. During systole the large arteries expand to accommodate the large blood volume coming from the heart. During diastole the arteries recoil forcing the blood forward, providing a continuous blood

flow through the system. The large arteries can therefore be seen as secondary pumps. These elastic tubes support the transfer of 1D wave energy between the kinetic energy of the blood and the potential energy of the walls and vice versa. The wave speed, c, depends upon the density of the blood and the distensibility (or compliance) of the arterial walls. The waves that propagate through the arterial system experience several reflections through the vascular system. These reflections are caused by discontinuities in the geometry and material properties of the arteries and bifurcations.

The effects of high blood pressure can harm the vessel walls. Blood vessels remodel themselves when there are chronic changes in blood pressure and flow rate. A reduction in pressure and flow causes the lumenal diameter and media mass to reduce. A rapid increase in flow rate or pressure leads to the increase in vessel bore and a reactive contraction of smooth muscle cells. If this increase is prolonged, structural changes occur and are characterised by proliferation of smooth muscle cells.

Vessel walls have non-linear visco-elastic material properties. Linear and non-linear elastic material follows the same path for loading and unloading. This is not true for visco-elastic materials. Most biosolids, also the vessel walls, show visco-elastic behaviour. Phenomena that characterise visco-elasticity are relaxation, creep and hysteresis. Stress relaxation refers to stress in a material that decreases when the material is suddenly strained and then maintained at a constant strain. When a material continually deforms with respect to time after it is suddenly stressed and then maintained at constant stress, it is known as creep. Hysteresis is the behaviour of a material when a different stress-strain relationship is obtained during loading and unloading when it is subjected to a cyclic load. The visco-elastic properties of the walls are relatively small.

2.1.4 Haemorheology

Rheology is the science that describes the interrelation between force, deformation and flow. When this is applied to blood, it studies the coupling of blood and blood vessels and is called haemorheology. Evidence shows that changes in the rheological properties of blood due to pathological disturbances might be the primary cause of many cardiovascular diseases.

Blood is a viscous incompressible liquid. It takes blood approximately one minute to circulate through the body. With every heart beat a pressure wave is generated that propagates much faster than the mass flow through the cardiovascular system. The propagation of this wave is due to the fluid-structure interaction.

The primary determinant of blood viscosity is the haemotocrit, which is linked to the red blood cell concentration. The plasma fibrinogen concentration is the second biggest determi-

nant of blood viscosity. Fibrinogen is the major determinant of red cell aggregation. Other plasma proteins have a much smaller effect on the viscosity because they are smaller and more symmetrical. However, in increased concentrations they may affect blood viscosity. When the viscosity of the blood increases, it can lead to hyperviscosity syndrome and can result in cerebral dysfunction, with headache, drowsiness and visual disturbance. Hyperviscosity syndrome is an extreme abnormality of the blood flow and can produce organ dysfunction. But even a minor increase in the viscosity of blood, due to increased fibrinogen or haematocrit, can affect tissue perfusion and result in tendency to vascular occlusion, leading to myocardial and cerebral infarction and pulmonary embolism. The plasma fibrinogen concentration is a risk factor for arterial occlusive disease and almost as potent as the level of serum cholesterol.

The blood plasma behaves like a Newtonian fluid, while the blood mixture (whole blood) exhibit non-Newtonian characteristics. This non-Newtonian effect is very small, except at low shear rates. It can be contributed by three factors: the red blood cells' tendency to aggregate at low shear rates to form three-dimensional microstructures, their tendency to align themselves with the flow field and their deformability. Whole blood shows shear thinning characteristics and thixotropic behaviour. Thixotropy refers to the dependence of material properties on the time over which shear has been applied. Beyond a shear rate of about $100\,\mathrm{s}^{-1}$ blood behaves like a Newtonian fluid because the ratio between blood viscosity and plasma viscosity is nearly constant. The Newtonian relation for shear stress sufficiently describes the behaviour [21]:

$$\tau = \mu\dot{\gamma} \tag{2.1}$$

where τ represents the shear stress, μ the dynamic viscosity and $\dot{\gamma}$ the shear rate.

When the viscosity decreases with an increase in shear rate, it is called shear thinning (Figure 2.5). Note that the viscosity is the slope of a curve at any point in the figure. For Newtonian flow the viscosity and therefore the slope is constant. For a shear thinning liquid the viscosity and slope of the curve becomes smaller as the strain rate increases. This shear thinning behaviour of blood can be accounted for by the erythrocytes' behaviour when shear stress is increased or decreased. When the shear stress in a vessel decreases, the individual red blood cells form shorter chains; when the shear stress keeps on decreasing, longer rouleaux form. When the shear rate is very low, the rouleaux align themselves in a side-to-side and end-to-side manner and a secondary structure is formed. This aggregating process is reversible. When a finite level of force is applied, the shear stress increases and structures start to disaggregate. This level of force, is often referred to as the yield stress. It is dependent on the haematocrit and fibrinogen concentration of the blood plasma. Other factors that influence the value of the yield stress parameter include the red cell shape and deformability. In sickle cell anaemia, for example, the deformability of the blood cells decreases, increasing the viscosity and yield stress

parameter. When the stress continues to increase, blood starts to flow. When the blood flows faster, the erythrocytes align themselves in the direction of flow, and the viscosity decreases.

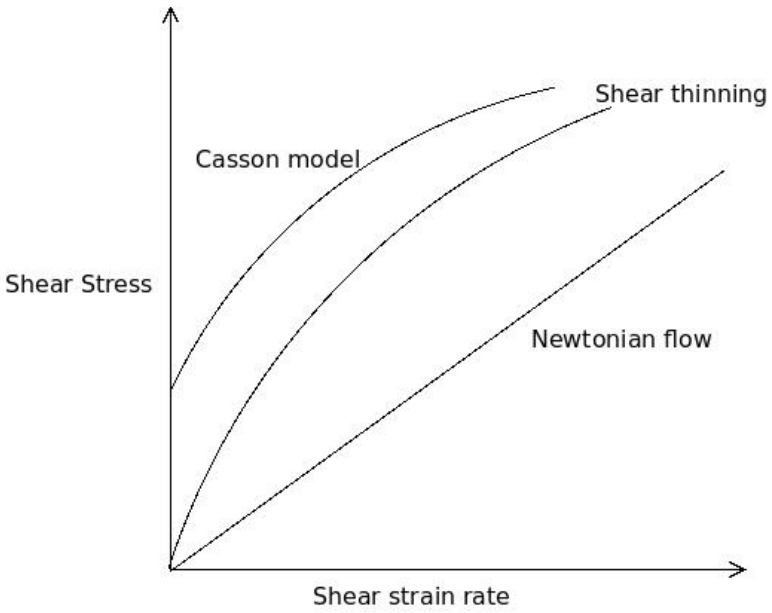

Figure 2.5: Shear thinning behaviour and the Casson model based on [21]

To account for the yield stress parameter a Casson model [6] can be used. The Casson model was originally derived for printer's ink. It includes the yield stress, under which blood behaves like a solid, and the shear thinning behaviour. Using the Casson model blood shear stress is represented by:

$$\sqrt{\tau} = \sqrt{\tau_0} + \sqrt{\mu\dot{\gamma}} \tag{2.2}$$

where τ_0 is the yield stress. It can be seen that when $\mu\dot{\gamma} \ggg \tau_0$ the above equation approaches the Newtonian equation (2.1).

A finite time is necessary for equilibrium in both the formation of the red blood cells' structures and alignment of the red blood cell to be reached. This causes the thixotropic behaviour of the blood.

2.1.5 Cardiovascular diseases

2.1.5.1 Atherosclerosis

Atherosclerosis is an inflammatory disease that can cause several complications including gangrene, aortic aneurysms, myocardial or cerebral infarction and carotid atheroma. It is commonly known as 'hardening' of the arteries. Atherosclerosis especially affects the large and medium arteries. It is characterised by fibrosis, lipid deposition and chronic inflammation. During the past 50 years its occurrence has increased dramatically.

The exact cause of atherosclerosis is unknown. There are some risk factors, but some patients with atherosclerosis have no obvious risk factors. Some of these risk factors include age, hypertension, diabetes, smoking, obesity, a sedentary lifestyle, low social-economic status and low birth weight. There is a strikingly wide variation in the distribution and severity of lesions between individuals. Studies of patients of different ages show that lesions progress from fatty streaks that are small and inconsequential to large and complicated lesions. When it progresses it can lead to complicated lesions that obstruct the lumen of the arteries (stenosis). These complications are chronic, cumulative and slowly progressive (it can take decades for symptoms to develop). Not much is known about the mechanisms which influence when and where the plaque develops. However, studies have shown that these lesions often occur at sites where turbulent flow normally occurs, on the outer walls of bifurcations or bends. There is substantial evidence to suggest that the localization of atherosclerosis is greatly influenced by the blood fluid mechanical factors [5].

2.1.5.2 Aneurysms

When a vessel forms a localised permanent dilatation, it is called an aneurysm. This is caused by a weakening of the vessel wall. Laplace formulated a law that expresses circumferential tension (T) as the product of the transmural pressure (P_t) and the radius (r) of the vessel [18]:

$$T = P_t r \tag{2.3}$$

This gives an explanation why enlarged vessels are more likely to rupture even when arterial pressures are quite normal. Untreated aneurysms can rupture and cause massive haemorrhage. Structural change in the connective tissue is a result of plastic deformation of the arterial wall.

Aneurysms can be divided into two types: fusiform aneurysms and saccular aneurysms (Figure 2.6). Fusiform aneurysms are cylindrical dilations where the artery's entire circumference is

weakened. Saccular aneurysms are balloon-like bulges and form as a result from a weakening of one side of the arterial wall.

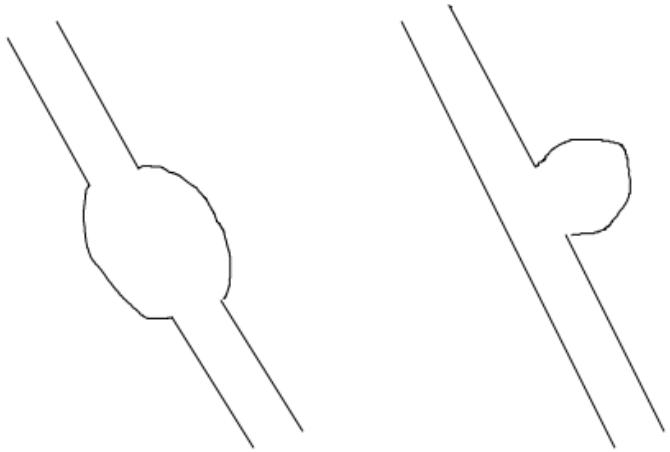

Figure 2.6: A fusiform aneurysm (left) is a cylindrical dilation, while a saccular aneurysm (right) forms a balloon-like bulge.

2.1.5.3 Hypertension

Chronic high blood pressure or hypertension is the most common cause of heart failure in many societies and a major risk for atherosclerosis. It is also a major risk factor for cerebral haemorrhage.

Hypertension can be divided into benign and malignant hypertension. Benign hypertension can be detected electrocardiographically, and is often associated with a concentric thickening of the left ventricle. Some patients also have coronary arterial atherosclerosis and consequently ischemic heart disease. Benign hypertension accelerates or precipitates other disorders including spontaneous intracerebral haemorrhage, aortic dissection and subarachnoid haemorrhage due to rupture of berry aneurysms. Malignant hypertension is characterised by a markedly raised diastolic pressure, over 130-140 mmHg, and progressive renal disease. The consequences of malignant hypertension include cardiac failure with left ventricular hypertrophy, blurred vision, severe headache and cerebral haemorrhage.

Hypertension has several effects on the vascular system. It accelerates atherosclerosis and thus ischemic heart disease is a frequent complication. It also causes thickening of the media of muscular arteries, affecting the smaller arteries especially.

2.1.5.4 Heart Failure

When the heart is unable to pump blood at the required rate for normal metabolism, cardiac failure occurs. Heart failure is a progressive disease and complicates almost all forms of severe cardiac disease. Cardiac failure has a poor prognosis. It has many causes including chronic valve disease, chronic arterial disease and the failure of the myocardium itself. The cardiac output is reduced in almost all forms of heart failure. This causes a degree of underperfusion and is called arterial underfilling. The body retains fluid and decreases blood volume to compensate. Mechanoreceptors in the left ventricle, the carotid sinus, the aortic arch and the renal afferent arterioles send signals to the cardioregulatory centres in the brain 'informing' it about the underfilling. The cerebral response causes tachycardia (rapid beating of the heart), increased myocardial contractility and constriction of the vessels. The cardiac ventricles undergo remodelling, changing in shape, size and composition. Alterations also occur in the network of connective tissue surrounding the cardiac muscle cells. Cardiac outputs fail to increase appropriately during exercise in most patients with heart failure, and later on it is decreased even at rest. This is a direct consequence of the heart's inability to pump normally.

The main causes of heart failure in adults are ischaemic heart disease, systemic hypertension, valvular heart disease and lung disease. Abnormal or inadequate circulation can also cause heart failure. This can be caused by induced shunts, fistulas, or by abnormal development of vessels called anomalies. A few years back fistulas in the hand were surgically inserted in an arteriovenous configuration for haemodialysis. This is because there is an adequate pressure difference between the arteries and veins. Studies have shown that this shunt disrupts the blood flow to the hand to such an extent, that the receptors send signals to the control centres which in turn send signals to the heart to increase the heart rate. Nowadays the fistulas are inserted in a venovenous configuration and pumps are used to create the pressure difference.

2.1.6 Treatment of cardiovascular diseases

When medicine fails to prevent or treat cardiovascular diseases, surgeons repair or alter the vessels with an operation. There are several different procedures such as grafting, stenting, coiling and clipping to correct vascular problems. Models can give insight into the flow behaviour and applied stress field in the vessels. It can also predict the flow outcomes and thus help with the planning of the procedures.

2.1.6.1 Grafting

When arteries are severely stenosed, two surgical procedures can be applied namely endarterectomy, that removes the plaque from the underlying media, and grafting. Grafts are either used

to replace or bypass the vessel. Replacement involves removing the diseased part of the artery and replacing it with another vessel sutured in between the remaining arteries. Bypasses leave the stenoses in place but provide an alternative route for blood flow.

The grafts used in these procedures are either from the veins of the patient or a donor, xenografts (vessels from different species) or artificially manufactured elastic grafts. Grafts can cause many complications in the vascular system. Veins used in coronary bypass are subjected to arterial pressures and may develop intimal thickening. This can progress to produce lesions that are indistinguishable from atherosclerosis and lead to recurrent ischemic heart disease. Artificial grafts and xenografts present a challenge of incorporating the material into the body without it being rejected by the immune system. Thrombosis of the graft can occur with all types of grafts when the blood flow is not optimal. This happens when the graft is either too short or too long or if the graft is inserted at a wrong angle. When the distal part of the graft is attached to a segment of the artery that is too narrow, the blood flow is impeded causing turbulence that might cause thrombi to form. Aneurysms may form at the graft junction if the flow is not optimal.

Better understanding of the flow patterns and stresses in grafts and graft junctions will aid in surgical planning of grafting. It may also help to predict the effects of graft geometry on the flow pattern and the mechanical interaction between the native arteries and the graft.

2.1.6.2 Stenting

A stent is a thread, rod or catheter that provides support for a stenosed vessel and maintains the patency of the vessel. To insert a stent is a minimally invasive procedure; a catheter is moved from a peripheral artery to the site of stenosis. Stenting has replaced the use of grafting in many situations. The stenosis is dilated with a balloon that is used to expand the wire mesh stent that supports the vessel walls. The stent becomes a permanent support for the vessel wall.

Restenosis is a common problem associated with stenting. Mathematical models can illustrate and predict the effect of stents on the artery and the process of remodelling. This can play an important role in developing more successful stents.

A recent development in treating fusiform aneurysms is external stenting. Not much information is available yet to determine the long-term outcome of external stenting.

2.1.6.3 Aneurysm clipping

Saccular aneurysms are surgically treated by placing a small metallic clip around the aneurysm's base to establish normal flow and preventing the aneurysm from rupturing. There is not much known about the effects of the presence of the clip and the isolated aneurysm on the artery after the operation. Mathematical models can help to determine the change in blood flow and simulate the damaging effects this procedure may have on the neighbouring vessels.

2.1.6.4 Coiling

Coiling is the procedure where thin metallic coils are used to fill a saccular aneurysm. A catheter is advanced under image guidance from a peripheral artery to the neck of the targeted aneurysm. Avoiding the formation of emboli or rupturing of the external wall, the metallic coils are advanced into the cavity. Blood clots around the coils and the free space form the artery's new lumen, comprising a large area of the aneurismal cavity. Therapeutic results are often unsatisfactory where the neck of the aneurysm is broad, the aneurysm is large or when a small angle is present between the inflow and the axis of the cavity. Another problem is that it is not always easy to determine how much coil must be added into an aneurysm or anomaly. Mathematical modelling can help with these and other problems regarding coiling.

2.2 Cardiovascular models

Cardiovascular models can be used in a variety of medical applications. These include diagnosing disease, surgical planning and prediction of the outcomes of procedures. In combination with current diagnostic tests such as cardiac stress tests, duplex ultrasound, computed tomographic (CT) angiography and magnetic resonance (MR) angiography, mathematical models can be of great value to identify the risk of cardiovascular disease in the early stages [19, 34]. Intervention plans can be based on a variety of factors extracted from patient specific clinical visualization aids. The intervention for carotid and coronary diseasse are currently based on the estimated diameter of stenosis. Data suggests that the plaque character and lesion anatomy are also important determinants of the outcome [34]. Mathematical models can help to utilise all the available data in such cases. For some cardiovascular diseases, such as atherosclerosis, more than one procedure may be suitable to treat it. Models can assist surgeons to choose between different procedures, such as inserting a stent or bypass graft, based on predicted outcomes. These models can either be 3D [44, 45] or 1D [42, 50]. Simulators based on numerical models can be used as training systems for surgeons [28]. Another application of mathematical

models of blood flow has been to use it as part of the anaesthesia simulator, SIMA(SIMulation in Anaesthesia) [25].

A cardiovascular model consists of different sub-models representing different organs such as the heart, the arteries and the veins. Different models are needed for large arteries, medium arteries and capillaries respectively. Large arteries (1-3 cm in diameter) deform under blood pressure to store elastic energy during the systole phase and return to their original shape during the diastolic phase, in such a way that they transport a substantial amount of blood flow from the heart to the organs [28]. In large arteries blood behaves like a Newtonian fluid [20, 28, 39]. Although the walls behave visco-elastically and are a source of physical dissipation [31], most modellers assume the effect is small enough to be ignored [10, 20, 39]. Smaller arteries have rigid walls and the blood behaves like a typical shear-thinning or non-Newtonian fluid. They are also characterised by strong branching. In capillaries, blood cannot be modelled as a homogeneous fluid, as the dimensions of the blood cells and platelets are of the same order as that of the vessel [28]. The blood flow is also influenced by the effect of wall permeability in these small vessels.

The vessel wall interacts chemically and mechanically with the blood flow [28]. The chemical interactions are dependent on the fluid dynamics of the blood. The blood flow induces stress on the vascular tissue and this affects the absorption process through the arterial walls [30]. Furthermore, the blood solutes are transported through the arterial network by the convection of the blood flow. Rappitsch *et al.* [32] developed a model that couples a blood flow model to a model for the transport of macromolecules (albumin and LDL) and gases (O_2 and CO_2). The flow model is based on the Navier-Stokes equations and the transport model is based on the advection-diffusion equation. They also studied the effects that blood dynamics have on the development of atherosclerosis (the hardening of the arteries as a result of fat, cholesterol and other substances building up in the walls of the arteries).

The vessel walls expand when blood pressure increases and the flow field changes as a result of the displacement of the wall. Pressure pulse waves propagate as a result of this fluid-structure interaction. In fact, if it weren't for such mechanical interactions, incompressible fluids such as blood would never show propagative phenomena [28]. The speed of the wave propagation in the large arteries is typically at least an order higher than the average speed associated with the bulk flow field, making the interaction problem rather complex [39]. Several different models of this interaction can be found in literature [8, 31, 52].

Multiscale models couple models of different physical dimensions to find the optimal balance between detail and computational cost [9]. 3D models based on the Navier-Stokes equations provide detailed descriptions of local flow features [50] but are resource and time intensive. Furthermore it is difficult to obtain information regarding 3D geometry and material properties

[20]. This makes it difficult to set up a large-scale simulation [36] and almost impossible to do a quick evaluation of alternate surgical options using only 3D models [50]. Using a multiscale approach, a 3D model would typically be used to model the carotid or other section that contains atherosclerosis or an aneurysm. Boundary conditions for the 3D model would then be computed by using a 1D network model. To model the smaller arteries and capillaries, lumped parameters or 0D models [23], such as a Windkessel model [48], are used. These models neglect the space dependency of vessels, in other words they treat a portion of the vessel as a lumped parameter, and simulate only the time-variation of the flow [36]. These models are based on Kirchoff's laws for hydraulic networks [10] and are analogous to electrical circuits [23], where the blood flow and pressure are treated the same as the current and the voltage of an electrical circuit respectively.

2.2.1 1D model for arterial network

1D models are commonly used to investigate wave propagation phenomena [10, 27]. The heart is a pump that creates pressure waves that propagate through the arterial network. Branches and discontinuities cause reflections of the waves. It is valid to consider blood flow to be quasi-1D, because the wavelengths of these pressure-flow waves are much larger than the diameter of the vessels [1, 20]. 1D models exploit the cylindrical morphology of vessels [10], which result in a 2D model. To eliminate the radial variable 1D models use the averaged value of flow and pressure over the cross sectional area of the arteries [36].

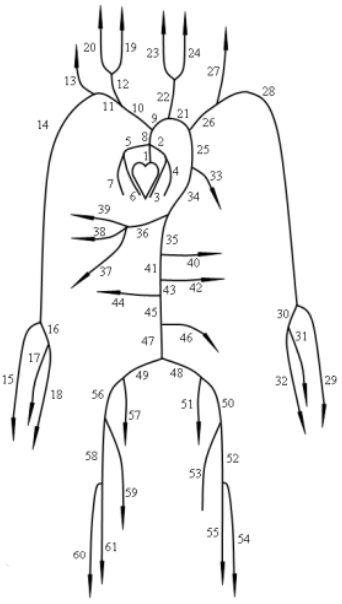

Figure 2.7: Arterial Tree [20]

While also being used to diagnose disease and to predict and rank outcomes in surgical planning [50], 1D models are used to identify anatomical variations by wave analysis to improve boundary conditions for 3D models and to derive methods to analyse in vivo pressure and velocity measurements [52]. The idea is that 1D models would be used as an everyday tool in clinical practice. The 1D arterial network can be represented by a tree-type diagram (Figure 2.7).

Although the classic linear solution of Womersley flow [53] isn't used much these days when solving flow in large arteries, it is still used to solve flow in the smaller arteries [14]. This solution employs a Fourier technique that treats each harmonic separately and then adds the results to calculate the axi-symmetric velocity profile. This method doesn't take into account the non-linear effects or the reflection of waves.

Blood flow through arteries can be modelled in the frequency and time domain. 1D linear pulse wave propagation methods are solved using a frequency domain approach [2, 15, 16]. They are based on the electromechanical analogy between flow through compliant tubes (such as arteries), and an electrical transmission system. These methods can be used because the linearised 1D Navier-Stokes equations show similarities to the electromagnetic wave equations in an electrical transmission line. Even though many simplifications have been made for the problem in hand, it is impossible to obtain an accurate analytical solution, due to the non-linear interaction between different parts of the system [29].

Models that function in the time domain are based on the nonlinear Navier-Stokes equations [20, 28, 39, 40, 45]. The system of equations is closed by coupling the solution of the fluid problem (characterised by pressure and velocity), to the structure problem (that solves the displacement of the vascular wall). This is done by an equation that implements the material properties and relates area to pressure. Several of these relations can be found in literature [35].

The problem is approximated to obtain a numerical solution. This is done by discretising both space and time derivatives and substituting algebraic operators in the place of the differential operators. The governing equations can be solved using different discretisation schemes. Barnard *et al.* [3] and Wang and Parker [51] uses the method of characteristics to solve the non-linear equations. Several researchers use the finite element method to discretise the non-linear problem. Research teams most frequently use the discontinuous Galerkin methods [50, 39, 8] to discretise the problem. Urquiza *et al.* [48] use the Galerkin least squares method. Nithiarasu and Thomas [46] developed the locally conservative Galerkin method which treats each element as a sub-domain with its own boundaries. This method was used by Mynard and Nithiarasu [20] to solve the problem in hand.

Some researchers use the finite difference method to discretise the governing equations. Smith *et al.* [40] used the two-step Lax-Wendroff method to solve the equations for the model of coronary flow. Olufsen *et al.* [24] and He *et al.* [13] use the two-step Lax-Wendroff method to solve the equations for non-linear flow in large arteries. Sheng *et al.* [37] use the two-step Lax-Wendroff method inside the vessel and the method of characteristics at the branching points.

The above discretisation schemes function on a co-located grid. In order to handle discontinuities and branching, an extra node or nodes are added. This creates additional equations to be solved, and increases the time needed to compute the solution. If a staggered grid can be used, where pressure and flow are calculated at different positions in the control volume, these nodes and equations could be eliminated. Pontrelli [27] used a staggered grid to solve the equations assuming visco-elastic material properties. He calculated the area, pressure and velocity at one point and the material properties at the staggered points. Mukhopadhyay [19] solved 2D flow in large arteries using a staggered grid. He evaluated the pressure and velocity at different points. No 1D model that uses the finite volume or difference disretisation on a staggered grid has been encountered so far.

Although much research has been done on 1D models, the understanding that it provides is still more explanatory than predictive. Furthermore, very little research has been done on venous haemodynamics [52]. Hence, there is still a lot of room for improvement in the 1D models.

2.3 Summary

This chapter discussed the vital role that the cardiovascular system plays in human beings. Disease can limit and alter the function of the cardiovascular system. Different surgical procedures exist to solve the problems caused by diseases. The flow patterns play an important role in both the diseases and their treatments. Mathematical models can assist surgeons and researchers to improve these procedures.

Mathematical models of several parts of the cardiovascular system can be found in literature. These models have different physical dimensions and can be coupled to form a multiscale model. The model for blood flow through vessels is a fluid structure interaction problem. 1D models are used to investigate wave propagation phenomena. Different discretisation schemes for the 1D problem are found in literature.

Chapter 3

The Mathematical Model

This chapter explains the mathematical and numerical backdrop implemented in developing a computer code which models blood flow through arteries. The system of equations that needs to be solved consists of the mass and momentum conservation equations as well as a constitutive equation that relates cross-sectional area to pressure. To simplify the way in which discontinuities and branching are dealt with, the equations are discretised by using a staggered grid.

The previous chapter referred to some of the methods used by researchers to solve these eqautions. We will use an iterative method, similar to the SIMPLE method [26], which drives the iterative solution algorithm to convergence by means of a pressure correction equation.

Blood is considered to be incompressible. The heart generates pressure waves that travel at the speed of sound each time it contracts. These waves are reflected by discontinuities and branches. To avoid non-physical reflections of these waves at the computational domain boundary, non-reflecting boundary conditions should be imposed. Non-reflecting boundary conditions allow the waves coming from inside the domain to travel unhindered out of the domain, emulating an artery that continues uniformly outside the boundary.

In this study branching is handled by positioning a control volume over the branch in such a way that the branch is in the middle of the control volume (Figure 3.1). The pressure and area are defined at this point. The flow into the control volume and flow out of the different branches is defined at the faces of this control volume. The equations are solved in the same manner as is the case for a single artery.

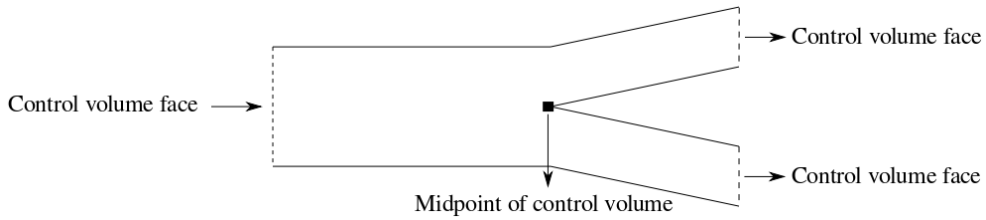

Figure 3.1: Control volume for branching showing the midpoint of the control volume and the control volume face.

3.1 The Incompressible Navier-Stokes equations

There are various ways to derive the 1D governing equations [10]:

Navier-Stokes with asymptotic analysis [3] - The derivation starts off with the Navier-Stokes equations for incompressible fluids and then an asymptotic analysis is performed, making the assumption that the radius of the vessel, r_0, is small relative to its length L, i.e. $\frac{r_0}{L} \ll 1$. This allows the simplification of the governing equations by neglecting the higher order terms in $\frac{r_0}{L}$.

Assume cylindrical symmetry [25] - Integrate the Navier-Stokes equations on a generic section where cylindrical symmetry is assumed.

Reynold's transport theorem [10] - Derive the governing equations from conservation principles using Reynolds' transport theorem. This method is general and does not need to make any simplifying assumptions regarding the geometry of the vessel section.

Even in the case of Reynold's transport theorem many researchers assume that the artery is circular, although some researchers describe it as elliptical and account for the shape in the resistance term of the momentum equation [4]. Some researchers assume that the velocity profile is flat with a thin boundary layer [25] and others assume Poiseuille flow [20].

The Reynold's transport theorem was used in this study. For the sake of completeness, the derivation will be shown in the following section.

For this study we made the following assumptions:

- Vessels are circular.
- Pressure and velocity are constant across the sectional area [20].

- The radial velocity is small compared to the velocity in the axial direction and is neglected [1].
- Displacement along the wall is only in the radial direction [28].
- There are no body forces acting on the blood [25].
- The arterial wall is impermeable [10].
- The velocity profile remains constant throughout the computational domain [40].
- The velocity profile is flat [40].

3.1.1 The derivation of the 1D equations

For the derivation of the governing 1D equations, using the above assumptions and the Reynolds' transport theorem, we follow the work of Formaggia *et al.* [10]. First Reynolds' transport theorem will be derived for a generic function, f, whereafter the result will be used to derive equations for the conservation of mass and momentum.

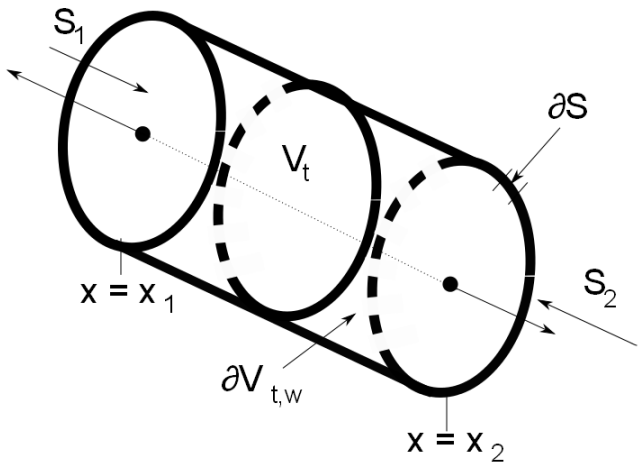

Figure 3.2: Notation that is used to describe a simple compliant tube

The artery is modelled as a simple compliant tube (Figure 3.2). It is assumed that the axis of the vessel coincides with the x axis. We consider the Reynolds' transport theorem for an arbitrary control volume V_t with boundary ∂V_t and outward pointing normal $\mathbf{n}$. The Reynold's transport theorem states that for a continuous function $f = f(t, \mathbf{x})$, we have:

$$\frac{d}{dt}\int_{V_t} f dV = \int_{V_t} \frac{\partial f}{\partial t} dV + \int_{\partial V_t} f \mathbf{u}_b \cdot \mathbf{n} d\sigma \tag{3.1}$$

where $\mathbf{u}_b$ is the velocity of the boundary of V_t, $\mathbf{x}$ represents (x, y, z) and σ refers to the area of control volume. The boundary is composed out of the arterial wall $\partial V_{t,\omega}$ and two end sections S_1 and S_2. At the end sections the normal component of $\mathbf{u}_b$ is 0, while on $\partial V_{t,\omega}$ the velocity of the wall, $\mathbf{u}_\omega$, is in the direction of the normal component of $\mathbf{u}_b$, so that:

$$\int_{\partial V_t} f \mathbf{u}_b \cdot \mathbf{n} d\sigma = \int_{\partial V_{t,\omega}} f \mathbf{u}_\omega \cdot \mathbf{n} d\sigma \tag{3.2}$$

Note that $\mathbf{u}_\omega$ is different from the fluid velocity $\mathbf{u} = (u_1, u_2, u_3)$ to allow for the presence of a lumen that is permeable. The relative velocity, ω, between the fluid at the lumen and the arterial wall is given by:

$$\omega = \mathbf{u}_\omega - \mathbf{u} \tag{3.3}$$

For the one-dimensional form, we need to express the functions as area-averaged values of the relevant variables. The area-averaged value of f is denoted by $\bar{f}$ and is given by:

$$\bar{f} = \frac{1}{A}\int_S f d\sigma \tag{3.4}$$

where $A = A(x,t) = \int_S d\sigma$ is the area of the cross-section S. We can write the volume integral as follows using this notation:

$$\int_{V_t} f dV = \int_{x_1}^{x_2} \left[\int_S f d\sigma\right] dx = \int_{x_1}^{x_2} A\bar{f} dx \tag{3.5}$$

where x_1 and x_2 are the x-coordinates of the end cross sections S_1 and S_2. We know that x_1 and x_2 are independent of time, thus the left-hand side term of Equation (3.1) can be written as:

$$\frac{d}{dt}\int_{V_t} f dV = \int_{x_1}^{x_2} \frac{\partial}{\partial t}(A\bar{f}) dx \tag{3.6}$$

Because the wall may be permeable the second term on the right-hand side of Equation (3.1) is more complex. This term is calculated as:

$$\int_{\partial V_{t,\omega}} f\mathbf{u}_\omega \cdot \mathbf{n} d\sigma = \int_{\partial V_{t,\omega}} f\omega \cdot \mathbf{n} d\sigma + \int_{\partial V_{t,\omega}} f\mathbf{u} \cdot \mathbf{n} d\sigma \tag{3.7}$$

Because $\partial V_{t,w} = \partial V_t \bigcup S_1 \bigcup S_2$ the last term of Equation (3.7) can be rewritten as:

$$\int_{\partial V_{t,\omega}} f\mathbf{u} \cdot \mathbf{n} d\sigma = \int_{\partial V_t} f\mathbf{u} \cdot \mathbf{n} d\sigma - \int_{S_1} f\mathbf{u} \cdot \mathbf{n} d\sigma - \int_{S_2} f\mathbf{u} \cdot \mathbf{n} d\sigma$$

$$\int_{\partial V_{t,\omega}} f\mathbf{u} \cdot \mathbf{n} d\sigma = \int_{\partial V_t} f\mathbf{u} \cdot \mathbf{n} d\sigma + \int_{S_1} f u_x d\sigma - \int_{S_2} f u_x d\sigma \tag{3.8}$$

If we apply Gauss's theorem to the first term on the right hand side of the equation we find:

$$\int_{\partial V_{t,\omega}} f\mathbf{u} \cdot \mathbf{n} d\sigma = \int_{\partial V_t} \nabla \cdot (f\mathbf{u}) dV + \int_{S_1} f u_x d\sigma - \int_{S_2} f u_x d\sigma \tag{3.9}$$

where u_x is the x-component of the velocity $\mathbf{u}$. Using area-averaged quantities, we can rewrite Equation (3.7) as follows:

$$\int_{\partial V_{t,\omega}} f\mathbf{u}_\omega \cdot \mathbf{n} d\sigma = \int_{\partial V_{t,\omega}} f\omega \cdot \mathbf{n} d\sigma + \int_{V_t} \nabla \cdot (f\mathbf{u}) dV - \int_{x_1}^{x_2} \frac{\partial}{\partial x} \left[A(\bar{f\bar{u}_x}) \right] dx \tag{3.10}$$

By substituting Equations (3.2), (3.6) and (3.10) into Equation (3.1) and applying Equation (3.5) we find:

$$\int_{x_1}^{x_2} \frac{\partial}{\partial t}(A\bar{f}) dx = \int_{x_1}^{x_2} \left(\int_S \frac{\partial f}{\partial t} d\sigma \right) dx + \int_{x_1}^{x_2} \left(\int_{\partial S} f\omega \cdot \mathbf{n} d\gamma \right) dx - \tag{3.11}$$

$$\int_{x_1}^{x_2} \frac{\partial}{\partial x} \left[A(\overline{fu_x}) \right] dx + \int_{x_1}^{x_2} \left(\int_S \nabla \cdot (f\mathbf{u}) d\sigma \right) dx \tag{3.12}$$

We know that this is true for any value of the end section coordinates x_1 and x_2. This makes it possible to give the final form of the one-dimensional transport theorem for a generic variable f as:

$$\frac{\partial}{\partial t}(A\bar{f}) + \frac{\partial}{\partial x}[A(\overline{fu_x})] = \int_S \left(\frac{\partial f}{\partial t} + \nabla \cdot (f\mathbf{u}) \right) d\sigma + \int_{\partial S} f\omega \cdot \mathbf{n} d\gamma \tag{3.13}$$

where γ represents the length of the control volume. This is a general conservation equation and applicable to both compressible and incompressible fluids. We can make use of the principles of mass conservation and balance of momentum to derive the governing equations.

Conservation of mass

For conservation of mass in the flexible tube we take $f = 1$ in Equation (3.13). If we assume that the fluid is incompressible, i.e. $\nabla \cdot \mathbf{u} = 0$ we get:

$$\frac{\partial A}{\partial t} + \frac{\partial}{\partial x}(A\bar{u}) = \int_{\partial S} \omega \cdot \mathbf{n} d\gamma \tag{3.14}$$

where A represents the cross sectional area, and $\bar{u}$ the averaged axial velocity. For impermeable flow, $\omega.\mathbf{n} = 0$ [50].

Balance of momentum

Similar to the conservation of mass, if we take $f = u$ in Equation (3.13) and again assume that the fluid is incompressible, we find:

$$\frac{\partial}{\partial t}(A\bar{u}) + \frac{\partial}{\partial x}\left[A(\overline{u^2})\right] = \int_S \left(\frac{\partial u}{\partial t} + \mathbf{u} \cdot \nabla u\right) d\sigma + \int_{\partial S} u\omega \cdot \mathbf{n} d\gamma \tag{3.15}$$

We can write this as:

$$\frac{\partial}{\partial t}(A\bar{u}) + \frac{\partial}{\partial x}\left[A(\overline{u^2})\right] = \int_S \frac{Du}{Dt} d\sigma + \int_{\partial S} u\omega \cdot \mathbf{n} d\gamma \tag{3.16}$$

where $\frac{D}{Dt} = \frac{\partial}{\partial t} + \mathbf{u} \cdot \nabla$ denotes the material derivative. It can be shown that [10]:

$$\int_S \frac{Du}{Dt} d\sigma = \int_S \left[f^b + \frac{1}{\rho}\left(-\frac{\partial p}{\partial x} + d\right)\right] d\sigma \tag{3.17}$$

where f^b represents the body force per unit volume in the axial direction, ρ the density of the blood, p the pressure and d the deviatoric stresses due to the viscosity of the fluid. Substituting this expressing into Equation (3.16) gives:

$$\frac{\partial}{\partial t}(A\bar{u}) + \frac{\partial}{\partial x}\left[A(\overline{u^2})\right] = \int_S \left[f^b + \frac{1}{\rho}\left(-\frac{\partial p}{\partial x} + d\right)\right] d\sigma + \int_{\partial S} u\omega \cdot \mathbf{n} d\gamma \tag{3.18}$$

This can be expressed with area-averaged values, Equation (3.5), as:

$$\frac{\partial}{\partial t}(A\bar{u}) + \frac{\partial}{\partial x}\left[A(\overline{u^2})\right] = \frac{A}{\rho}\left(\rho\bar{f}^b - \frac{\partial p}{\partial x} + \bar{d}\right) + \int_{\partial S} u\omega \cdot \mathbf{n} d\gamma \tag{3.19}$$

The term $(\overline{u^2})$ will be difficult to evaluate and is handled by defining a momentum-flux correction coefficient α (also known as the Coriolis coefficient). We can express $(\overline{u^2})$ as:

$$(\overline{u^2}) = \frac{1}{A}\int_S u^2 d\sigma = \alpha\bar{u}^2 \tag{3.20}$$

The Coriolis coefficient is not dependant on the axial direction because a constant velocity profile throughout the computational domain was assumed. The coefficient is given by

$$\alpha = \frac{\int_S s(y)^2 d\sigma}{A} \tag{3.21}$$

where $s(y)$ is a velocity profile and $S = S(t, x)$ refers to a generic axial section. The radial direction is denoted by y. Blood flow in arteries is often described by a power law of the type $s(y) = \vartheta^{-1}(\vartheta + 2)(1 - y^{\vartheta})$, where ϑ is a constant with a typical value of $\vartheta = 9$ for a flat profile [40]. This renders a momentum flux coefficient value of $\alpha = 1.1$. For parabolic flow $\alpha = \frac{4}{3}$. In this study we follow most researchers and assume $\alpha = 1.0$. This is quite realistic since the velocity profile is almost flat.

The term d which represents the viscous forces is taken to be a linear function of the area-averaged velocity $\bar{u}$ and has the form:

$$\frac{A}{\rho}d = -K_R\bar{u} \tag{3.22}$$

K_R is the resistance to the flow per unit length of tube. It consists of viscous and inertial components. The viscous terms are proportional to u and the inertial terms to du/dt. We ignore the inertial component of the resistance term [20, 4]. This is because the pressure drop due to inertia is insignificant for a low Womersley parameter, $W = r\sqrt{w\rho/\mu}$ [53]. In this equation w is the angular frequency of a given harmonic and μ is the dynamic viscosity. Quarteroni and Mynard [28] pointed out that the effects of inertia can be modelled by adding

terms to the equation describing the interaction between the fluid and the wall, Equation (3.34). The viscous resistance can be formulated in various ways and is dependant on the velocity profile and rheological factors. However, flow is considered to be laminar in the major arteries. Although most modellers assume a flat velocity profile when calculating the α value, they assume parabolic flow profile when calculating K_R [8, 20, 31, 50]. This parabolic flow profile is also called Poiseuille flow and assumes fully developed steady flow. We follow these assumptions which results in $K_R = \frac{8\pi\mu}{\rho}$. When a flat flow profile is assumed, $K_R = \frac{22\pi\mu}{\rho}$ [28]. These expressions will not be valid where the flow is non-Newtonian (in the arterioles or capillaries) or turbulent (in some disease states).

The final form for the conservation of momentum is:

$$\frac{\partial}{\partial t}(A\bar{u}) + \frac{\partial}{\partial x}\left[\alpha A\bar{u}^2\right] = A\bar{f}^b - \frac{A}{\rho}\frac{\partial p}{\partial x} - K_R\bar{u} + \int_{\partial S} u\omega \cdot \mathbf{n} d\gamma \tag{3.23}$$

3.1.2 Governing equations

The cross-sectional flow, Q, can be written in terms of the area and the velocity:

$$Q = uA \tag{3.24}$$

The conservation Equations (3.14) and (3.23) can be rewritten in terms of the cross-sectional flow [10]:

$$\frac{\partial A}{\partial t} + \frac{\partial Q}{\partial x} = \int_{\partial S} \boldsymbol{\omega}.\boldsymbol{n} d\gamma \tag{3.25}$$

$$\frac{\partial Q}{\partial t} + \frac{\partial}{\partial x}(\alpha\frac{Q^2}{A}) + \frac{A}{\rho}(\frac{\partial p}{\partial x}) + K_R\frac{Q}{A} = A\bar{f}^b + \int_{\partial S} u\boldsymbol{\omega}.\boldsymbol{n} d\gamma \tag{3.26}$$

The body forces, $\bar{f}^b$, are negligible, although gravity could be included in this term at a later stage of the research. For impermeable flow ($\omega.\boldsymbol{n} = 0$) Equation 3.25 can be written as:

$$\frac{\partial A}{\partial t} + \frac{\partial Q}{\partial x} = 0 \tag{3.27}$$

The Q, A, p system is derived directly from the conservation of mass and momentum and is widely used [28, 39, 50]. The second term in Equation (3.26) known as the convective

acceleration term can be difficult to determine and must be linearised if left in that form. This linearisation is undesirable because it slows down convergence of the linearised solution algorithm and can introduce instabilities. Greyvenstein [11] eliminated this term by rewriting the equations in the non-conservative form and expressing the momentum conservation in terms of the total pressure. The total pressure is defined as:

$$p_0 = p + \frac{1}{2}\rho u^2 \tag{3.28}$$

To make it possible to write the equations in terms of total pressure, the system of equations should be expressed in terms of velocity. If α is taken to be equal to 1, the weak form of the Q, A, p system is equivalent to a u, A, p system for smooth solutions [10]. By rearranging Equation (3.26) and performing some algebra we can eliminate the convective acceleration term:

$$\begin{aligned}
\frac{\partial Q}{\partial t} + \frac{\partial}{\partial x}(\frac{Q^2}{A}) + \frac{A}{\rho}(\frac{\partial p}{\partial x}) + K_R\frac{Q}{A} &= 0 \\
\frac{\partial}{\partial t}(uA) + \frac{\partial}{\partial x}(\frac{u^2A^2}{A}) + \frac{A}{\rho}(\frac{\partial p}{\partial x}) + K_R\frac{uA}{A} &= 0 \\
u\frac{\partial}{\partial t}(A) + A\frac{\partial}{\partial t}(u) + u\frac{\partial}{\partial x}(uA) + uA\frac{\partial}{\partial x}(u) + \frac{A}{\rho}(\frac{\partial p}{\partial x}) + K_R u &= 0 \\
u\left[\frac{\partial A}{\partial t} + \frac{\partial}{\partial x}(uA)\right] + A\left[\frac{\partial u}{\partial t} + u\frac{\partial u}{\partial x} + \frac{1}{\rho}\frac{\partial p}{\partial x} + K_R\frac{u}{A}\right] &= 0
\end{aligned} \tag{3.29}$$

We may write the mass conservation, Equation (3.27), in terms of the velocity:

$$\frac{\partial A}{\partial t} + \frac{\partial}{\partial x}(uA) \;=\; 0 \tag{3.30}$$

Equation (3.29) can then be written as:

$$\rho\frac{\partial u}{\partial t} + \rho u\frac{\partial u}{\partial x} + \frac{\partial p}{\partial x} + \rho K_R\frac{u}{A} = 0 \tag{3.31}$$

This is the non-conservative form of momentum conservation. We can alter this equation further:

$$\begin{aligned} \rho\frac{\partial u}{\partial t} + \frac{1}{2}\frac{\partial(\rho u^2)}{\partial x} + \frac{\partial p}{\partial x} + \rho K_R \frac{u}{A} &= 0 \\ \rho\frac{\partial u}{\partial t} + \frac{\partial}{\partial x}\left[\frac{1}{2}\rho u^2 + p\right] + \rho K_R \frac{u}{A} &= 0 \end{aligned} \tag{3.32}$$

If we use the definition of total pressure, Equation (3.28), Equation (3.32) can be rewritten as:

$$\rho\frac{\partial u}{\partial t} + \frac{\partial p_0}{\partial x} + \rho K_R \frac{u}{A} = 0 \tag{3.33}$$

This form of the momentum conservation equation is linear as it contains the convective acceleration term implicitly, which will make it easier to solve the equation.

3.2 Equations for the arterial wall dynamics

This system of equations has 3 variables, A, p_0 and Q (or $\underline{u}$), to solve for and 2 equations, Equations (3.27) and (3.33) to solve it with. To close the system a third equation is required. The constitutive equation represents the fluid-structure interaction and relates A to p. The mechanics of the wall are complex, therefore an empirical or mathematical simplification is made. This fluid-structure relation can be a linear elastic model, non-linear elastic model [8, 22, 35, 37, 38, 40], collapsible tube model [4] or a visco-elastic model. The most accurate would be a visco-elastic model [28, 31], but it is also the most complicated model. We use a non-linear model as the effects of wall viscosity are assumed to be small. There are many different non-linear models with the general form:

$$p = p_{ext} + \phi(A, A_0, \beta) \tag{3.34}$$

Where p_{ext} represents the external pressure of the artery, A_0 the area of the artery when $p_{ext} = 0$ and β a function that represents the mechanical properties of the arterial wall. We follow Formaggia *et al* [8] using the relation as:

$$p = p_{ext} + \beta(\sqrt{A} - \sqrt{A_0}) \tag{3.35}$$

where

$$\beta = \frac{\sqrt{\pi}hE}{A_0(1-\sigma)} \tag{3.36}$$

where E is Young's modulus, h the thickness of the wall of the vessel and σ Poisson's ratio. The vessel wall is assumed to be incompressible, thus $\sigma = 0.5$.

Using Equation (3.28), Equation (3.35) can be rewritten as:

$$p_0 = p_{ext} + \beta(\sqrt{A} - \sqrt{A_0}) + \frac{1}{2}\rho\left(\frac{Q}{A}\right)^2 \tag{3.37}$$

Now we have three equations, Equations (3.30), (3.33) and (3.37) to solve the three variables A, p_0 and Q.

3.3 Discretisation

To discretise and solve the equations a method developed by Greyvenstein [11] was used. Equations (3.30) and (3.33) were discretised by integrating them over a typical control volume. A staggered grid (Figure 3.3) was used. This grid contains two different groups of control volumes. The control volumes that are indicated with the solid lines are associated with momentum conservation and those indicated with the dashed lines are associated with the mass conservation. The midpoints of the different groups are defined in such a way that the values of the midpoints of one group's control volumes are also the values on the walls of the other group's control volume. I is the node in the centre of the control volume associated with momentum conservation. i is the node in the middle of the control volume associated mass conservation. Q_I was defined at the centre of the control volume associated with momentum conservation and p_{0_i} and A_i at the centre of the control volume associated with mass conservation. The length of the control volume is $\triangle x$. Values of A at the faces of the mass conservation control volume are indicated with A_I or A_{I-1} and calculated by interpolation.

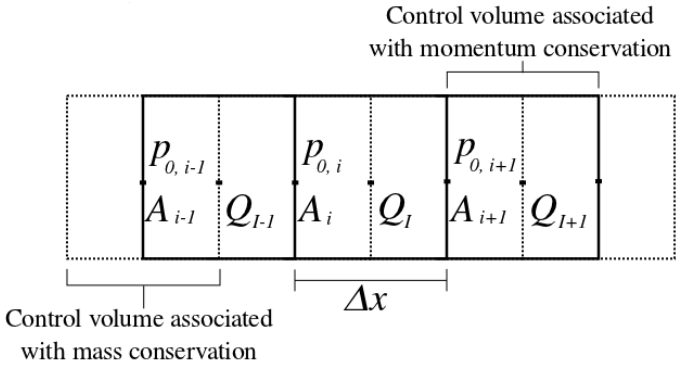

Figure 3.3: Staggered grid control volumes

The equation for momentum conservation, Equation (3.33) should be integrated over the 1D control volume and over time. This will be done in two steps. Integration over the control volume gives:

$$\int_V \rho \frac{\partial u}{\partial t} dV + \int_V \frac{\partial p_0}{\partial x} dV + \int_V K_R \frac{u}{A} dV = 0 \tag{3.38}$$

We can use the midpoint integration rule and rewrite Equation (3.38) as:

$$\left(\rho \frac{\partial u}{\partial t}\right)_I \delta V_I + \frac{\partial p_0}{\partial x}|_I \delta V_I + \left(\rho K_R \frac{u}{A}\right)_I \delta V_I = 0 \tag{3.39}$$

Note that $\delta V_I = A_I \triangle x_I$. For this study $\triangle x$ is the same for each increment and we can write $\triangle x_I = \triangle x$. Thus Equation (3.39) becomes:

$$\begin{aligned} \rho \frac{\partial u_I}{\partial t} A_I \triangle x + \frac{p_{0_{i+1}} - p_{0_i}}{\triangle x} A_I \triangle x + \rho K_R \frac{u_I}{A_I} A_I \triangle x &= 0 \\ \rho \frac{\partial u_I}{\partial t} \triangle x + p_{0_{i+1}} - p_{0_i} + \rho K_R \frac{u_I}{A_I} \triangle x &= 0 \end{aligned} \tag{3.40}$$

Where p_{0_i} and $p_{0_{i+1}}$are the total pressures at the midpoints of the adjacent mass conservation control volumes. A_I and u_I are the values of the velocity and area at the midpoint of the momentum conservation control volume respectively.

To discretise in time we follow the approach of Versteeg and Malalasekera [49]. The first term is discretised by using a first order (backward) differencing scheme:

$$\rho \frac{\partial u_I}{\partial t} \triangle x = \rho \frac{u_I - u_I^o}{\triangle t} \triangle x \tag{3.41}$$

Note that the superscript $[]^o$ refers to the known values of the variable calculated at the previous time-step and the values that are calculated at the current time-step have no superscript.

To determine the other two terms, we should make an assumption about the variation of the variables over time. We can either use the values of the variables at the previous time-step, the current time-step or a combination of the two. This approach can be generalised by introducing a relaxation or weighting parameter with a value between 0 and 1. This parameter

prescribes whether the time integration is explicit ($\theta = 0$), implicit ($\theta = 1$) or Crank-Nicholson type ($\theta = 0.5$). This results in:

$$\rho\frac{(u_I - u_I^o)}{\triangle t}\triangle x + \theta\left[(p_{0_{i+1}} - p_{0_i}) + \rho K_R\frac{u_I}{A_I}\triangle x\right] + (1-\theta)\left[(p_{0_{i+1}} - p_{0_i}) + \rho K_R\frac{u_I}{A_I}\triangle x\right]^o = 0 \tag{3.42}$$

where $0 \leq \theta \leq 1$. The variable that should be conserved is not the velocity u but the volume flow rate Q. We substitute $u = \frac{Q}{A}$ and $K_R = \frac{8\pi\mu}{\rho}$ into Equation (3.42):

$$\frac{\rho}{\triangle t}\left[\frac{Q_I}{A_I} - \left(\frac{Q_I}{A_I}\right)^o\right]\triangle x + \theta\left[(p_{0_{i+1}} - p_{0_i}) + \frac{8\pi\mu Q_I}{A_I^2}\triangle x\right] + (1-\theta)\left[(p_{0_{i+1}} - p_{0_i}) + \frac{8\pi\mu Q_I}{A_I^2}\triangle x\right]^o = 0 \tag{3.43}$$

We can discretise the mass conservation, Equation (3.30), similarly. This results in:

$$\frac{A_i - A_i^o}{\triangle t}\triangle x + \theta(Q_I - Q_{I-1}) + (1-\theta)(Q_I - Q_{I-1})^o = 0 \tag{3.44}$$

3.4 Solving the equations

To find all the unknowns p_{0_i}, Q_I and A_i we must solve Equations (3.37), (3.43) and (3.44) simultaneously. An iterative procedure was used to do this. A field of guessed pressures of $\bar{p}_0$ was used to solve the preliminary areas $\bar{A}$ and flow rates $\bar{Q}$ using an altered form of Equations (3.43) and (3.44). For the first iteration of a time step the pressures from the previous time step can be used, and for the following iterations the corrected pressures from the previous iteration can be used.

Now we need the corrected values for the variables:

$$\begin{aligned} A &= \bar{A} + A' \\ Q &= \bar{Q} + Q' \\ p_0 &= \bar{p}_0 + p_0' \end{aligned} \tag{3.45}$$

The variables with the accents ($A^{'}$, $Q^{'}$, $p_0^{'}$) are the corrections that should be made, and these with overbars ($\bar{A}$, $\bar{Q}$, $\bar{p_0}$) are the preliminary guessed values.

We can relate the area correction to the pressure corrections in the following manner. We start by rewriting Equation (3.37):

$$\beta\sqrt{A} = p_0 - p_{ext} + \beta(\sqrt{A_0}) - \frac{1}{2}\rho\left(\frac{Q}{A}\right)^2 \tag{3.46}$$

The partial derivative of Equation (3.46) can be taken with respect to p_0. This gives:

$$\frac{\beta}{2\sqrt{A}}\frac{\partial A}{\partial p_0} = 1 - \frac{\rho Q}{A^2}\frac{\partial Q}{\partial p_0} + \frac{\rho Q^2}{A^3}\frac{\partial A}{\partial p_0} \tag{3.47}$$

Rearranging Equation (3.47) gives:

$$\left(\frac{\beta}{2\sqrt{A}} - \frac{\rho Q^2}{A^3}\right)\frac{\partial A}{\partial p_0} = 1 - \frac{\rho Q}{A^2}\frac{\partial Q}{\partial p_0} \tag{3.48}$$

If we assume that $\partial A \approx A^{'}$, $\partial Q \approx Q^{'}$ and $\partial p_0 \approx p_0^{'}$ we get:

$$\left(\frac{\beta}{2\sqrt{A}} - \frac{\rho Q^2}{A^3}\right)A^{'} = p_0^{'} - \frac{\rho Q}{A^2}Q^{'} \tag{3.49}$$

Now we can solve $A^{'}$:

$$A^{'} = \frac{1}{\left(\frac{\beta}{2\sqrt{A}} - \frac{\rho Q^2}{A^3}\right)}p_0^{'} - \frac{\rho Q}{A^2\left(\frac{\beta}{2\sqrt{A}} - \frac{\rho Q^2}{A^3}\right)}Q^{'} \tag{3.50}$$

For the area-total pressure node point i it can be written:

$$A_i^{'} = \frac{1}{\left(\frac{\beta}{2\sqrt{A_i}} - \frac{\rho\left(\frac{Q_{I-1}+Q_I}{2}\right)^2}{A_i^3}\right)}p_{0_i}^{'} - \frac{\rho\left(\frac{Q_{I-1}+Q_I}{2}\right)}{A_i^2\left(\frac{\beta}{2\sqrt{A_i}} - \frac{\rho\left(\frac{Q_{I-1}+Q_I}{2}\right)^2}{A_i^3}\right)}\left(\frac{Q_{I-1}^{'}+Q_I^{'}}{2}\right) \tag{3.51}$$

An equation to calculate the guessed values can be obtained by substituting $\bar{Q}$ into Equation (3.43):

$$\begin{aligned} \frac{\rho}{\triangle t}\left[\frac{\bar{Q}_I}{A_I}-\left(\frac{\bar{Q}_I}{A_I}\right)^o\right]\triangle x+\theta\left[(\bar{p}_{0_{i+1}}-\bar{p_{0_i}})+\frac{8\pi\mu\bar{Q}_I}{A_I^2}\triangle x\right] \quad + \\ (1-\theta)\left[(p_{0_{i+1}}-p_{0_i})+\frac{8\pi\mu Q_I}{A_I^2}\triangle x\right]^o \quad = \quad 0 \end{aligned} \tag{3.52}$$

An equation for $Q^{'}$ can be found by substituting the corrected values of Equation (3.45) into Equation (3.43) and subtracting Equation (3.52) from it. This gives:

$$\frac{\rho}{A_I}\centerdot\frac{Q_I^{'}}{\triangle t}\centerdot\triangle x+\theta(p_{0_{i+1}}^{'}-p_{0_i}^{'})+\frac{8\theta\pi\mu Q_I^{'}}{A_I^2}\centerdot\triangle x=0 \tag{3.53}$$

To solve for $Q_i^{'}$:

$$Q_I^{'}=a_I p_{0_i}^{'}-a_I p_{0_{i+1}}^{'} \tag{3.54}$$

with

$$a_I=\frac{\theta}{\left[\frac{\rho}{A_I}\frac{\triangle x}{\triangle t}+\frac{8\theta\pi\mu\triangle x}{A_I^2}\right]} \tag{3.55}$$

Substituting the corrected values into the mass conservation Equation (3.44) produces:

$$\frac{\triangle x}{\triangle t}\centerdot A_i^{'}+\theta\left(Q_I^{'}-Q_{I-1}^{'}\right)+\frac{\bar{A}_i-A_i^o}{\triangle t}\centerdot\triangle x+\theta\left(\bar{Q}_I-\bar{Q}_{I-1}\right)+(1-\theta)\left(\bar{Q}_I-\bar{Q}_{I-1}\right)^o=0 \tag{3.56}$$

Substitute the Equations (3.51) and (3.54) into Equation (3.56). This gives:

$$\begin{aligned} \frac{\triangle x}{\triangle t}\left[k_i p_{0_i}^{'}-r_i\left(Q_{I-1}^{'}+Q_I^{'}\right)\right]+\theta a_I(p_{0_i}^{'}-p_{0_{i+1}}^{'})-\theta a_{I-1}(p_{0_{i-1}}^{'}-p_{0_i}^{'}) \quad &= \quad b_i \\ \frac{\triangle x}{\triangle t}\left[k_i p_{0_i}^{'}-r_i\left(\theta a_{I-1}(p_{0_{i-1}}^{'}-p_{0_i}^{'})+\theta a_I(p_{0_i}^{'}-p_{0_{i+1}}^{'})\right)\right]+ \quad & \qquad (3.57) \\ \theta a_I(p_{0_i}^{'}-p_{0_{i+1}}^{'})-\theta a_{I-1}(p_{0_{i-1}}^{'}-p_{0_i}^{'}) \quad &= \quad b_i \qquad (3.58) \end{aligned}$$

where

$$b_i = -\left\{ \frac{\bar{A}_i - A_i^o}{\triangle t} \cdot \triangle x + \theta \left(\bar{Q}_I - \bar{Q}_{I-1} \right) + (1-\theta) \left(Q_I - Q_{I-1} \right)^o \right\} \tag{3.59}$$

$$k_i = \frac{1}{\left(\frac{\beta}{2\sqrt{A_i}} - \frac{\rho \left(\frac{Q_{I-1}+Q_I}{2} \right)^2}{A_i^3} \right)} \tag{3.60}$$

$$r_i = \frac{\rho \left(Q_{I-1} + Q_I \right)}{4A_i^2} \cdot k_i \tag{3.61}$$

Solving for $p_{0_i}^{'}$, we can rearrange Equation (3.58):

$$c_i p_{0_i}^{'} = c_{i-1} p_{0_{i-1}}^{'} + c_{i+1} p_{0_{i+1}}^{'} + b_i \tag{3.62}$$

where

$$\begin{aligned} c_{i,i} &= k_i \cdot \tfrac{\triangle x}{\triangle t} + a_I \left(\theta - r_i \cdot \tfrac{\triangle x}{\triangle t} \right) + a_{I-1} \left(\theta + r_i \cdot \tfrac{\triangle x}{\triangle t} \right) \\ c_{i-1} &= a_{I-1} \left(\theta + r_i \cdot \tfrac{\triangle x}{\triangle t} \right) \\ c_{i+1} &= a_I \left(\theta - r_i \cdot \tfrac{\triangle x}{\triangle t} \right) \end{aligned} \tag{3.63}$$

3.4.1 Steady state solution

A steady state solution (of the system) will be used as the initial condition for the transient calculations. For a steady state problem $\frac{\partial}{\partial t} = 0$. The system of equations reduces to a simpler but still non-linear set of equations. This can be solved with the Newton-Rhapson method.

The system can be further reduced if we notice that when we choose to work with Q as primary variable, the mass conservation, Equation (3.30), for steady state implies that Q is a constant. When $\frac{\partial}{\partial t} = 0$ is assumed Equation (3.33) can be rewritten in term s of p_0 and discretised:

$$p_{0,i} = p_{0,i-1} - \frac{8\pi\mu Q_I}{\bar{A}_I^2} \triangle x \tag{3.64}$$

The pressure-area relation, Equation (3.37), can be rewritten in terms of A and discretised:

$$A_i = \left[\frac{p_{0,i} - p_{ext} + \beta\sqrt{A_{0,i}} - \frac{1}{2}\rho\left(\frac{Q_i}{A_i}\right)^2}{\beta^2} \right] \tag{3.65}$$

A simple iterative procedure can be used to solve for A and p_0 for each increment.

In CFD (Computational Fluid Dynamics) applications when a bifurcation is modelled in a network that is not closed, the flow or pressure at the outlet of each branch has to be specified [49]. For the steady state solution the flow remains constant through each branch. This has the implication that we can specify the steady state flow for each branch at the bifurcation (Figure 3.4).

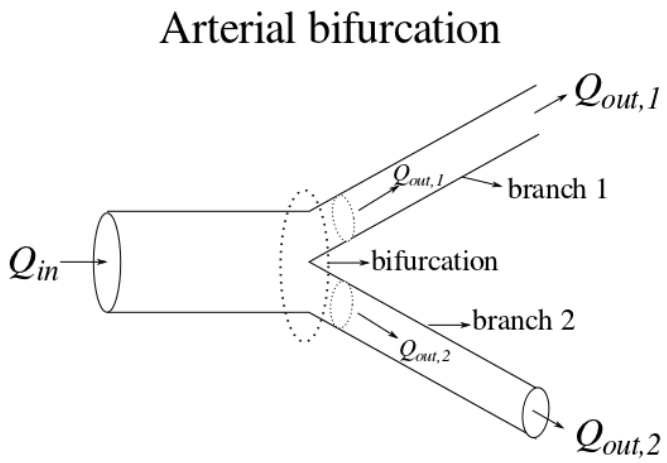

Figure 3.4: Modelling of an arterial bifurcation

3.5 Boundary conditions

The cardiovascular system is a closed system consisting of many parts that can be represented by different mathematical models. Because we are modelling sections of the system, it is necessary to introduce boundary conditions. Typically the flow domain is 'cut off' at two sides. The boundary where the flow enters into the domain is referred to as the inlet. The boundary where the flow exits the domain is known as the outlet. There are several ways to specify the inlet conditions for the computational domain when modelling a section of the cardiovascular system. Most models either prescribe the aortic volume flow rate or pressure as an inlet condition [15, 22, 50, 40]. In the physical cardiovascular system there are forward and

backward moving pressure waves at this boundary. When the desired values of pressure, area or velocity at the inlet are prescribed, the backward travelling waves reflect at this boundary. These are known as reflecting boundary conditions. The total reflection causes behaviour that is not physiological. A non-reflecting type boundary condition would correspond better to the physical system.

Quarteroni *et al.* [28] and Mynard and Nithiarasu [20] imposed non-reflecting boundary conditions by prescribing only the forward component of pressure, flow or area. The backward waves pass unhindered through the boundary as if the vessel extends uniformly beyond the boundary. The resulting primary variables can be calculated as a combination of the forward and backward travelling waves (Figure 3.5). This corresponds better to the physical system, where forward and backward moving waves can be found. Non-reflecting boundary conditions are made possible by the characteristic system, which expresses the system in terms of characteristic variables that are associated with forward and backward-travelling waves.

The characteristic system calculates forward and backward-moving wavefronts. The pressure or flow at a point can be described as a combination of several of these forward and backward-moving wave fronts [20]. We distinguish between **physical pressure waves** or pulses and **characteristic wavefronts**.

Physical pressure waves or pulses are generated by the pump action of the heart. They propagate through the cardiovascular system and reflect partially at branches and other discontinuities. These pressure waves travel at the speed of sound of the system superimposed on the steady-state velocity ie. $|u + c|$. Thus pressure waves propagate forward at a speed of $u + c$ and backwards at a speed of $u - c$. The speed of sound of the system is determined by [20]:

$$c = \sqrt{\frac{\beta\sqrt{A}}{2\rho}} \tag{3.66}$$

Characteristic wavefronts refer to the infinitesimal changes in one of the characteristic variables, ω_1 or ω_2 and are mathematical phenomena. Wavefronts are also generated by the heart and are also reflected at discontinuities. To determine the characteristic variables of the wavefronts the system of equations, Equations (3.30) and (3.33) can be linearized and de-coupled by expressing it in quasi-linear form and deriving the characteristic system [38]. The characteristic system provides characteristic lines and characteristic variables. The characteristic variables (ω_1, ω_2) remain constant along the characteristic lines $(\frac{dx}{dt} = \lambda_{1,2})$ (Figure 3.6). The mathematical derivation of the characteristic lines and variables is described in Section 3.4.

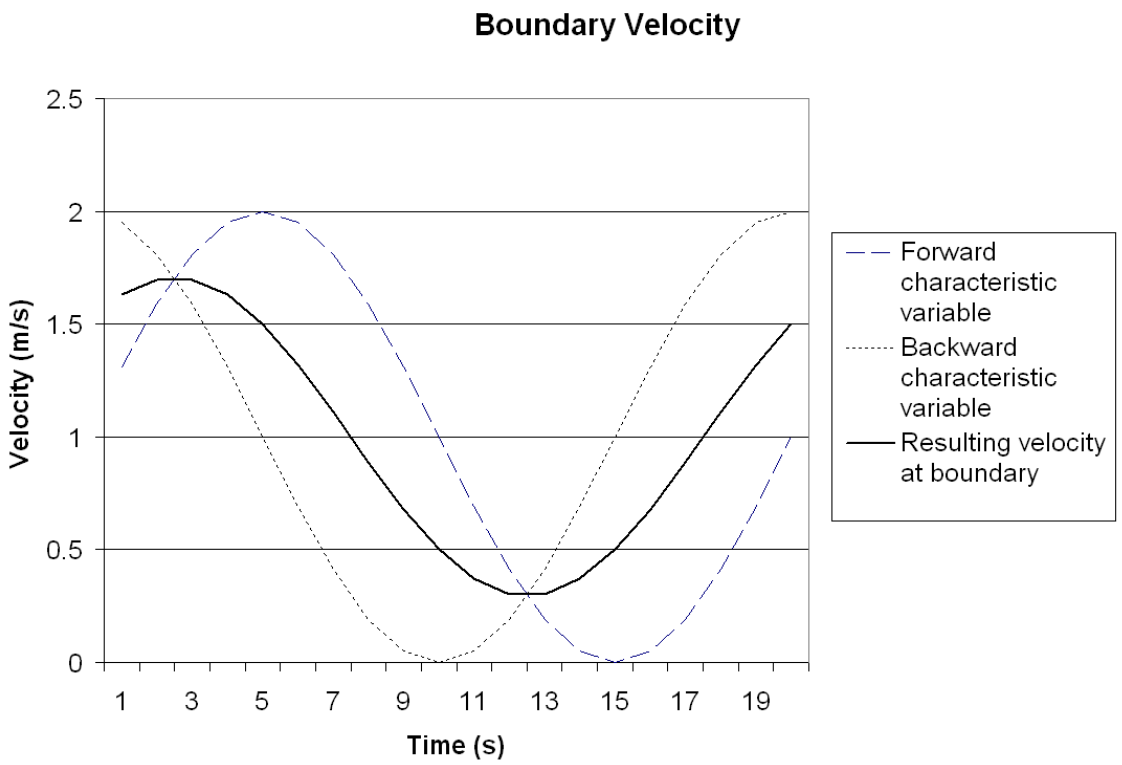

Figure 3.5: Forward and backward waves superimposed on each other contribute to the inlet velocity

The characteristic system facilitates the prescription of non-reflecting boundary conditions. At the inlet the forward component of a primary variable is prescribed and the characteristic variable associated with the forward travelling wave is calculated from it. The backward characteristic variable can be determined with the use of linear extrapolation along the characteristic line on the $x-t$ plane (Figure 3.6). When both the characteristic variables are known, the rest of the variables can be calculated (see Equations (3.81) and (3.83)).

The boundary conditions for a 'cut off' outlet can be prescribed in a similar way. The forward moving characteristic variable can be determined by linear extrapolation along the characteristic line on the $x-t$ plane. If it is assumed that there are no backward moving wave fronts entering the system at the outlet, the characteristic value associated with the backward running wave remains constant at the boundary through time.

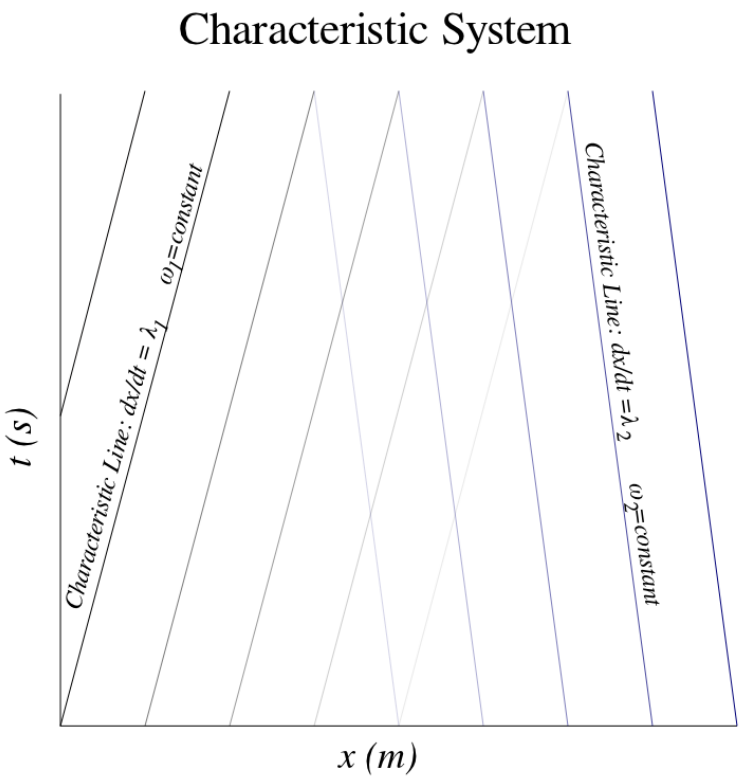

Figure 3.6: The characteristic system in the $x-t$ plane showing the characteristic lines $\frac{dx}{dt} = \lambda_1, \lambda_2$ where the characteristic variables ω_1, and ω_2 are constant.

3.5.1 Characteristic system

The characteristic system is useful because along the characteristic lines the partial differential equations become ordinary differential equations. The expression of the characteristic variables and the characteristic lines (λ_i) are not dependant on the choice of the governing variables (either a A, Q system or a A, u system) [10]. The characteristic variables are derived for the A, u system but are also valid for the A, Q system.

The system of equations, Equation (3.30) and (3.33), can be written in quasi-linear form when the spatial derivative of Equation (3.35) is taken and substituted into Equation (3.31):

$$\frac{\partial}{\partial t}\mathbf{U} + \mathbf{H}(\mathbf{U})\frac{\partial \mathbf{U}}{\partial x} + \mathbf{B}(\mathbf{U}) = 0 \tag{3.67}$$

where,

$$\mathbf{U} = \begin{bmatrix} A \\ Q \end{bmatrix}, \mathbf{H}(\mathbf{U}) = \begin{bmatrix} 0 & 1 \\ \frac{\beta}{2\rho\sqrt{A}} & u \end{bmatrix} \text{ and}$$

$$\mathbf{B}(\mathbf{U}) = \begin{bmatrix} 0 \\ \frac{1}{\rho}\left(8\pi\mu\frac{u}{A} + \frac{\partial p_{ext}}{\partial x} - \frac{\beta}{2\sqrt{A_0}}\frac{\partial A_0}{\partial x} + (\sqrt{A} - \sqrt{A_0})\frac{\partial \beta}{\partial x}\right) \end{bmatrix}.$$

The matrix $\mathbf{H}$ possesses two real eigenvalues when $A > 0$. This implies that it is a strictly hyperbolic system of equations. For a physically relevant system, where blood is able to flow, it is indeed necessary that $A > 0$ [38]. The eigenvalues of $\mathbf{H}$ can be determined as:

$$\lambda_{1,2} = u \pm c \tag{3.68}$$

The two eigenvalues are distinct if $c \neq 0$, resulting in the existence of a complete set (left and right) of eigenvectors for $\mathbf{H}$ [28]. The left eigenmatrix $\mathbf{L}$ corresponding to $\lambda_{1,2}$ is:

$$\mathbf{L} = \begin{bmatrix} \mathbf{l}_1^T \\ \mathbf{l}_2^T \end{bmatrix} = \begin{bmatrix} \frac{c}{A} & 1 \\ \frac{-c}{A} & 1 \end{bmatrix} \tag{3.69}$$

where the i-th left eigenvector is indicated by $\mathbf{l}_i$ so that $\mathbf{l}_i^T\mathbf{H} = \lambda_i\mathbf{l}_i^T$. If we premultiply Equation (3.67) with $\mathbf{L}$, we can rewrite it in component form as:

$$\mathbf{l}_i\frac{\partial \mathbf{U}}{\partial t} + \lambda_i\mathbf{l}_i\frac{\partial \mathbf{U}}{\partial x} + \mathbf{l}_i\mathbf{B}(\mathbf{U}) = 0 \qquad i = 1, 2 \tag{3.70}$$

We define the characteristic variables of our hyperbolic system as follows:

$$\frac{\partial \omega_1}{\partial \mathbf{U}} = \mathbf{l}_1, \qquad \frac{\partial \omega_2}{\partial \mathbf{U}} = \mathbf{l}_2 \tag{3.71}$$

In the case where $\mathbf{B}(\mathbf{U}) = \mathbf{0}$, the system of equations, Equation (3.67), can be written as a decoupled system of equations in terms of the characteristic variables. Near the boundaries, the spatial derivatives of β, A_0 and p_{ext} can be assumed to be zero. If the viscous resistance is small $\mathbf{B}(\mathbf{U}) \approx \mathbf{0}$ near the boundaries. The decoupled system is given by:

$$\frac{\partial \omega_i}{\partial \mathbf{U}}\frac{\partial \mathbf{U}}{\partial t} + \lambda_i \frac{\partial \omega_i}{\partial \mathbf{U}}\frac{\partial \mathbf{U}}{\partial x} = 0 \tag{3.72}$$

$$\frac{\partial \omega_i}{\partial t} + \lambda_i \frac{\partial \omega_i}{\partial x} = 0 \qquad i = 1, 2 \tag{3.73}$$

We define $\lambda_i = \frac{\partial x}{\partial t}$ as characteristic lines on which the following holds true:

$$\frac{\partial \omega_i}{\partial t} + \frac{\partial \omega_i}{\partial x}\frac{\partial x}{\partial t} = 0 \tag{3.74}$$

$$\frac{\partial \omega_i}{\partial t} = 0 \qquad i = 1, 2 \tag{3.75}$$

Thus ω_i for $i = 1, 2$ is constant along the lines where $\lambda_i = \frac{\partial x}{\partial t}$.

Equation (3.71) can be rewritten in component form as:

$$\begin{bmatrix} \frac{\partial \omega_1}{\partial A} \\ \frac{\partial \omega_1}{\partial u} \end{bmatrix} = \begin{bmatrix} \frac{c}{A} \\ 1 \end{bmatrix}, \begin{bmatrix} \frac{\partial \omega 2}{\partial A} \\ \frac{\partial \omega_2}{\partial u} \end{bmatrix} = \begin{bmatrix} \frac{-c}{A} \\ 1 \end{bmatrix} \tag{3.76}$$

Alternatively it can be written as:

$$\begin{bmatrix} \frac{\partial \omega_1}{\partial \mathbf{U}} \\ \frac{\partial \omega_1}{\partial \mathbf{U}} \end{bmatrix} = \begin{bmatrix} \frac{c}{A} \\ 1 \end{bmatrix}$$

$$\begin{bmatrix} \partial \omega_1 \\ \partial \omega_1 \end{bmatrix} = \begin{bmatrix} \frac{c}{A} \\ 1 \end{bmatrix} \begin{bmatrix} \partial A & \partial u \end{bmatrix}$$

$$\partial \omega_1 = \frac{c}{A}\partial A + \partial u \tag{3.77}$$

similarly

$$\partial \omega_2 = \frac{-c}{A}\partial A + \partial u \tag{3.78}$$

The characteristic variables may be integrated:

$$\begin{aligned}\int \partial\omega_1 =& \int \frac{c}{A}\partial A + \int \partial u \\ \omega_1 =& \sqrt{\frac{\beta}{2\rho}} \int A^{-\frac{3}{4}}\partial A + u \\ \omega_1 =& u + 4\sqrt{\frac{\beta}{2\rho}} A^{\frac{-1}{4}} \\ \omega_1 =& u + 4c \end{aligned} \tag{3.79}$$

similarly

$$\omega_2 = u - 4c \tag{3.80}$$

Seeing that $\beta > 0$, the primary variables can be expressed in terms of the characteristic variables by adding or subtracting the two equations, Equation (3.79) and (3.80):

$$A = \frac{(\omega_1 - \omega_2)^4}{1024}\left(\frac{\rho}{\beta}\right)^2 \tag{3.81}$$

$$u = \frac{1}{2}(\omega_1 + \omega_2) \tag{3.82}$$

$$Q = \frac{1}{2}A(\omega_1 + \omega_2) \tag{3.83}$$

3.5.2 Prescribing the boundary conditions

From physiological conditions we know that $u < c$ (the flow is subcritical). This implies that $\lambda_1 > 0$ and $\lambda_2 < 0$. The sign of the eigenvalues has the consequence that ω_1 is associated with the wave moving forward and ω_2 with the wave travelling backward [20]. This led to the conclusion that only one boundary condition must be specified at both boundaries. At both the inlet and outlet, the outgoing characteristic can be determined by linear extrapolation along the characteristic lines in the $x - t$ plane (Figure 3.6). The characteristic values at time-step n can be calculated and used to determine the values for the next time-step $n + 1$ at the inlet and outlet (Figure 3.7):

$$\omega_2^{n+1}|_{x=x_0} = \omega_2^n|_{x=x_0-\lambda_2^n \triangle t} \tag{3.84}$$

and

$$\omega_1^{n+1}|_{x=x_L} = \omega_1^n|_{x=x_L-\lambda_1^n\triangle t} \tag{3.85}$$

with x_0 and x_L the coordinates of the inlet and outlet. The coordinates $x = x_0 - \lambda_2^n \triangle t$ and $x = x_L - \lambda_1^n \triangle t$ can be determined with an iterative process which will be discussed in the next chapter.

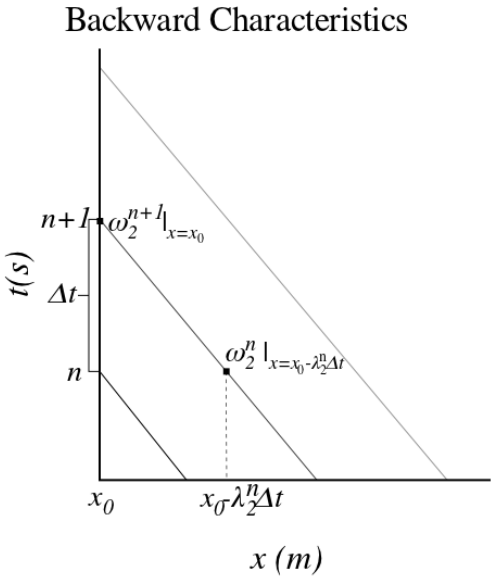

Figure 3.7: Finding the value of ω_2 at the inlet using extrapolation along the λ_2 characteristic line

3.5.2.1 The inlet conditions

Either the total value of one of the primary variables (area, pressure or flow) or the forward component of one of these variables can be prescribed at the inlet [20]. The remaining variables can be calculated from the characteristic variables and the constitutive equation. It is more physically intuitive to prescribe the forward component of a variable. This can be done by prescribing the incoming characteristic (ω_1) [50]. To prescribe the forward pressure, rearrange Equation (3.81):

$$\omega_1^{n+1} = \omega_2^0 + 8(A^{n+1})^{\frac{1}{4}}\sqrt{\frac{\beta}{2\rho}} \tag{3.86}$$

and substitute Equation (3.35) into Equation (3.86):

$$\omega_1^{n+1} = \omega_2^0 + 4\sqrt{\frac{2}{\rho}}\sqrt{(\bar{p}^{n+1} - p_{ext}) + \beta\sqrt{A_0}} \tag{3.87}$$

$\bar{p}$ is the prescribed pressure and the superscript 0 of ω_i^0 denotes the initial value of ω_i. When no backward waves reach the inlet, $\omega_2^0 = \omega_2$. The outgoing characteristic can be calculated from the previous time-step as described in the previous section. With both characteristic values ω_1 and ω_2 known, the primary variables can be calculated using Equation (3.81) for the area and Equation (3.83) for the mass flow. With area and mass flow known, the total pressure can be calculated using Equation (3.37).

3.5.2.2 The outlet conditions

Generally, after some bifurcations the diameter of the arteries becomes smaller, the stiffness of the walls larger and the flow behaviour of the system changes. The mathematical model that has been discussed until now is only valid for the large arteries. Therefore the 1D model has to be truncated. Researchers use different lumped parameter models to represent the downstream branches [52]. One approach is to use a lumped resistance with a reflection coefficient, so that a given proportion of the forward travelling wave is reflected [39, 50]. Another approach is to use a Windkessel element (consisting of two resistors and a capacitor) [48]. This approach includes the capacitive effect that can be observed by the phase lag in reflected waves in physical systems. Olufsen [22, 24] developed a linear tree model for the smaller arteries. This tree model is impedance based and similar to models used for the analysis of electrical cable networks. Mynard and Nithiarasu [20] investigated the use of a single tapering vessel as a terminal element. The terminal vessel has several step decreases in the A_0 or step increases in the material properties, causing increases in local characteristic impedance. This will cause reflections at each stepping point.

For this study we modelled the downstream effects as purely resistive. This does not accurately reflect the physical system, and could be improved upon in later studies. The causes of the reflections (branching and changes in vessel properties) can also be described as a change in the characteristic impedance according to linear transmission theory [20]. The characteristic impedance, Z_0, is analogous to Ohm's Law and relates the flow of a wave to the applied pressure. It may be expressed as:

$$Z_0 = \frac{1}{Y_0} = \frac{\rho c_0}{A_0} \tag{3.88}$$

where Y_0 is called the characteristic admittance and c_0 is the intrinsic wave speed of the vessel. From Equation (3.66) it can be seen that the impedance depends only on the material properties and geometry of the vessel. The reflection coefficient, R, expresses the ratio of the incoming and outgoing waves' amplitudes and is given as:

$$R = \frac{Y_{0p} - \sum_{j=1}^{n} Y_{0j}}{Y_{0p} + \sum_{j=1}^{n} Y_{0j}} \tag{3.89}$$

where the underscript p denotes the parent vessel and j the daughter vessels. When there is a 'wall' at the end of a vessel, $\sum_{j=1}^{n} Y_{0j} = 0$ and there is a total positive reflection ($R = 1$). When there is a opening with no downstream resistance (such as an artery that is cut open), $\sum_{j=1}^{n} Y_{0j} \to \infty$ and there is a total negative reflection ($R \to \infty$). For a well-matched branching no reflection occurs ($R = 0$). Although Equation (3.89) is strictly only valid for a linear model, it can be used to set boundary conditions for a outlet where only the resistive effects of the downstream is taken into account. This approach determines the incoming characteristic variable from the change in the outgoing characteristic variable. For a forward travelling wave front the terminal reflection coefficient, R_t, is:

$$R_t = -\frac{\triangle\omega_2}{\triangle\omega_1} = \frac{\omega_2^{n+1} - \omega_2^0}{\omega_1^{n+1} - \omega_1^0} \tag{3.90}$$

The value of the outgoing characteristic variable, ω_1, can be calculated from the previous time-step by linear extrapolation (Section 3.5.2). The incoming characteristic variable, ω_2, can be calculated by rearranging Equation (3.90):

$$\omega_2^{n+1} = \omega_2^0 - R_t(\omega_1^{n+1} - \omega_1^0) \tag{3.91}$$

With both the characteristic values known, the primary variables can be calculated with Equation (3.81) and Equation (3.83).

3.6 Discontinuities

A discontinuity in a artery is a sudden change in the material properties (β) or the unstressed area (A_0). Cardiovascular diseases can cause discontinuities. Atherosclerotic plaque decreases A_0 and increases β while aneurysms increase A_0 and decrease β. Surgical procedures also induce discontinuities. A vascular stent or graft may change both A_0 and β.

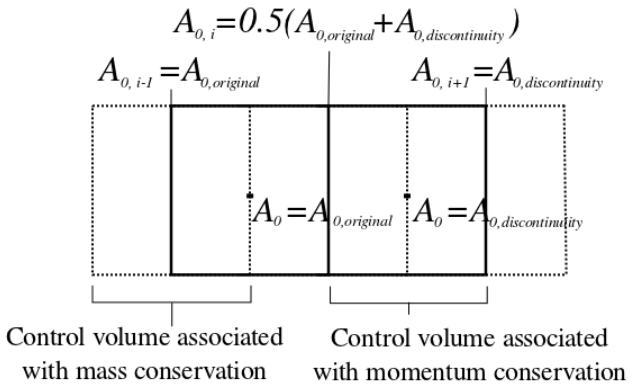

Figure 3.8: Spreading a discontinuity in A_0 across a cell

The finite volume method has been developed for continuum mechanics. However, several techniques to handle discontinuities have been successfully implemented [49].

As β, E, h and A_0 are not constant along the length of the artery, it is stored as vectors in the computer code. It is natural to define β_i, E_i, h_i and A_{0i} at the centre of the control volume associated with mass conservation as it is relevant to the fluid-structure interaction, Equation (3.37). Computational experiments done in this study showed that it is better to implement the discontinuity in the centre of the control volume associated with momentum conservation, thus spreading it over a cell (Figure 3.8).

3.7 Bifurcation

When considering branching (Figure 3.4), it is useful to represent the arteries with nodes in a surrounding control volume (Figure 3.9). The control volume associated with p_{02} and A_2 is indicated with a dotted line. The control volumes associated with Q_1, Q_2 and Q_3 are between the nodes associated with total pressure and area (as in the previous sections).

3.7.1 Discretisation for bifurcation

The equation for mass conservation, Equation (3.27), for the control volume associated with the bifurcation can be discretised in a similar way as in Section 3.3. Note that for the control volume associated with the bifurcation $\delta V_{bifurcation} = A_2(\frac{1}{2}\triangle x_1 + \frac{1}{2}\triangle x_2 + \frac{1}{2}\triangle x_3)$. The discretised equation for mass conservation can be written as:

$$\frac{A_2 - A_2^o}{\triangle t}(\frac{1}{2}\triangle x_1 + \frac{1}{2}\triangle x_2 + \frac{1}{2}\triangle x_3) + \theta(\sum_{k=1}^{3} s_k Q_k) + (1-\theta)(\sum_{k=1}^{3} s_k Q_k)^o = 0 \tag{3.92}$$

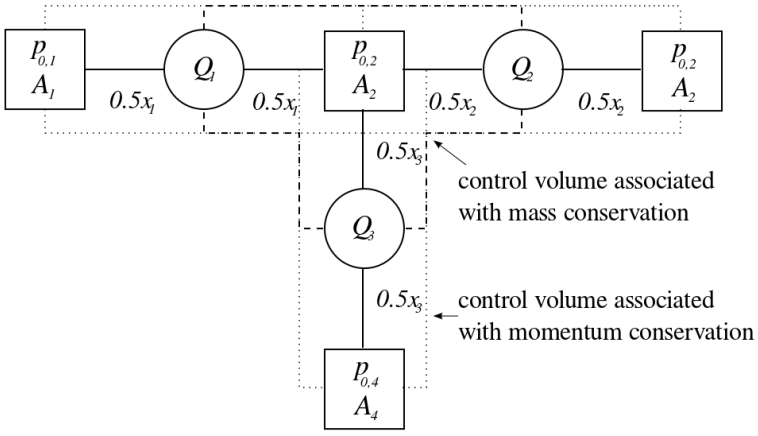

Figure 3.9: Branch network diagram

The symbol s_k indicates the direction of flow. In accordance with conventional control volumes $s_k = -1$ is used when flow is into the control volume and $s_k = +1$ is used when flow is out of the control volume.

There is no change to the equations for momentum conservation for the control volume associated with Q_1 and Q_2. For Q_3 the equation becomes:

$$\begin{aligned} \frac{\rho}{A_{2-4}}\frac{(Q_3 - Q_3^o)}{\triangle t}\triangle x + \theta\left[(p_{0_4} - p_{0_2}) + \frac{8\pi\mu Q_3}{A_{2-4}^2}\triangle x\right] & \\ +(1-\theta)\left[(p_{0_4} - p_{0_2}) + \frac{8\pi\mu Q_3}{A_{2-4}^2}\triangle x\right]^o &= 0 \end{aligned} \tag{3.93}$$

The values for A_{2-4} and A_{2-3} are calculated as the interpolated values at the centre of the Q-control volumes in the same way as previously.

It can be assumed that the effect of storage in the branch as a result of the change in area is small. Therefore we can write $|Q_1| \approx |Q_2| + |Q_3|$. The equation that relates p_0 to A, Equation (3.37), can then be written as:

$$p_{0_2} = p_{ext} + \beta(\sqrt{A_2} - \sqrt{A_0}) + \frac{1}{2}\rho\left(\frac{\frac{1}{2}(|Q_1| + |Q_2| + |Q_3|)}{A_2}\right)^2 \tag{3.94}$$

3.7.2 Solving the branch equations

To solve the equations we proceed in the same manner as in Section 3.4. The branch doesn't affect the equations for the correction of Q, Equation (3.54). This is because the control volumes of the bifurcation associated with the momentum conservation has a identical structure to that of the single artery.

The control volume of the bifurcation associated with the mass conservation has two outlets and a inlet. Because we assumed that the effect of storage in the branch as a result of change in area is small, $|Q_1| \approx |Q_2| + |Q_3|$. Therefore the correction for A, Equation (3.50), for the area-total pressure node in the control volume associated with the bifurcation can be written as:

$$A_2^{'} = \frac{1}{\left(\frac{\beta}{2\sqrt{A_2}} - \frac{\frac{1}{2}\rho\left(\frac{|Q_1|+|Q_2|+|Q_3|}{2}\right)^2}{A_2^3}\right)} p_{0_2}^{'} - \frac{\rho\left(\frac{|Q_1|+|Q_2|+|Q_3|}{2}\right)}{A_2^2\left(\frac{\beta}{2\sqrt{A_2}} - \frac{\rho\left(\frac{|Q_1|+|Q_2|+|Q_3|}{2}\right)^2}{A_2^3}\right)} \left(\frac{|Q_1^{'}| + |Q_2^{'}| + |Q_3^{'}|}{2}\right) \tag{3.95}$$

When we substitute Equation (3.54) and Equation (3.95) into the conservation of mass for a branch, Equation (3.92), we can solve for $p_0^{'}$:

$$c_{(2,2)} p_{0_2}^{'} = c_{(2,1)} p_{0_1}^{'} + c_{(2,3)} p_{0_3}^{'} + c_{(2,4)} p_{0_4}^{'} + b_2 \tag{3.96}$$

with

$$\begin{aligned} c_{(2,2)} = k_2 \cdot \frac{\frac{1}{2}\triangle x_1 + \frac{1}{2}\triangle x_2 + \frac{1}{2}\triangle x_3}{\triangle t} + a_2 \left(\theta - r_2 \cdot \frac{\frac{1}{2}\triangle x_1 + \frac{1}{2}\triangle x_2 + \frac{1}{2}\triangle x_3}{\triangle t}\right) + \\ a_1 \left(\theta + r_2 \cdot \frac{\frac{1}{2}\triangle x_1 + \frac{1}{2}\triangle x_2 + \frac{1}{2}\triangle x_3}{\triangle t}\right) + a_4 \left(\theta - r_2 \cdot \frac{\frac{1}{2}\triangle x_1 + \frac{1}{2}\triangle x_2 + \frac{1}{2}\triangle x_3}{\triangle t}\right) \\ c_{(2,1)} = a_1 \left(\theta + r_2 \cdot \frac{\frac{1}{2}\triangle x_1 + \frac{1}{2}\triangle x_2 + \frac{1}{2}\triangle x_3}{\triangle t}\right) \\ c_{(2,3)} = a_3 \left(\theta - r_2 \cdot \frac{\frac{1}{2}\triangle x_1 + \frac{1}{2}\triangle x_2 + \frac{1}{2}\triangle x_3}{\triangle t}\right) \\ c_{(2,4)} = a_4 \left(\theta - r_2 \cdot \frac{\frac{1}{2}\triangle x_1 + \frac{1}{2}\triangle x_2 + \frac{1}{2}\triangle x_3}{\triangle t}\right) \end{aligned} \tag{3.97}$$

and

$$b_2 = -\left\{\frac{\bar{A}_2 - A_2^o}{\triangle t} \cdot \left(\frac{1}{2}\triangle x_1 + \frac{1}{2}\triangle x_2 + \frac{1}{2}\triangle x_3\right) + \theta\left(\bar{Q}_2 + \bar{Q}_3 - \bar{Q}_1\right) + (1-\theta)\left(Q_2 + Q_3 - Q_1\right)^o\right\} \tag{3.98}$$

with

$$r_2 \quad = \tfrac{1}{4}\rho\left(\tfrac{(|Q_1|+|Q_2|+|Q_3|)}{A_2^2}\right) \cdot k_2 \tag{3.99}$$

$$k_2 = \frac{1}{\left(\frac{\beta}{2\sqrt{A_2}} - \frac{\rho\left(\frac{|Q_1|+|Q_2|+|Q_3|}{2}\right)^2}{A_2^3}\right)} \tag{3.100}$$

3.8 Summary

This chapter has considered the theory of the mathematical model that describes blood flow in large expandable arteries. The derivation of the equations from the Reynold's transport theorem was shown and used for the derivation of the equations for mass and momentum conservation. In this system of equations there are three variables and two equations. A third equation, the constitutive equation, is used to close the system. This equation is in the form of a non-linear relation between pressure and area. The system of equations was discretised using a staggered control volume grid. The pressure and area were defined at the wall of the control volume and the flow at the centre of the control volume on this grid. The iterative method that was used to solve the system of equations was discussed. This method is similiar to the SIMPLE algorithm. To accommodate the forward and backward moving waves that are found in the cardiovascular system, non-reflecting boundary conditions based on the characteristic system should be used. The way in which discontinuities should be handled on the staggered grid was explained. The last tool that is necessary to model the arterial network, the way to implement branching, was also discussed. The mathematical methods and techniques discussed in this chapter are the theoretical basis from which a computer code to model the arterial network was developed.

Chapter 4

Implementation

The mathematical model was implemented as a computer code written in GNU Octave [7], hereafter referred to as the Octave program. The computer code consists of several functions. The core of the program is an iterative procedure similar to the SIMPLE algorithm.

This chapter will give a general overview of the layout of the computer code. It will also give attention to functions that are special in some way. These include the iterative procedures for the steady state solution and characteristic values. The post-processing of pressure will also be discussed.

4.1 Outlay of program

The heart of the Octave program is an iterative procedure that is repeated for every time-step (Figure 4.1). To initiate the guess-values for the first time-step an iterative steady state procedure is used. This procedure will be discussed in more depth in the following section. Non-reflecting boundary conditions are prescribed for each time-step. The iterative procedure calculates converged values for the primary variables (p_0, Q and A). At the end of each time-step the outgoing characteristics, that will be used to prescribe the boundary conditions for the next time-step, are determined.

At the beginning of each time-step non-reflecting boundary conditions are imposed. At the inlet this is done by prescribing the static pressure, $\bar{p}$, and calculating the forward characteristic variable, ω_1, using Equation (3.87). For this study we assumed that there is no backward travelling wave entering the domain. Thus ω_2 remains constant at the outlet through time. The backward characteristic variable at the inlet, ω_2, and the forward characteristic variable

at the outlet, ω_1, are available from the previous time-step. The boundary values for the primary variables can now be calculated by the application of Equations (3.81) and (3.83). With A_{inlet} and Q_{inlet} known, $p_{0,inlet}$ (the stagnation pressure at the inlet) can be calculated using Equation (3.37). With the boundary values known, the iterative process can be used to determine all the variables in the computational domain.

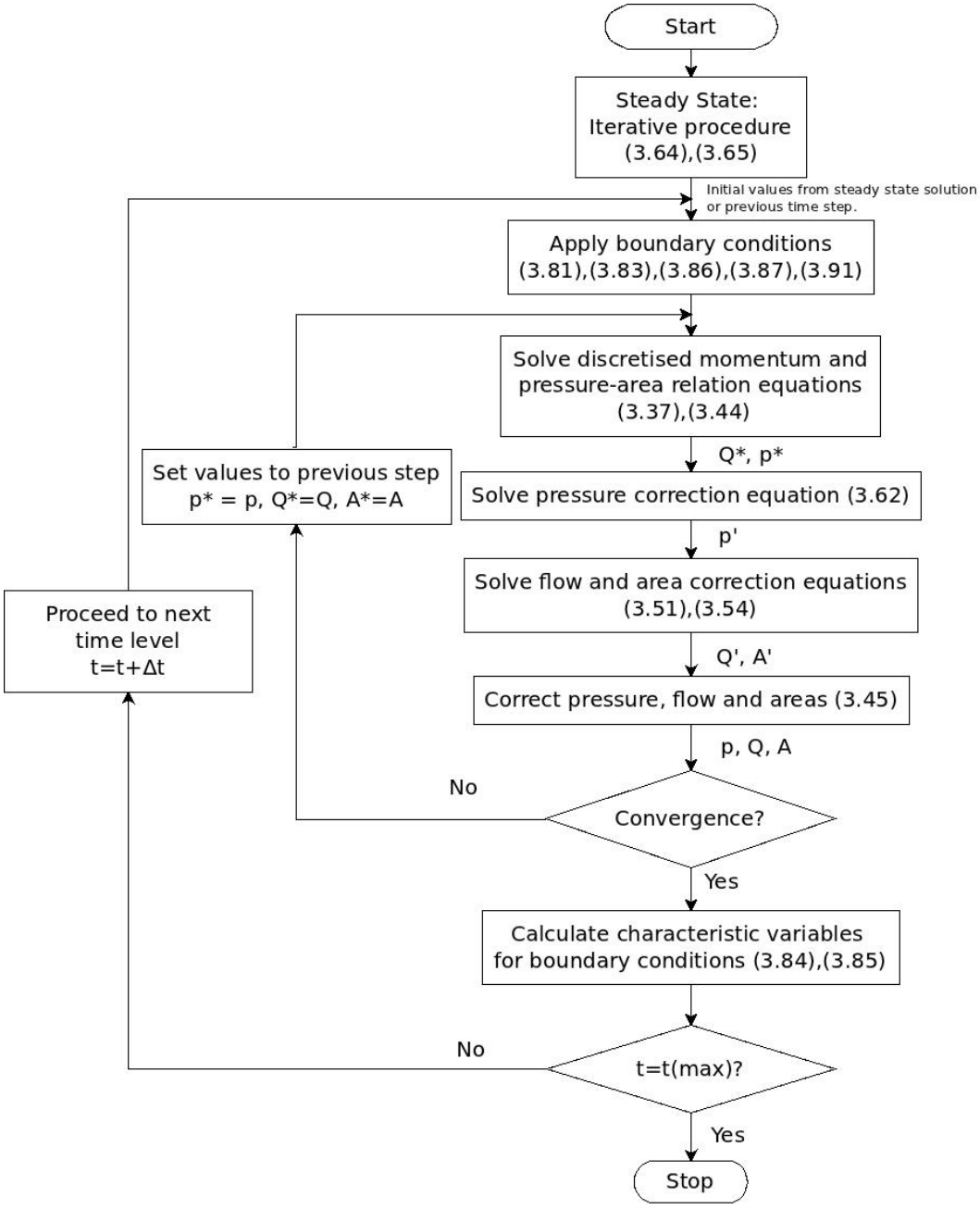

Figure 4.1: Outlay of program

The iterative procedure imposes momentum conservation and the pressure-area relation and

then uses the pressure correction equation, Equation (3.62), to impose continuity. When the updated values from the previous iteration or time-step are substituted into the discretised momentum and constitutive equations, mass conservation will not be satisfied. After the correction equations are implemented mass conservation is satisfied, but momentum conservation and the pressure-area relation are not. With each iteration the discrepancy between the conservation equations decreases until $p' \approx 0$ and convergence is reached.

When convergence is reached the outgoing characteristics (ω_2 at the inlet's side and ω_1 at the outlet's side) are calculated. The iterative procedure to determine the outgoing characteristics will be discussed in Section 4.3. This iterative cycle repeats itself for every time-step. The calculation stops when the maximum number of time-steps have been reached.

4.2 Steady state iteration

To determine the initial condition of the system, the steady-state solution can be used. The steady-state solution can be determined by using the Newton-Rhapson method. Steady-state mass conservation implies that flow, Q, is constant through the length of the artery. This makes it unnecessary to solve the system simultaneously as a whole. The values of p_0 and A for each increment are dependant only on each other and the values of the previous increment. This makes it possible to use a simple iterative procedure to calculate p_0 and A for each consecutive element using Equation (3.64) and Equation (3.65). The pseudo code for the iterative procedure follows:

```
for i = 1 to number_of_increments

    A[i] = A[i-1]
    difference_Area = 1
    while difference_Area≠0
        p_0[i] = p_0[i-1]-8*PI*Q[i]*deltax/A^2[i]
        A_updated[i] = (p_0[i]-p_ext+beta*Sqrt(A_0[i])
           -0.5*rho*(Q/A[i])^2)/beta^2
        difference_Area = A_updated[i]-A[i]
        A[i] = A_updated[i]
    end

end
```

The iterative procedure that repeats itself for every increment makes use of momentum conservation and the pressure-area relation. Momentum conservation is used to update the value of p_0. The value of A is updated next by using the relation of area to pressure. If the value of A does not change during the current iteration the values of p_0 and A for the increment have converged. The values for the next increment are calculated in the same way.

4.3 Calculating the outgoing characteristic values

At the end of each time-step the outgoing characteristic values, $\omega_2|_{x=x_0-\lambda_2^n \triangle t}$ at the inlet and $\omega_1|_{x=x_L-\lambda_1^n \triangle t}$ at the outlet, should be calculated to prescribe the boundary conditions for the next time-step (Section 3.5.1). The x-coordinate where the characteristic values should be calculated is dependent on λ, Equation (3.85). The characteristic line λ is in turn a function of Q and A, Equation (3.68). But Q and A are again a function of x. An iterative procedure is therefore needed to determine al the values. When the x-coordinate is determined, the outgoing characteristics can be determined using Equations (3.79) and (3.80). The pseudo code for the iterative function at the inlet follows:

```
initiate x_guess
initiate x_error=1
xincrement = FALSE
while x_error~=0

    while xincrement is FALSE
    increment_test=2

        if x_guess is outside domain

            print error
            xincrement = TRUE

        else if x_guess is in first increment

            b=x_b/△x
            A_guess = (1-b)*A_in +b*A[2]
            if x_guess is in first half of increment

              c=2*b
              Q_guess = (1-c)*Q_in + c*Q[1]

            else

              c=b-0.5
              Q_guess = (1-c)*Q[1] + c*Q[2]
```

```
            end
            xincrement=TRUE
        elseif x_guess is in increment=increment_test
            b=x_b/delta_x
            A_guess = (1-b)*A[increment_test-1] + b*A[increment_test]
            if x_guess is in first half of increment
              c=b+0.5
              Q_guess = (1-c)*Q[increment_test-2] + c*Q[increment_test-1]
            else
              c=b-0.5
              Q_guess = (1-c)*Q[increment_test] + c*Q[increment_test-1]
            end
            xincrement=TRUE
        end
        increment_test +=1
    end
    lambda= Q_guess/A_guess-SQRT(beta*SQRT(A_guess)/2*rho)
    x_updated = x_in - lambda*delta_t
    x_error = x_updated - x_guess
    x_guess = x_updated
end
omega_2 = Q_guess/A_guess-4*SQRT(beta*SQRT(A_guess)/2*rho)
```

The function starts with a guessed value for x. Then it determines the increment in which x is situated. It then determines x_b, x_c (Figure 4.2). These values are used to determine weighting values (b, c) for the linear interpolation of A and Q. With A_{guess} and Q_{guess} known, λ can be calculated and x updated. When the values have converged, ω_2 can be calculated.

4.4 Post processing the results

Although the solution is found in terms of p_0 it is useful to display p. This is partly because the blood pressure that can be measured is the static pressure. It will also make it easier to compare our results with the results of other researchers. To make it more comfortable

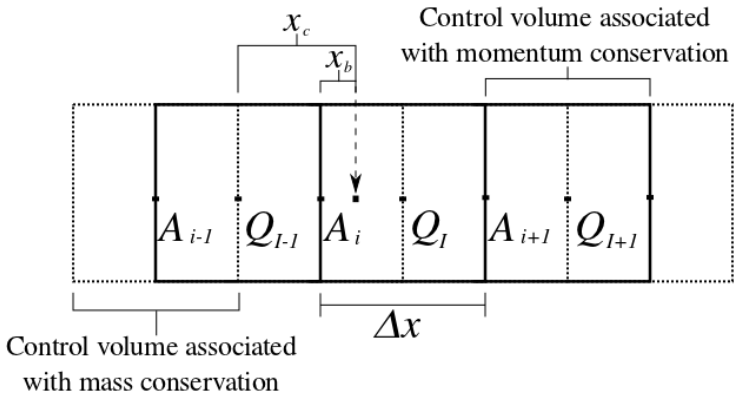

Figure 4.2: Staggered grid showing x_b and x_c that is used to interpolate the values of A and Q.

to track the wave with time we display the pressure as the variation between transient and steady state pressure. The pseudo code for the pressure that will be displayed was processed as follows:

```
p_steady = p_0_steady - (0.5*rho*(Q/A)^2)
p_display = p_0 - 0.5*rho*(Q/A)^2 - p_steady
```

4.5 Summary

The computer code that models the cardiovascular system was discussed briefly in this chapter. Attention was given to the general outlay of the program and the iterative procedure that is found in the computer code. The computer code uses a iterative procedure to determine the steady state solution. The forward component of pressure is prescribed to obtain the ingoing characteristic at the inlet. Combining the ingoing characteristic with the outgoing characteristic, calculated at the previous time-step, non-reflecting boundary conditions are prescribed. An iterative procedure similar to the SIMPLE algorithm determines the variables for each time-step. At the end of each time-step, another iterative procedure calculates the outgoing characteristics. Post-processing ensures that the results that will be displayed are in a form that can easily be compared with the results available in literature.

Chapter 5

Simulations

This chapter discusses the results of the test cases that were run to demonstrate the ability of the computer code to solve problems. First we look at the steady state solution, then at different transient solutions for a single artery and lastly at more complex cases with branching.

5.1 Steady state

The steady state solution is used as the initial conditions for the transient solution. It also gives us additional insight to the flow behaviour. Different variables can be solved for using mass and momentum conservation. The time needed to calculate steady state solutions for different variables gives an indication of which variables to use in the transient solution. Different programs were written in EES (Engineering Equation Solver) [17] to compare the solution times between a collocated and staggered grid, when cross-sectional area is expressed in terms of area A or radius r, as well as when the momentum equations are expressed in terms of volume flow rate Q or velocity u. When writing a program with EES, it is only necessary to provide the discretised equations. The built-in Newton-Rhapson solver does all the hard work. This makes it easy to compare different discretised equations and programs using different variables.

The domain that was chosen to perform this steady state investigation had a length of L =0.1 m, a relaxed area of A_0 =7.069$\times 10^{-4}\, m^2$, the material properties remained constant through the length with $\beta = 417871\, Pa/m^3$. The domain was divided into 800 increments resulting in $\delta x = 1.25 \times 10^{-4}\, m$. The properties of blood were taken as $\rho = 1060\, kg/m^3$ and $\mu = 0.035\, Pa \cdot s$. An external pressure of $p_{ext} = 8600\, Pa$ was chosen. A lower limit on the

guess values, $A_0 \geq 0$, was enforced to ensure that the system of equations can be solved with EES. Table 5.1 shows the results from the investigation.

Table 5.1: Comparing solution times for steady state solution using EES.

Program	EES							
Method	Newton-Rhapson							
Grid	Co-located				Staggered			
A/r	A		r		A		r	
Q/u	Q	u	Q	u	Q	u	Q	u
Time(s)	0.1	0.2	0.1	0.2	0.1	0.3	0.1	0.2

Note that the shape of the artery resulting from the steady state problem of all the programs is the same. From these results we observed that to express the system in terms of flow, Q, instead of velocity, u, makes the biggest impact on the solution time. There is not a significant difference in solution time when the cross-sectional area is expressed in terms of radius, r, rather than the area, A, itself. This is especially true in the cases where the system is expressed in terms of the flow, Q. There is also not a big difference in solution time when a co-located grid or a staggered grid is used. When a staggered grid is used and the system is expressed in terms of A and u, the program takes the longest time to solve. For the work that follows we chose to express the system in terms of Q and A. Because the method used to solve the transient solution makes use of a staggered grid, the following investigations were performed on a staggered grid.

EES provides memory space for up to 6000 variables. For a transient problem or even a more complex steady-state problem that includes several branches this amount of space will not be sufficient. A second investigation using the Octave programming language was done to determine the method with the fastest solution time. The results are shown in Table 5.2.

Table 5.2: Comparing solution time for steady state solution using EES and Octave.

Program	EES		Octave			
Method	Newton-Rhapson		Newton-Rhapson		Iterative	
Increments	200	800	200	800	200	800
Time(s)	0.0	0.1	2.2	54.0	0.0	0.1

The Newton-Rhapson method takes a lot longer to solve the problem than the iterative procedure discussed in Section 4.2. The iterative method solves the problem in the same time as EES. When the viscosity and, in effect, the pressure loss is too large (or the artery is too long), the artery reaches a point where the area is zero for all practical reasons. The Newton-Rhapson

method is unable to solve any part of the problem when this happens. This is because the whole system and all the increments are solved simultaneously. The iterative method on the other hand will show the results before that point and show a zero area and pressure for the remaining part of the artery. This makes it easier to debug the steady state solution.

Figure 5.1 shows the effects that viscosity has on the area and pressure of the artery. As expected, in the case of the inviscid flow there is no pressure drop. Note that as viscosity increases so does the non-linearity of the solution and pressure loss. When the material properties and external pressure around a vessel are constant for a vessel section, the area will decrease due to the pressure loss that results from the viscosity.

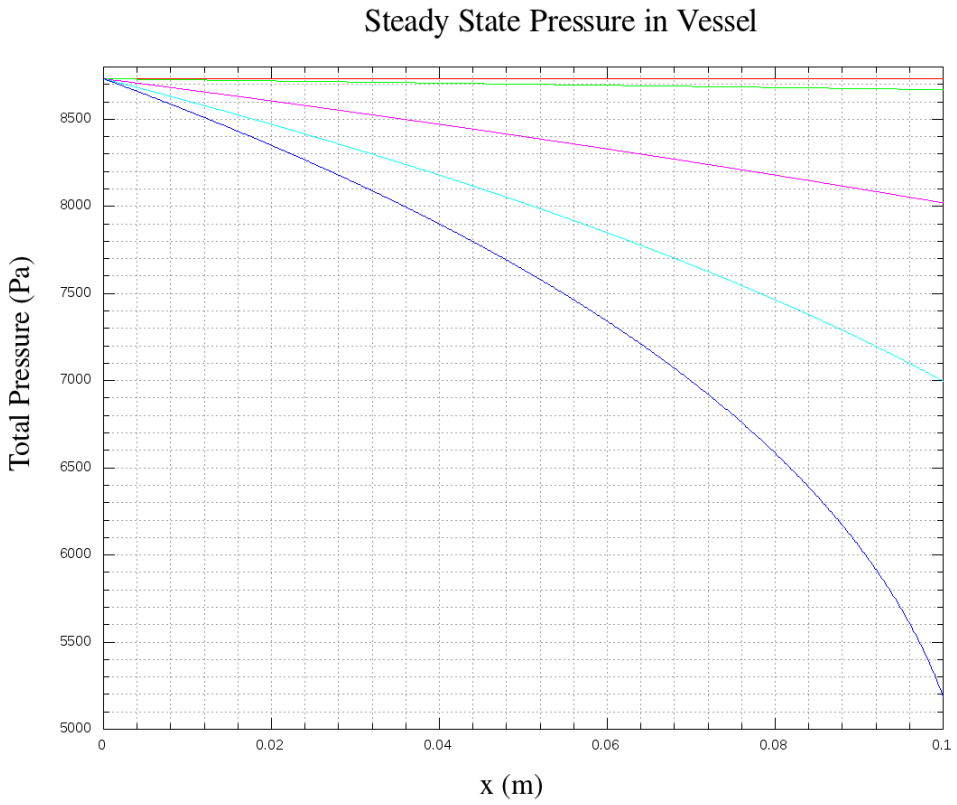

Figure 5.1: Steady State pressure of blood vessel showing the effects of viscosity. Inviscid flow ($\mu \approx 0\, Pa \cdot s$) is shown in red. Different viscous flows are also shown ($\mu = 0.035\, Pa \cdot s$ in green, $\mu = 0.35\, Pa \cdot s$ in magenta, $\mu = 0.7\, Pa \cdot s$ in cyan and $\mu = 1\, Pa \cdot s$ in blue).

5.2 Transient cases

5.2.1 Single artery

This section discusses results of investigations of transient simulations on a single artery. Each variable that has an effect was isolated and varied while all the other variables were kept constant. Mynard [20] presented results in terms of pressure pulse graphs at different time intervals. However not enough information is available to reproduce exact results. As will be outlined in the next sections, it is important to do for example mesh independence studies to be sure that results presented do not suffer discretisation type of influences that could have been resolved. For this study assumptions with regard to the initial blood velocity u, input wave shape and relaxed area A_0 were made to best match the given graphs. Firstly the effects that different time integration schemes have on the shape of the pressure pulse will be investigated. In this same section we demonstrate the effects of varying time-step and increment length. The following four sections (Section 5.2.1.2- Section 5.2.1.5) look into:

- The effect of viscosity on the pressure peak.
- The non-linearity of the solution by using different pressure inputs.
- The effect on the solution when the speed of sound of the system is varied.
- The reflections caused by discontinuities.

The single artery test case section is closed with a focus on the boundary conditions. It shows how the wave propagates at the boundaries when different values for the reflection coefficient are used. For the transient simulations p_{ext} was chosen as zero. The density was chosen as $\rho = 1060\,kg/m^3$. Note that the pressure that is displayed in the transient cases is the static pressure, p, and not the total pressure, p_0.

5.2.1.1 Numerical experiments

Sensitivity with regard to values associated with space and time discretisation and time integration were investigated. Note that the physical problem doesn't change at all, only the way in which it was solved.

Figure 5.2 shows the effect of different time integration schemes, namely Euler implicit, explicit and Crank-Nicholson. Snapshots were taken at $t = 0.03\,s$, $t = 0.045\,s$ and $t = 0.06\,s$. The three peaks represent the three snapshots. For this experiment $\mu \approx 0$ and the amplitude of

the pulse is expected to remain constant. As will be outlined below, sensitivity towards time integration, time-step, and increment size of the results correlate well with what is usually observed in the CFD field [49]. The Courant number, Cr, can be calculated as $Cr = \frac{c\triangle t}{\triangle x}$. The value for the speed of sound is calculated by Equation (3.66) as $c = 3.33$. As discussed in Section 3.3, for time integration θ may vary between zero and one. For a more explicit type of solution, i.e. $\theta < 0.5$, the solution becomes unstable when $Cr > 1$. Thus, the explicit solution is only stable for a very small time step or a large increment length (For similar results, when $\triangle x = 0.002\,m$ and a very small time step, $\triangle t < 0.00006$, is used for the explicit case, the solution time is two orders higher than when a second order Crank-Nicholson time integration is done with a time step of $\triangle t = 0.0001\,s$). The blue line in Figure 5.2 represents the Crank-Nicholson time integration ($\theta = 0.5$). Note that the amplitude of the pulse remains constant. The red line in the figure represent a first order Euler implicit solution ($\theta = 1$). The solution is unconditionally stable but only accurate for very small time steps. For $\triangle t = 0.0001\,s$ the pulse is smeared: the amplitude decreases, while width of the pulse increases. This is called numerical diffusion or dispersion. For all the subsequent test cases the Crank-Nicholson time integration scheme was used.

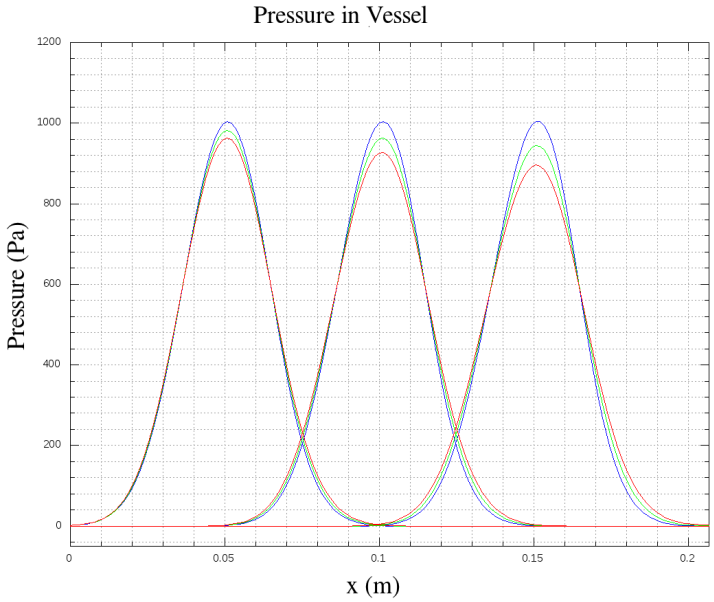

Figure 5.2: Wave propagation with varying α (time integration). Blue lines show the Crank-Nicholson scheme ($\alpha = 0.5$), green lines show an implicit solution ($\alpha = 0.75$) and red lines show the fully implicit time integration ($\alpha = 1$).

The next numerical experiment was done on the size of the time-step. Figure 5.3 shows the effect of different sized time-steps. As above snapshots were taken at $t = 0.03\,s$, $t = 0.045\,s$ and $t = 0.06\,s$. The three peaks represent the snapshots. The first run was done with $\triangle t = 0.001\,s$ ($Cr = 1.665$) and is represented with a blue line. When smaller time-steps were used, the pulse

propagated at a faster speed, converging to the analytical solution. This is shown by the green line where $\triangle t = 0.0005\,s$ ($Cr = 0.8325$) and the red line where $\triangle t = 0.0001\,s$ ($Cr = 0.167$). The actual speed of the wave was determined by $u_{wave} = \frac{\triangle x}{\triangle t}$. This was compared to the speed of sound, c, of the wave. For $\triangle t = 0.0001\,s$, the actual speed of the wave was very close to the speed of sound of the wave, and is thus a more accurate representation of the propagation. When the time-step was decreased some more ($\triangle t = 0.00005\,s$ - represented by the magenta line) the solution was very close to the solution of a slightly bigger time-step ($\triangle t = 0.0001\,s$). The solution could be considered as converged. The time that it took to solve the system when $\triangle t = 0.00005\,s$ was two orders higher than when $\triangle t = 0.0001\,s$. To achieve a balance between time needed and accuracy of the solution $\triangle t$ was chosen to be $0.0001\,s$.

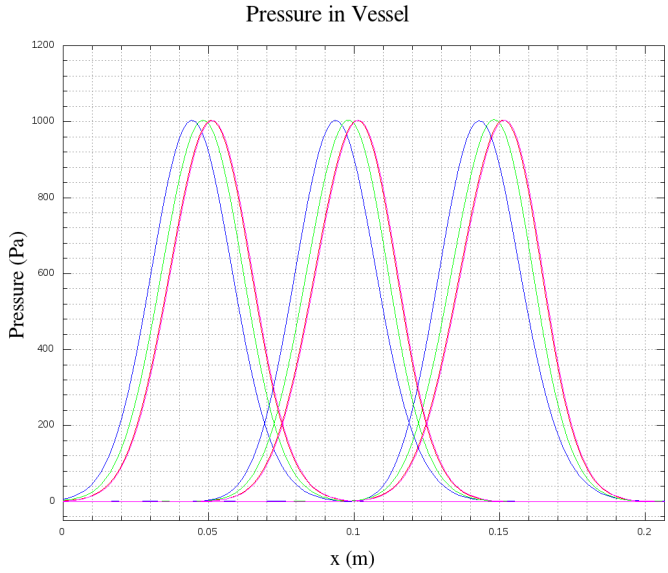

Figure 5.3: Wave propagation with varying time-step ($\triangle t = 0.001\,s$ (blue), $\triangle t = 0.0005\,s$ (green), $\triangle t = 0.0001\,s$ (red) and $\triangle t = 0.00005\,s$ (magenta)).

The lengths of the increments also have an effect on the accuracy of the solution [49]. Figure 5.4 shows snapshots that were taken at $t = 0.03\,s$ and $t = 0.045\,s$ of different increment lengths ($\triangle x = 0.00267\,m$ (blue), $\triangle x = 0.00107\,m$ (green), $\triangle x = 0.00053\,m$ (red) and $\triangle x = 0.0002\,m$ (cyan)). The two peaks represents the different snapshots. The length of the increments did not have quite the impact that the size of the time-step had on the speed of the wave propagation. A very small increase in propagation speed could be observed between the blue line ($\triangle x = 0.00267\,m$) and the red line ($\triangle x = 0.00053\,m$) when the number of increments in the artery were increased, indicating a mesh independant solution. The shape of the pulse became smoother as the increment length decreased. There was a significant increase in solution time when the number of increments were increased (Table 5.3). A balance between accuracy and solution time had to be found again. $\triangle x$ was chosen to be close to $0.00107\,m$

for subsequent experiments.

The choice of $\triangle x = 0.00107\,m$ and $\triangle t = 0.001\,s$ for further calculations, concludes the mesh and timestep independency tests.

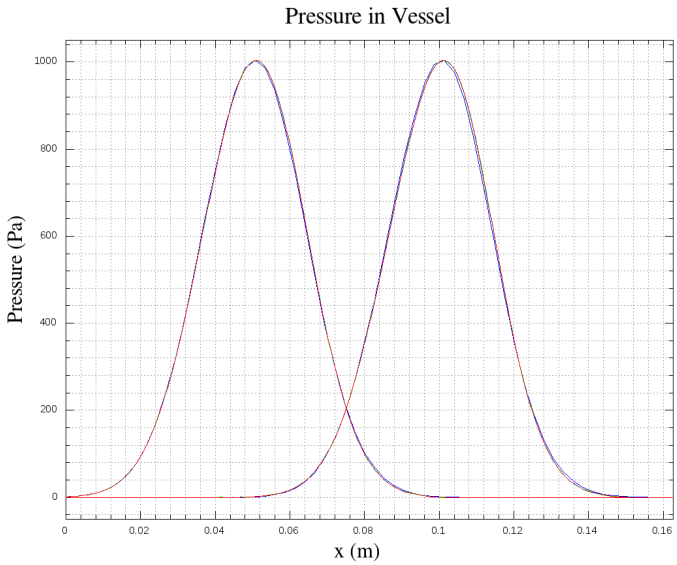

Figure 5.4: Wave propagation with varying increment lengths. ($\triangle x = 0.00267\,m$ (blue), $\triangle x = 0.00107\,m$ (green), $\triangle x = 0.00053\,m$ (red) and $\triangle x = 0.0002\,m$ (cyan)).

Table 5.3: Time required to obtain solution for varying increment lengths.

increments	$\triangle x\ (m)$	Cr	solution time (s)
60	0.00267	0.125	31.04
150	0.00107	0.311	90.98
300	0.00053	0.628	207.37
800	0.00020	1.665	1280.02

5.2.1.2 Effect of viscosity

As outlined in Section 5.1, viscosity is a measure of the resistance a fluid presents when it is being deformed. When the viscosity of a fluid increases, the resistance to flow increases and the pressure drop also increases. Figure 5.5 shows the effect viscosity has on the pressure drop.

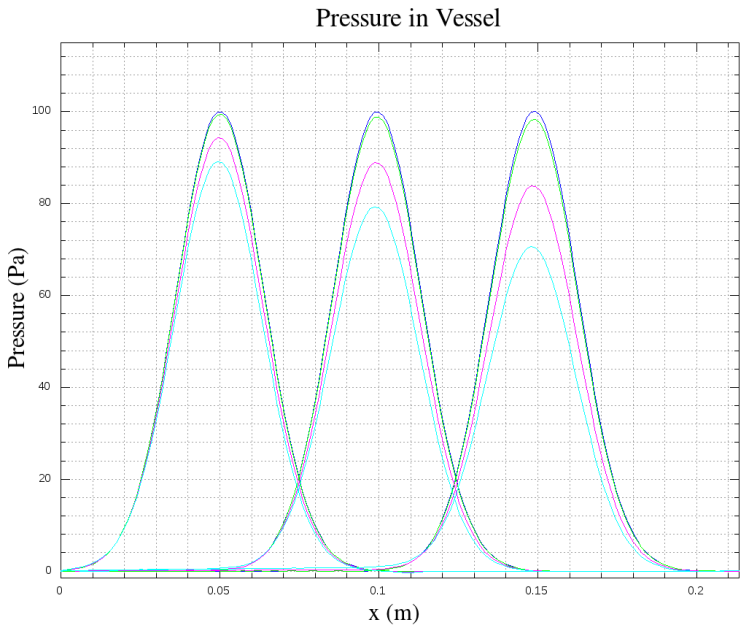

Figure 5.5: A pulse that propagate in fluids with different viscosities. The blue line indicates an inviscid fluid. Viscous fluids are indicated with green ($\mu = 0.0035\,Pa \cdot s$), magenta ($\mu = 0.035\,Pa \cdot s$) and cyan ($\mu = 0.07\,Pa \cdot s$).

For this investigation the length of the artery was chosen $L = 0.2\,m$, the cross-sectional area $A_0 = 0.0001\,m^2$, the initial velocity used for the steady state initialisation step $u = 0.05\,m/s$ and the material properties $\beta = 2296740\,Pa/m$. The program was run for different viscosities and as previously explained, snapshots were taken at $t = 0.03\,s$, $t = 0.045\,s$ and $t = 0.06\,s$. The three peaks represents the three snapshots. As expected with increased viscosity, the pressure drop increased. The pulse propagation for an inviscid fluid is shown in blue. Viscous fluids are indicated with green ($\mu = 0.0035\,Pa \cdot s$), magenta ($\mu = 0.035\,Pa \cdot s$) and cyan ($\mu = 0.07\,Pa \cdot s$).

It is difficult to validate whether the current implementation calculates the correct pressure drop as it depends on multiple non-linear relationships. What we can do, is to test whether the pressure drop due to the viscosity is of the right order (thus, do we capture at least the obvious first order behaviour). To do this we look at a control volume with a length L and radius r that has been rotated for an angle θ as depicted in Figure 5.6.

Of interest are the terms from the Navier-Stokes equation that are responsible for the pressure loss:

$$\nabla\mu(\nabla u) = -\frac{\partial p}{\partial z} \tag{5.1}$$

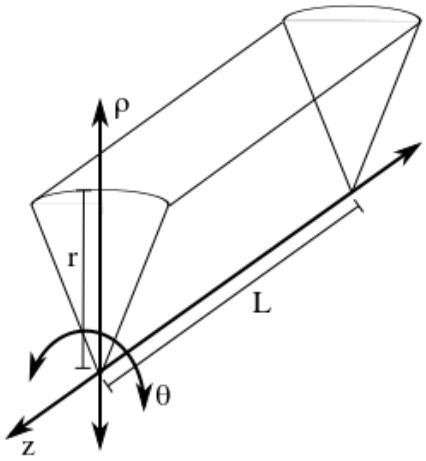

Figure 5.6: Control volume of a pipe

We integrate Equation (5.1) over the control volume for a pipe with length L:

$$\int_V \nabla\mu(\nabla u)dV = -\int_V \frac{\partial p}{\partial z}dV \tag{5.2}$$

where V is the volume of the control volume. When Gauss's theorem is applied to the left hand side of the equation and the midpoint integration rule to the right hand side of the equation, Equation (5.2) becomes:

$$\int_{dV} \mu(\nabla u)\cdot\mathbf{n}\mathrm{dS} = -V\frac{\partial p}{\partial z} \tag{5.3}$$

where $\mathbf{n}$ denotes the unit normal vector on the face of the control volume, dS. The change in the z-direction is $\partial z = L$ and the volume of a pipe is $V = \pi r^2 L$. We can rewrite the left hand side of the Equation (5.3) as the sum over all the faces of the control volume:

$$\sum_f \mu(\nabla u)\cdot\mathbf{A_f} = -\pi r^2 L\frac{\partial p}{L} \tag{5.4}$$

where $\mathbf{A_f}$ denotes the area vector on each face and ∂p the pressure drop over the control volume with length L. Using cylindrical polar coordinates the gradient of the velocity can be written as:

$$\nabla u = (\frac{\partial u}{\partial \rho}, \frac{1}{r}\frac{\partial u}{\partial \theta}, \frac{\partial u}{\partial z}) \tag{5.5}$$

The change in velocity in the θ-direction is $\frac{\partial u}{\partial \theta} \approx 0$. Although there might be a small change in velocity in the z direction in the region where the pressure wave propagates, we assume $\frac{\partial u}{\partial z} \approx 0$. The change in the ρ-direction is $\frac{\partial u}{\partial \rho} = \frac{0-u}{r}$. Equation (5.4) can now be expanded:

$$\begin{aligned} \mu[(\frac{0-u}{r},0,0)\cdot(2\pi rL,0,0)+(\frac{0-u}{r},0,0)\cdot(0,0,\pi r^2)+\cdots & \\ (\frac{0-u}{r},0,0)\cdot(0,0,-\pi r^2) \quad] &= -\pi r^2 L\frac{\partial p}{L} \\ \frac{2\mu u}{r^2} &= \frac{\partial p}{L} \end{aligned} \tag{5.6}$$

Table 5.4 tabulates the different values for viscosity that was used in Figure 5.5, the pressure loss as calculated by the current implementation and the pressure loss as calculated by Equation (5.6). The pressure loss that was calculated by the current implementation is of the same order as the pressure loss calculated by Equation 5.6.

Table 5.4: Validating the pressure loss.

$\mu(Pa.s)$	$\frac{\partial P}{\partial L}(\frac{Pa}{m})$	$\frac{\partial p}{L}(\frac{Pa}{m})$
	Octave	Equation (5.6)
0	0	0
0.0035	11.8	11.0
0.035	109.4	110.0
0.07	198.3	219.9

5.2.1.3 Effect of different pressure inputs

For an unstretched artery Equation (3.66) can be written as:

$$c_0 = \sqrt{\frac{\beta\sqrt{A_0}}{2\rho}} \tag{5.7}$$

This value was calculated as $c_0 = 3.291\,m/s$. Similar to what was discussed in Section 3.5, the total speed of the foot of the wave, u_{wf}, can be calculated as $u_{wf} = c_0 + u$. This results in a value of $3.341\,m/s$.

The speed of the computed wave can be calculated as:

$$u_{wfc} = \frac{\triangle x}{\triangle t} \tag{5.8}$$

The value of u_{wfc} was calculated as $u_{wfc} = 3.324\,m/s$. When this was compared to the theoretical value, the error in the speed of the wave, ϵ_{speed}, was calculated as $0.52\,\%$.

It is not possible to verify the speed of the peak of the wave analytically. This is because non-linear effects start to take an effect. For a small pulse the non-linear effects are small, for a big pulse it is larger. To verify the results, it was compared to Mynard's results [20]. As mentioned in Section 5.2.1, it is difficult to compare results as some of the necessary values, such as u and the form of the input wave, are not mentioned in their work.

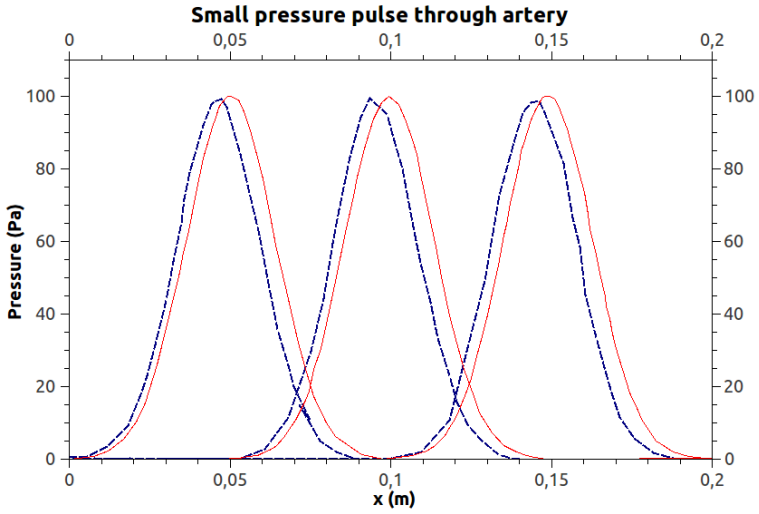

Figure 5.7: Pulse propagation for a small pressure pulse. Mynard's [20] results are shown as blue dotted lines, while the results from this study is represented by red solid lines.

Figures 5.7 and 5.8 show a small and larger pulse propagating through the vessel respectively. The solid red line represents the results from this study, while Mynard's results were shown by blue dotted lines. Snapshots were taken at $t = 0.03\,s$, $t = 0.045\,s$ and $t = 0.06\,s$ and is represented by the three peaks on the figure. The general behaviour of the wave from this study compares well with the wave from Mynard's research. As discussed in Section 5.2.1.1 the wave speed and width of the wave is also a function of the order of discretisation (numerical technique), mesh and time step size and it is unclear whether this has been investigated by Mynard [20]. Note that the peak of the larger pulse travels faster than the peak of the small pulse and than the foot of the pulse. This is due to the fact that the speed of sound c is dependant on the area, Equation (3.66). When the pressure pulse is larger it follows from the constitutive equation, Equation (3.37), that the area at the peak of the pulse will be larger. If the area is larger the speed of sound of the system at the wavefront will be larger. For a very long vessel the pulse will become skewed with the front steeper than the back. The peak will eventually 'catch up' with the foot and a shock will form. In the human body the vessels are shorter than would be needed to form a shock.

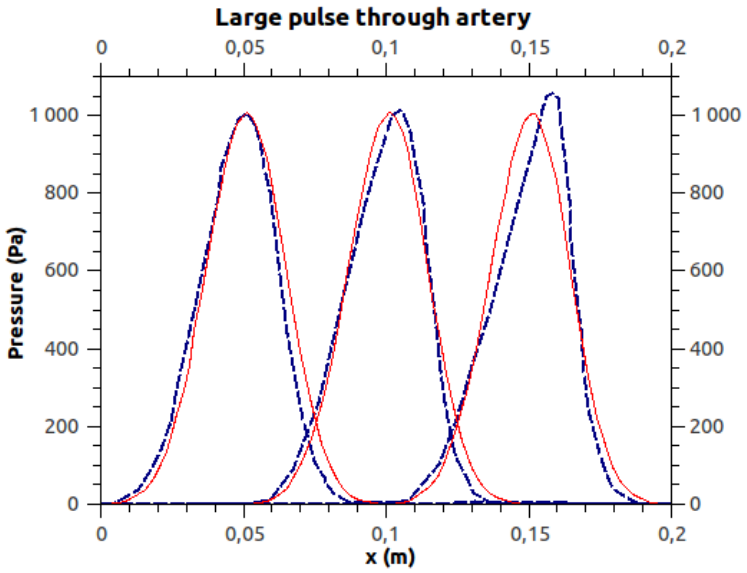

Figure 5.8: Pulse propagation for a larger pressure pulse. Mynard's results are shown by blue dotted lines, while the results from this study is represented by red solid lines.

5.2.1.4 Effect of varying the speed of sound of system

The shape and propagation speed of the pressure pulse is dependant on the speed of sound, c, of the system. The speed of sound of the system is dependant on the relaxed area, A_0, of the system and the material properties, β, Equation (3.66). Although A_0 doesn't appear in Equation (3.66), A does. A is dependant on A_0. Note that β is also dependant on A_0 and when A_0 increases, β decreases, Equation (3.36). When A_0 increases, c decreases and when A_0 decreases, c increases. When β increases, c increases and when β decreases, c decreases. Thus when one of these values changes, the speed at which the pressure pulses propagate also changes. The propagation speed is not directly dependant on A_0 or β but only on the value of c.

Figure 5.9 shows the effect that different values of c have on the propagation speed of the pressure pulse. Snapshots were taken at $t = 0.03\,s$ and $t = 0.06\,s$. For the first two cases the value of A_0 was increased and is represented by the green and red lines in Figure 5.9. For the last cases the value of β was changed and is shown by the blue and black lines in Figure 5.9. When the value of c was low, the pulse travelled slower and was narrower. When the value of c was large, the pulse travelled faster and the pulse was wider. When the value of A_0 was changed, it also affected the amplitude of the wave. This is because pressure is related to relaxed area and area in the pressure-area relation, Equation (3.37). The material properties β only affects the speed of the wave and not the amplitude of the wave as well.

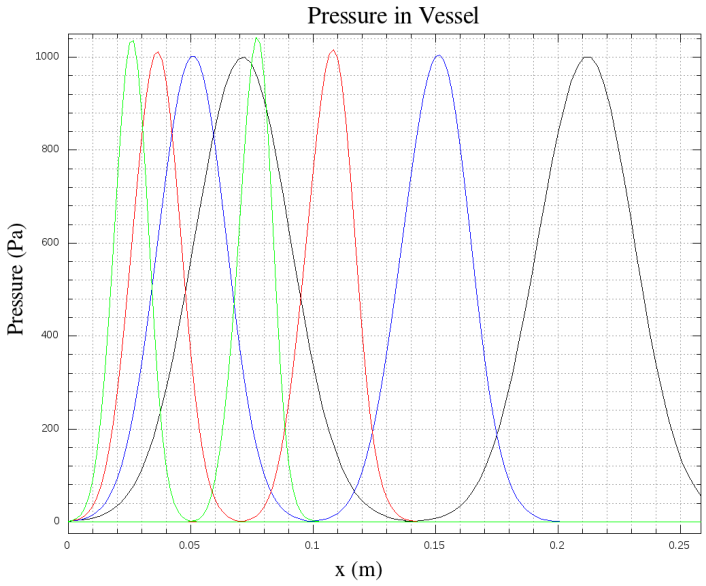

Figure 5.9: Waves with different values of c propagating through the vessel ($c = 1.6457$ (green), $c = 2.3274$ (red), $c = 3.2195$ (blue) and $c = 4.6548$ (black)).

5.2.1.5 Discontinuities

This section investigates the effect that discontinuities have on the pressure waves. There are two types of discontinuities that we will discuss, a sudden change in relaxed area A_0 and a sudden change in material properties β. In the vascular system, these discontinuities are caused by cardiovascular diseases such as aneurysms and athereosclerosis as was discussed in Section 2.1.5. Although most of these diseases cause a discontinuity in both A_o and β, we chose to illustrate the effect that these discontinuities have on the pressure wave seperately. This was done so that the effect that each type of discontinuity produces would be clear and also that it would be easy to compare the results with the results from Mynard's study [20]. When a pressure pulse reaches a discontinuity the amplitude changes, there is a positive or negative reflection and the sound of speed of the system c also changes. This change in c changes the shape and speed of the pressure pulse. Snapshots for all the test cases were taken at $t = 0.03\,s$, $t = 0.045\,s$ and $t = 0.06\,s$ and is represented by the three peaks on the figure.

Increase in material properties - The first case considered a sudden increase in β when A_0 was kept constant for the test case (Figure 5.10). This demonstrates what happens when there is an increase in wall thickness or Young's modulus, Equation (3.36). This corresponds to the physical dissease atherosclerosis, the hardening of arteries. (Section 2.1.5.1). Note that in the disease's case A_0 usually also decrease. A partial positive reflection can be observed and

the amplitude and speed of the transmitted pulse is larger than that of the pulse before the discontinuity. In Figure 5.10 Mynard's results [20] are shown by a dashed line, while results from this study are shown by a solid line. The general behaviour corresponds well to Mynard's results [20].

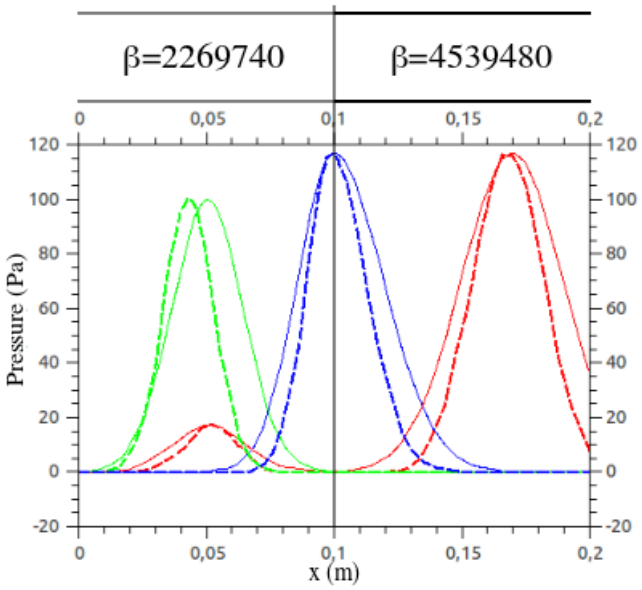

Figure 5.10: Single vessel showing reflected and transmitted waves due to a step increase in β. Waves are shown at $t = 0.03\,s$ (green), $t = 0.045\,s$ (blue) and $t = 0.06\,s$ (red). Results from this study is shown by solid lines, while Mynard's results [20] are represented by dashed lines.

Decrease in material properties - After the atherosclerotic region in the vessel, the vessel wall becomes more elastic again. This corresponds to a sudden decrease in β (Figure 5.11) or more physically a decrease in wall thickness or Young's modulus. Although A_0 usually increase in the case of the disease, it was kept constant for the test case. The amplitude and speed of the transmitted pulse are smaller than those of the original pulse. There is a partial negative reflection. The general behaviour compare favourably with Mynard's results [20].

Sudden increase in relaxed area - In the case of an aneurysm (Section 2.1.5.2), the artery suddenly becomes larger (Figure 2.6). Figure 5.12 shows the effect of a sudden increase in A_0. A partial negative reflection takes place at the discontinuity. For this case it wasn't clear whether Mynard [20] calculated β as a function of A_0 or kept it constant throughout the artery.

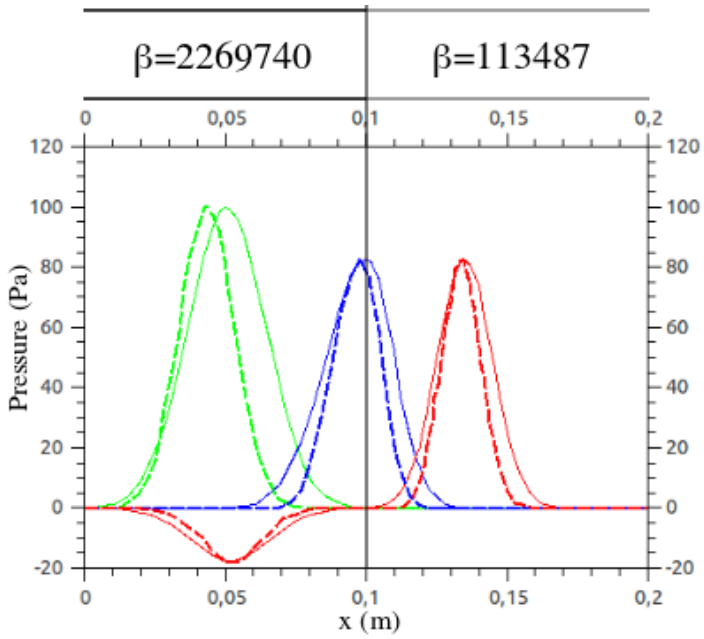

Figure 5.11: Single vessel showing reflected and transmitted waves due to a step decrease in β. Waves are shown at $t = 0.03\,s$ (green), $t = 0.045\,s$ (blue) and $t = 0.06\,s$ (red). Results from this study is shown by solid lines, while Mynard's results [20] are represented by dashed lines.

The linear reflection coefficient, Equation (3.89), was calculated by Mynard as $R = -0.25$. The concept of a linear reflection coefficient is not strictly speaking valid for a non-linear system. However small pulses approach linear behaviour, thus it is a good approximation. The transmission coefficient was calculated as $T_p = 0.75$ [20]. The calculated values predict that the amplitude of the transmitted wave will be 85 % of the amplitude of the original wave and the amplitude of the reflected wave will -25% of the amplitude of the orginal wave. Mynard's results are shown by the dashed lines. The results from this study, when β was kept constant, are illustrated by the solid lines. In both studies, the changes in amplitude, as predicted by the reflection and transmission coefficients, corresponded well to the calculated results. The speed of the reflected and transmitted wave also corresponded well with Mynard's results.

In Section 5.2.1.4 we discussed the effect that a change of A_0 has on the speed of the wave. We expect that when A_0 increases, the speed of the wave should decrease. This is not the case when β is kept constant. Another line on Figure 5.12 (the lines with dashes and dots) shows the effect the discontintuity had on the wave when β was calculated for each increment as a function of A_0. Now the speed of the transmitted pulse decreased.

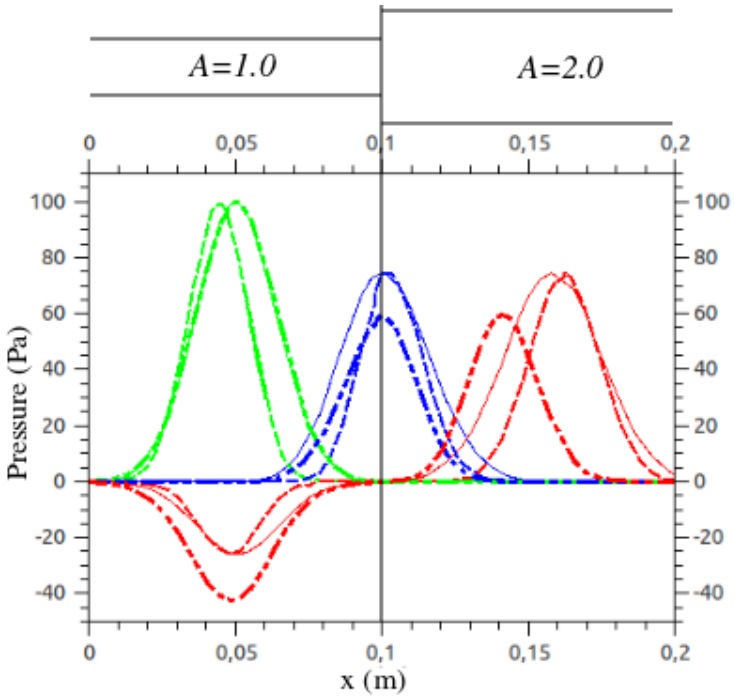

Figure 5.12: Reflected and transmitted waves due to a step increase in A_0. β is constant through vessel. Waves are shown at $t = 0.03\,s$ (green), $t = 0.045\,s$ (blue) and $t = 0.06\,s$ (red). Results from this study is shown by solid lines, while Mynard's results [20] are represented by dotted lines.

Sudden increase in relaxed area - Figure 5.13 shows the effect that a sudden decrease in A_0 has on the pressure pulse. This corresponds to the region in the artery where the outlet of an aneurysm is. For this case it was also not clear whether Mynard [20] calculated β as a function of A_0 or kept it constant throughout the artery. A partial positive reflection can be observed. This is because a decrease in A_0 corresponds to an increase in characteristic impedance. The linear reflection coefficient, Equation (3.89) was calculated by Mynard as $R = 0.25$ [20]. The transmission coefficient was calculated as $T_p = R + 1$, $T_p = 1.25$. The calculated values predict that the amplitude of the transmitted wave will be 125 % of the amplitude of the original wave and the amplitude of the reflected wave will 25% of the amplitude of the orginal wave. Mynard's results are shown by the dashed lines. The results from this study, when β was kept constant, are illustrated by the solid lines. In both studies, the changes in amplitude, as predicted by the reflection and transmission coefficients, again corresponded well to the calculated results. The speed of the reflected and transmitted wave also corresponded well with Mynard's results.

In Section 5.2.1.4 we predicted that when A_0 decreases, the speed of the wave would increase. This is not the case when β is kept constant. Another line on Figure 5.13 (the lines with dashes

and dots) shows the effect the discontintuity had on the wave when β was calculated for each increment as a function of A_0. Now the speed of the transmitted pulse increased.

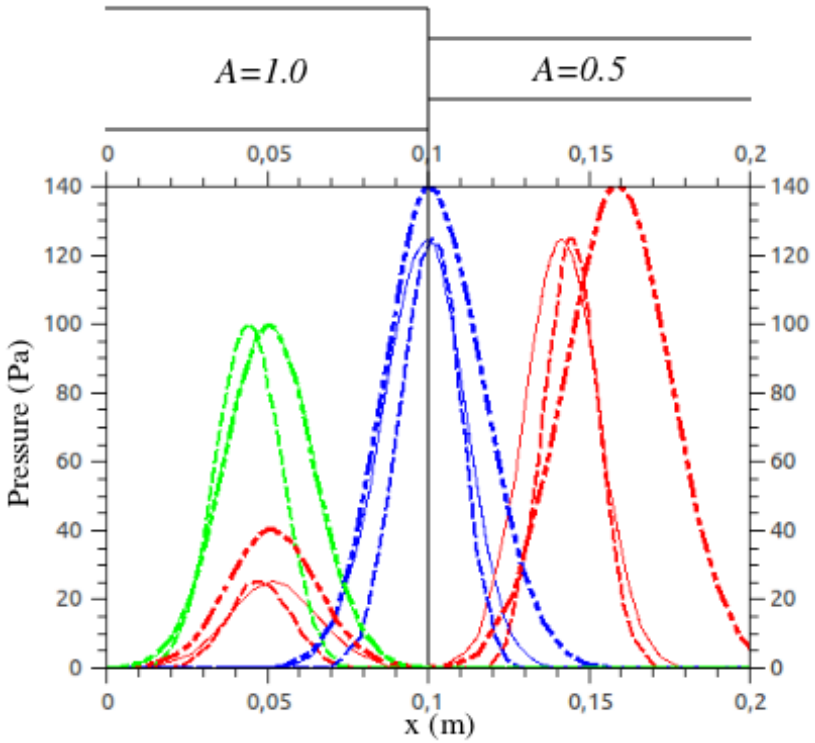

Figure 5.13: Reflected and transmitted waves due to a step decrease in A_0. β is constant through vessel Waves are shown at $t = 0.03\,s$ (green), $t = 0.045\,s$ (blue) and $t = 0.06\,s$ (red). Results from this study is shown by solid lines, while Mynard's results [20] are represented by dotted lines.

5.2.1.6 Boundaries

This section demonstrates the influence that the reflection coefficient R has on the propagation of the pulse at the boundary. The reflection coefficient is strictly only valid for a linear model, as discussed in Section 3.5.2.2. Furthermore the assumptions that were made when deriving the characteristic values ω_i should hold (Section 3.5.1). These assumptions include that the initial velocity u, as calculated for the steady state, should be close to zero. The change in external pressure p_{ext}, relaxed area A_0 and material properties β near the boundaries should also approach zero. Furthermore the viscosity should be very small.

The inlet pressure pulse for the first test cases was $100\,Pa$. When the pressure pulse is this small, it behaves linearly. This made it possible to simulate a non-reflecting boundary. For the following test cases the length of the artery was $0.15\,m$. The fluid was inviscid ($\mu \approx 0$)

and the initial velocity $u = 0.05\,m/s$. Snapshots were again taken at $t = 0.03\,s$, $t = 0.045\,s$ and $t = 0.06\,s$. This time a snapshot was also taken at $t = 0.075\,s$. The green line shows the pulse at $t = 0.03\,s$, the blue line at $t = 0.045\,s$, the red line at $t = 0.06\,s$ and the magenta line at $t = 0.075\,s$.

When $R = 0$ the pulse moved through the boundary unhindered (Figure 5.14). Note that the magenta line ($t = 0.075\,s$) is a straight line. This shows that there was no part of the wave that was reflected.

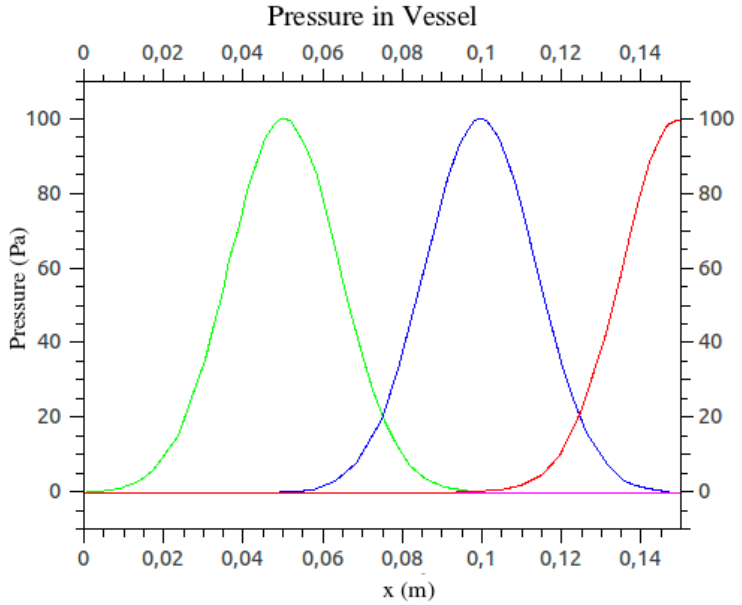

Figure 5.14: Propagtion of a small pressure pulse ($P = 100\,kPa$) when $R = 0$. Snapshots were taken at $t = 0.03\,s$ (green), $t = 0.045\,s$ (blue), $t = 0.06\,s$ (red) and $t = 0.075\,s$ (magenta).

When $R = 1$, there was a total positive reflection at the boundary (Figure 5.15). At $t = 0.06\,s$ (red line) half of the wave was already reflected and was travelling backwards through the artery. The forward and backward part of the wave was superimposed on each other and this explains why the amplitude of the pressure pulse represented by the red line is very large. At $t = 0.075\,s$ (magenta line) the whole pulse had been reflected and was travelling backwards. Note that the shape of the pulse at $t = 0.045\,s$ (blue line) and at $t = 0.075\,s$ (magenta line) is almost identical. This is because the behaviour of the pulse is linear (See Section 5.2.1.3).

Figure 5.16 shows a total negative reflection at the boundary. This occurs when $R = -1$. At $t = 0.06\,s$ (red line) half of the wave had undergone a negative reflection. The negative backward wave and the positive frontward wave cancelled each other out. At $t = 0.075\,s$ (magenta line) the whole wave had undergone a negative reflection.

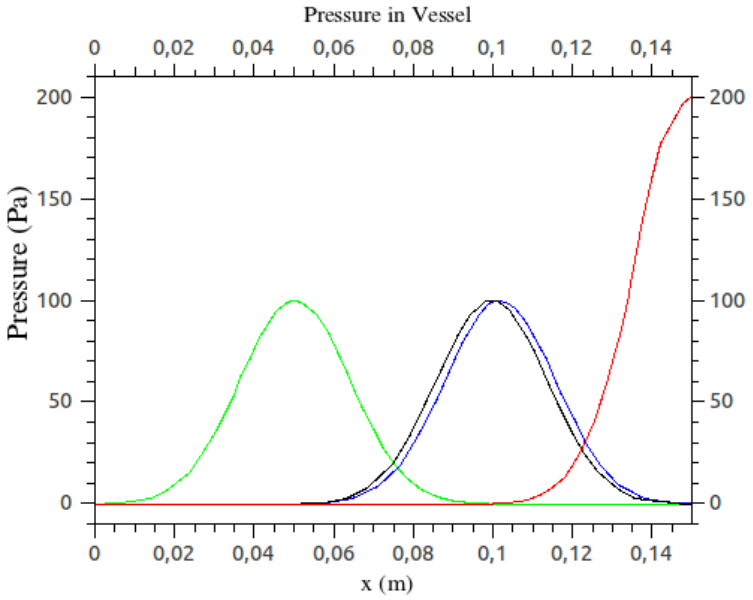

Figure 5.15: Propagtion of a small pressure pulse ($P = 100\,kPa$) when $R = 1$. Snapshots were taken at $t = 0.03\,s$ (green), $t = 0.045\,s$ (blue), $t = 0.06\,s$ (red) and $t = 0.075\,s$ (magenta).

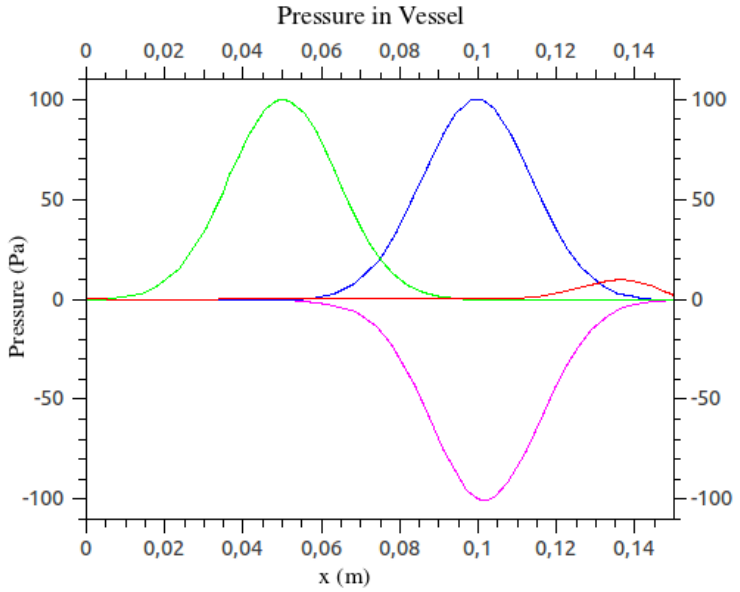

Figure 5.16: Propagtion of a small pressure pulse ($P = 100\,kPa$) when $R = -1$. Snapshots were taken at $t = 0.03\,s$ (green), $t = 0.045\,s$ (blue), $t = 0.06\,s$ (red) and $t = 0.075\,s$ (magenta).

The test cases above were repeated for a larger input pressure wave of $1\,000\,Pa$. This is closer to the pressure wave in the body, which is in the order of $16\,000\,Pa$. Results are displayed in

Figure 5.17. At this pressure the non-linear effects were no longer negligible. The green line is a snapshot taken at $t = 0.03\,s$ and the blue line at $t = 0.045\,s$. The three red lines show three different reflections that are caused by different reflection coefficients, $R = -1$, $R = 0$ and $R = 1$. The top red line shows the positive reflection when $R = 1$. Similar to the more linear illustration, the backward and frontward travelling parts of the wave were superimposed on each other and the amplitude of the wave seems to have doubled in size. The red line in the middle represents the pulse when $R = 0$. Unlike the more linear case, where there had been no reflection, a very small part of the pulse was reflected. The bottom red line shows the negative reflected wave, or $R = -1$. This small amplitude is a result of the parts of the wave that cancels each other out. A black line represents the positive reflected wave at $t = 0.075\,s$. As discussed in Section 5.2.1.3 the peak of the wave was propagating at a faster speed than the foot of the wave. The peak of the wave at $t = 0.075\,s$ is left of the peak of the wave at $t = 0.045\,s$. This is different from the more linear simulation illustrated in Figure 5.15. The magenta line shows the reflected wave due to the non-linear effects at $t = 0.075\,s$. The cyan line shows the negative reflected wave at $t = 0.075\,s$.

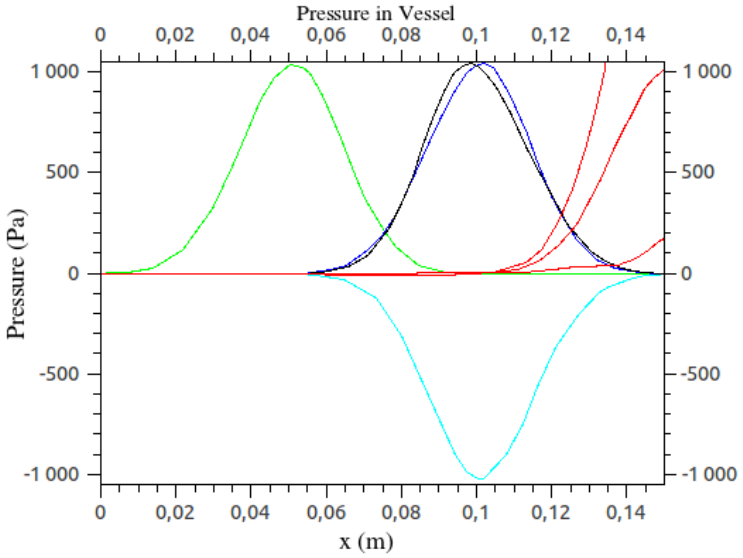

Figure 5.17: Propagtion of a larger pressure pulse ($P = 1000\,kPa$) for different values of R. Snapshots were taken at $t = 0.03\,s$ (green) and $t = 0.045\,s$ (blue). There are three red lines ($t = 0.06\,s$). The top one show the reflection when $R = 1$, the one in the middle when $R = 0$ and the bottom one when $R = -1$. Different colours were used to show the reflected waves at $t = 0.075\,s$. The magenta line shows the reflected wave when $R = 0$, The black line shows the reflected wave when $R = 1$ and the cyan line shows the reflected wave when $R = -1$.

5.2.2 Branching

The test case in this section demonstrates the effect of branching on the pressure pulse. Figure 5.18 shows the simple branch that was modelled. The test case consisted of a parent artery with two branches, one a bit smaller than the other. The length of the parent branch was $0.1\,m$. Both branches were also $0.1\,m$ long. The relaxed area of the first branch was a fraction of that of the parent: $A_{0,branch1} = 0.2A_{0,parent}$. The relaxed area of the second branch was also a fraction of that of the parent: $A_{0,branch2} = 0.8A_{0,parent}$. The material properties were also different for the branches: $\beta_{branch1} = \beta_{branch2} = 1.2\beta_{parent}$. A large inlet pulse was prescribed $(1000\,Pa)$.

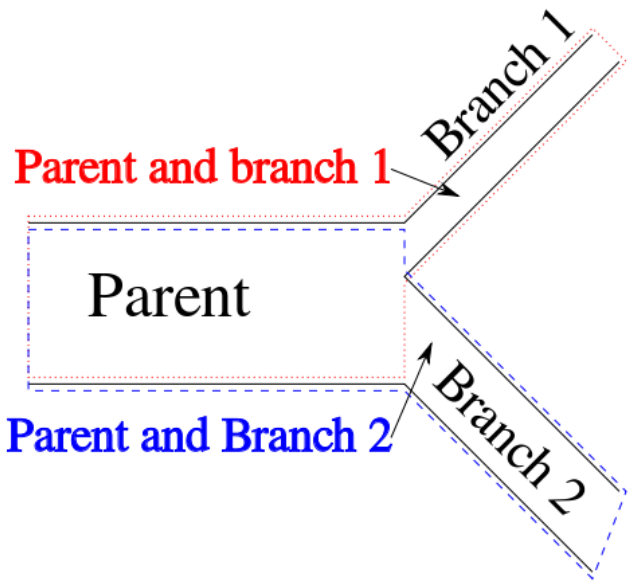

Figure 5.18: The parent artery and its two branches that were used to demonstrate the effects of branching.

Figure 5.19 shows propagation through the parent and first branch. A small positive reflection occurs. The speed of the wave increases in the branch. This is what we expect when there is a decrease in A_0 and an increase in β.

Figure 5.20 shows the wave that is transmitted to the second branch. In this branch the speed of the transmitted wave is only slighty faster. This is because there is only a slight decrease in A_0.

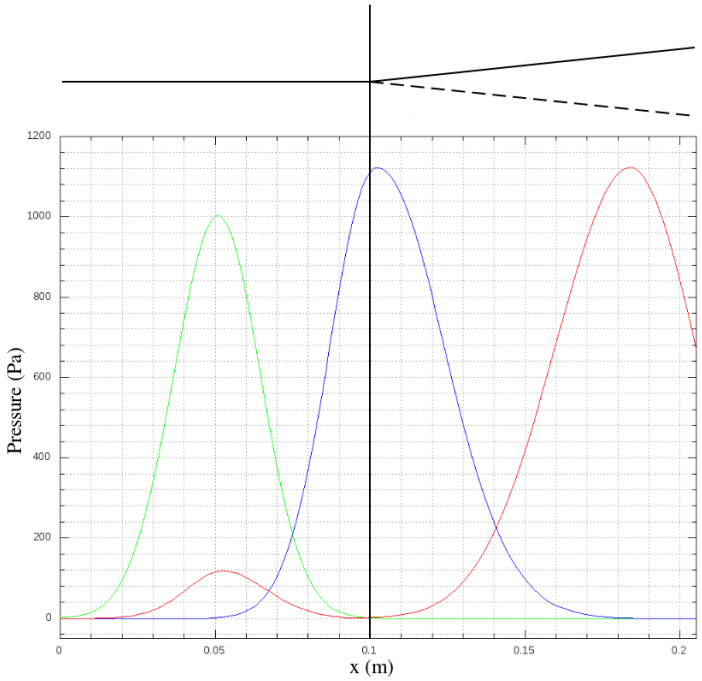

Figure 5.19: Wave propagating through parent and branch 1. ($A_{0,branch1} = 0.2A_0$). Snapshots were taken at $t = 0.03\,s$ (green), $t = 0.045\,s$ (blue) and $t = 0.06\,s$ (red).

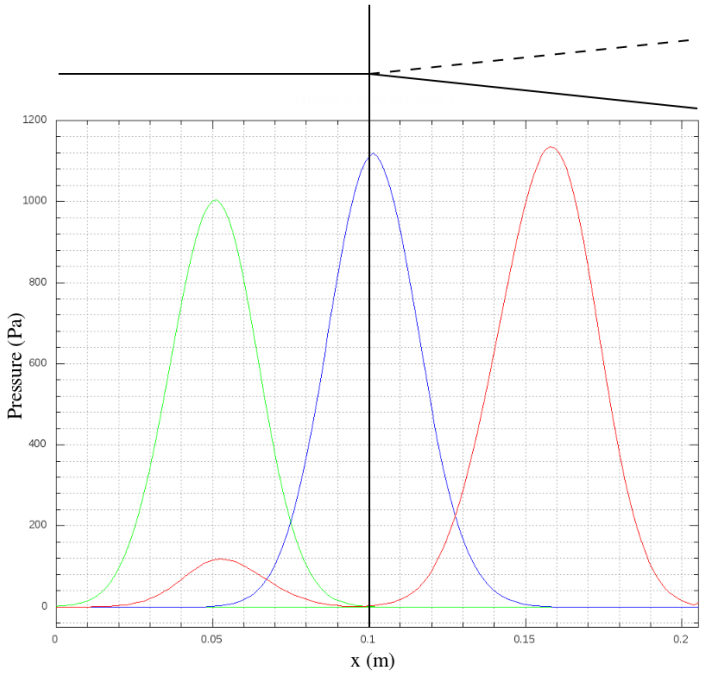

Figure 5.20: Wave propagating through parent and branch 2 ($A_{0,branch2} = 0.8A_0$). Snapshots were taken at $t = 0.03\,s$ (green), $t = 0.045\,s$ (blue) and $t = 0.06\,s$ (red).

5.2.3 More complex test case

The last test case is a artery with two branches and one of its branches branches again into two branches (Figure 5.21). The cross sectional areas of branch 1 and branch 2 are equal and half the size of the parent branch. The cross sectional areas of branch 3 and branch 4 are equal and half the size of branch 2. The material becomes stiffer after each branching point ($\beta_{branch1} = \beta_{branch2} = 1.2\beta_{parent}$ and $\beta_{branch3} = \beta_{branch4} = 1.5\beta_{parent}$). All the branches are $0.1\,m$ long.

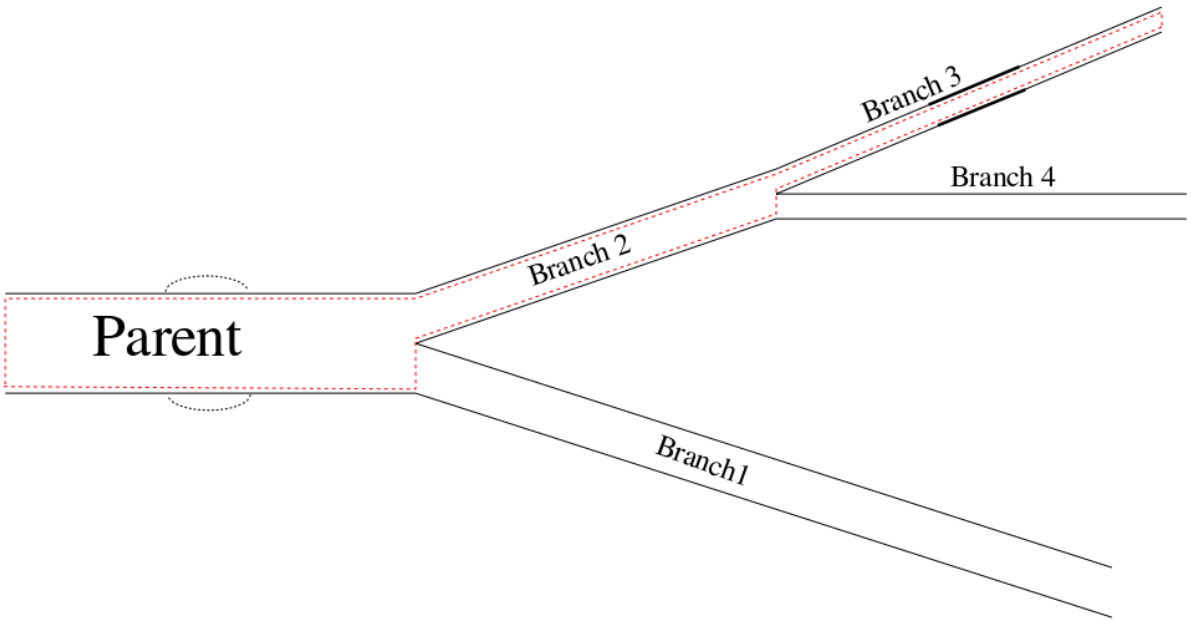

Figure 5.21: Configuration of four branches used for the more complex test case. The red line shows the branches that will be shown in the following graphs.

The test case consists out of two parts. The first part of this test case was done without any discontinuities present. The second test case was done with an aneurysm modelled in the parent vessel and a hardening in branch 3. Figure 5.22 shows the pressure wave at different time-steps for the parent vessel, branch 2 and branch 3. At $t = 0.03\,s$, the magenta wave shows a wave similar to the input wave. At $t = 0.045\,s$ the cyan wave shows an increase in amplitude at the first branching point. At $t = 0.06\,s$ (black line) the part of the wave that was reflected at the first branching point can be seen travelling backwards. At $t = 0.0675\,s$ (orange line) the transmitted wave reached the second branching point and the amplitude increased again. At $t = 0.075\,s$ the blue line shows the first reflected wave exiting the computational domain. The reflected wave caused by the second branching point can also be seen breaking away from the transmitted wave. The green line ($t = 0.09\,s$) shows the original wave exiting the domain

withouth any reflection. At $t = 0.09\,s$ the wave that was reflected at the second branching point had reached the first branching point and a part was re-reflected. This is a negative reflection and the re-reflected wave can be seen travelling forward at $t = 0.105\,s$ (red line).

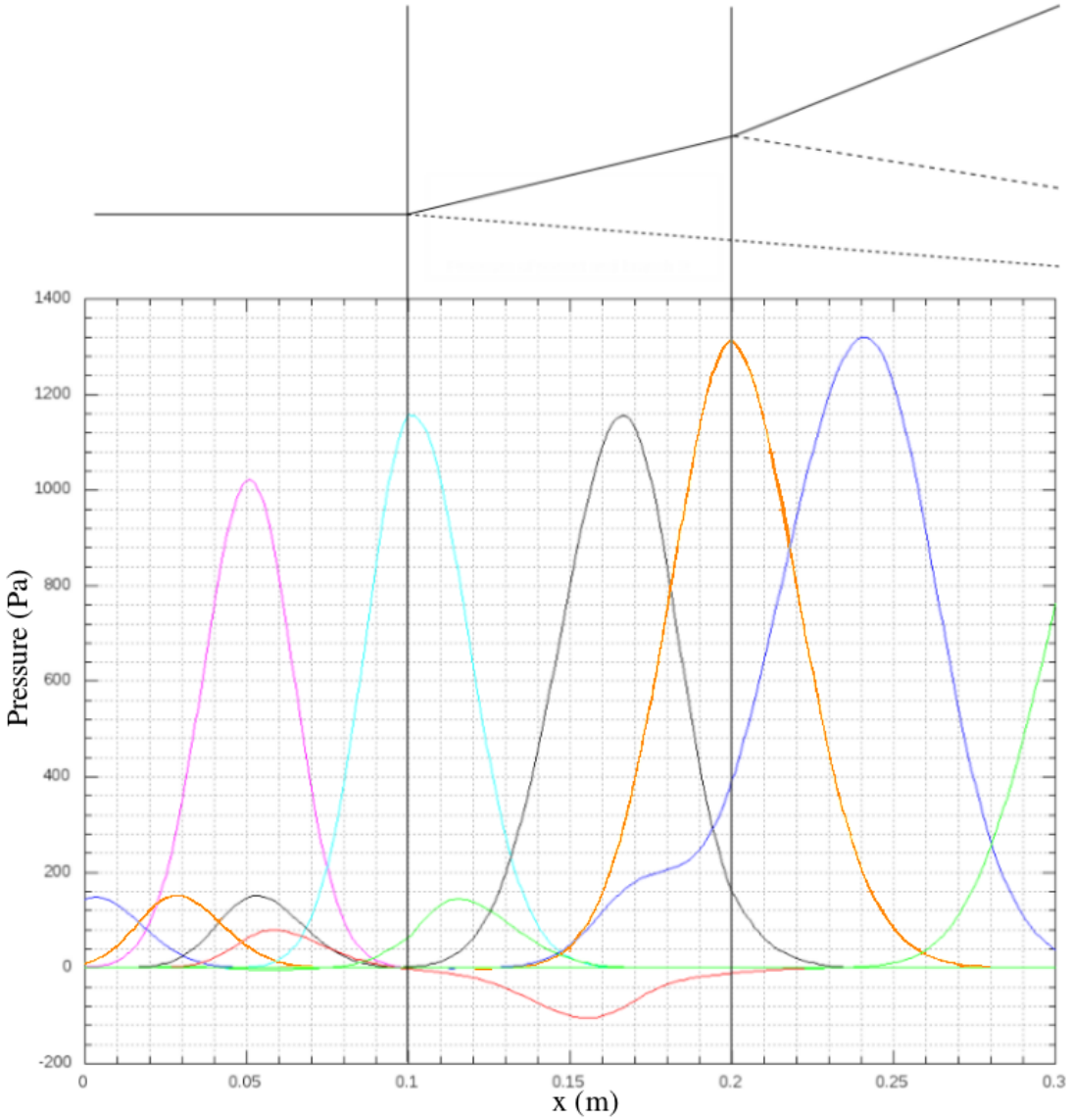

Figure 5.22: Propagation of pressure wave for complex test case. Snapshots were taken at $t = 0.03\,s$ (magenta), $t = 0.045\,s$ (cyan), $t = 0.06\,s$ (black), $t = 0.0675\,s$ (orange), $t = 0.075\,s$ (blue), $t = 0.09\,s$ (green) and $t = 0.105\,s$ (red).

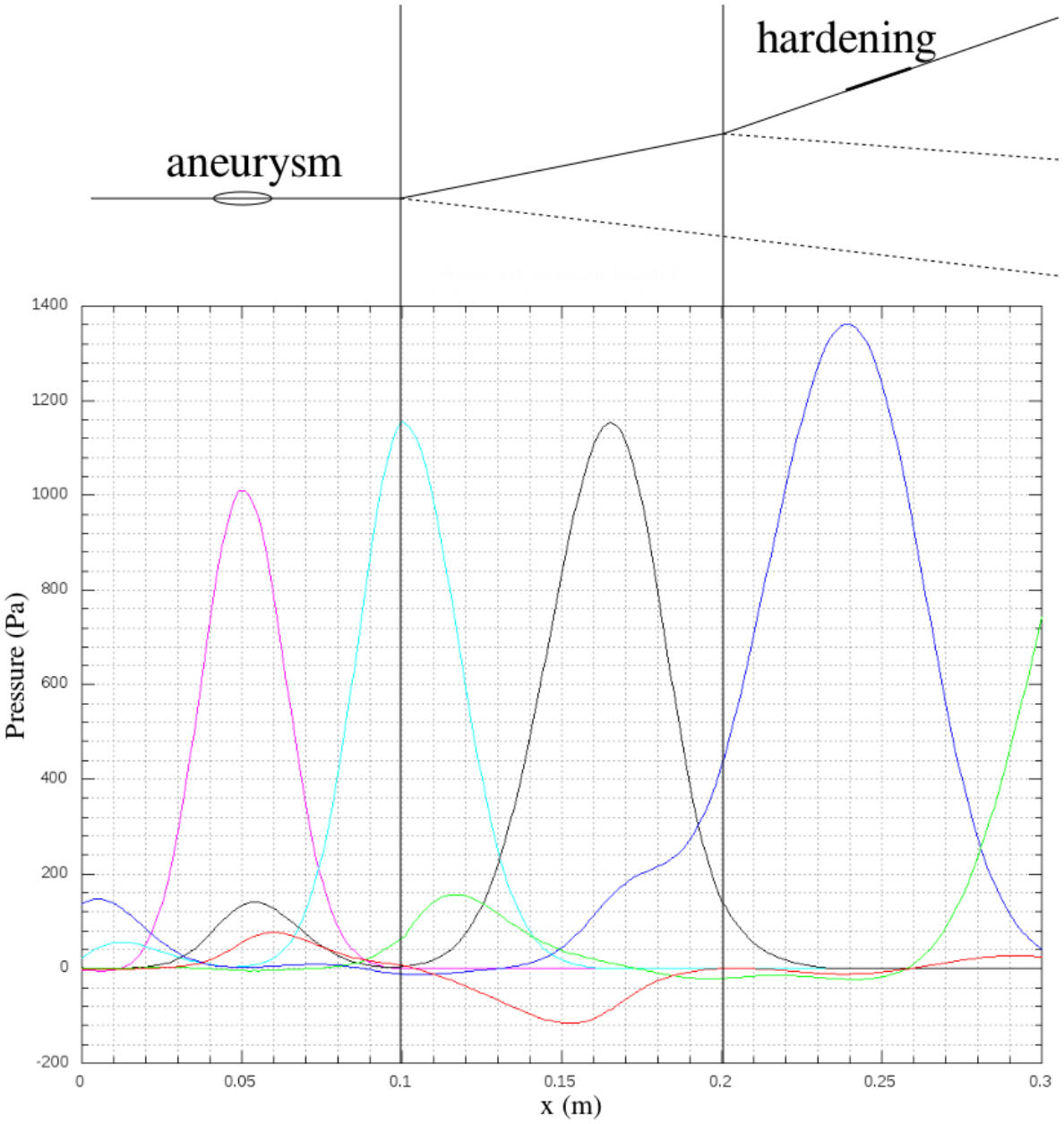

Figure 5.23: Propagation of pressure wave for complex test case with an aneurym in the parent branch and a hardening of the arterial wall in branch 3. Snapshots were taken at $t = 0.03\,s$ (magenta), $t = 0.045\,s$ (cyan), $t = 0.06\,s$ (black), $t = 0.075\,s$ (blue), $t = 0.09\,s$ (green) and $t = 0.105\,s$ (red).

The second part of this case included an aneurysm like discontinuity in the parent branch and a hardening of the arterial wall in branch 3. The same behaviour as in the first part can be seen with few exeptions. At $t = 0.045\,s$ (cyan line) the reflected wave that was caused by the 'aneurysm' can be seen near $x = 0.01\,m$. The blue line ($t = 0.075\,s$) shows many backward and

forward travelling waves. Near to the inlet is the backward moving wave that was caused by the first branching point. Between $x = 0.05\,m$ and $x = 0.1\,m$ the rereflections of this reflected wave that was caused by the 'aneurysm' can be seen. The green and red lines ($t = 0.09\,s$ and $t = 0.105\,s$) also show many backward and frontward travelling waves that were caused by the branching and discontinuities.

5.3 Summary

The result of several test cases were discussed in this chapter. The steady state solution is important as it is used as the initial condition for the transient case. Experiments with discretisation were done with the help of EES. A further investigation was done on how viscosity affects the solution.

For the transient cases seperate effects were demonstrated and then combined for a more complex test case. Several numerical experiments demonstrated the effect that the size of the increment and time-step as well as the time integration scheme have on the solution. The damping effect that viscosity has ons the pressure pulse was illustrated. When the pressure input was small, the solution was more linear. When the pressure input was larger, the speed of the peak of the wave was greater than its foot. The effect that β and A_0 have on the sound of speed of the system was demonstrated by waves moving at different speeds for different values of β and A_0. A section showed that when there is a discontinuity part of the wave is reflected and part of the wave is transmitted. The reflections are either partially positive or negative and depend on the discontinuity. It was shown that it is possible to prescribe either a non-reflecting, positive reflecting or negative reflecting boundary. The use of the reflection coefficient R is strictly only valid when the problem is almost linear. This is the case for small pressure input waves. When a larger input pressure wave was used, the solution was non-linear. A very small part of the wave was reflected when a non-reflecting boundary was prescribed. This was due to the non-linear effects of the solution.

The effect that branching has on the solution was also shown. At a branch, part of the wave was reflected. This reflection depends on the relaxed area and material properties of the branches.

A more complex test case combined the different effects studied by the computer code.

Chapter 6

Conclusions and recommendations

The aim of this research was to develop a 1D network code to model blood flow and pressure pulses through large arteries in the systemic circulation. The goal was to find a method that handles discontinuities and branching naturally. The plan was to discretise the partial differential equations using a staggered grid. A further goal was to implement non-reflecting boundary conditions so that the outgoing waves proceed unhindered (with no reflections) through the computational boundaries. Where results were available from other researchers, they were used to compare with the results from the computer code.

The literature survey covered the physiology and pathology of the cardiovascular system and gave an overview of the different models that are available in the literature. The biological section gave attention to the haemorheology and treatments available for cardiovascular diseases. There are different models for different parts of the cardiovascular system. Multiscale models couple models of different physical dimensions to find the optimal balance between detail and computational cost. An overview of the different discretisation schemes that are used to model 1D flow through arteries was given.

The mathematical model was explained in great detail. A derivation of the model from Reynold's transport theorem was given. The equations were reformulated to eliminate the convective acceleration term in the momentum conservation equation. This was done by rewriting the equations in terms of the total pressure rather than the static pressure. To close the system of equations a 'constitutive' equation was used to relate the total pressure to the area of the vessel through the material properties. The staggered grid configuration used to discretise the equations was shown. The iterative method that was used to solve the system of equations is similar to the SIMPLE method. Non-reflecting boundary conditions were derived by finding characteristic lines on which characteristic variables remain constant. The relaxed area and material properties were written in vector form. This way discontinuities are

handled naturally and do not need any special treatment. When there was a branch in the artery, a special control volume was used with three cell walls which represent the inflow and two outflows. The pressure and area were defined at the centre of the control volume.

Several steady state simulations were done with EES using different variables and discretisation schemes. Based on that results, we chose to continue with Q, A and p_0 as primary variables. In Octave a Newton-Rhapson and iterative method was used to solve the steady state. The iterative method was faster and the results was used as the initial conditions for the transient cases. When the viscosity increases so does the pressure loss, and therefore the problem becomes more non-linear.

Test cases showed the effects that different parameters had on the transient cases of a single artery. When the viscosity increased, the pressure loss also increased and the amplitude of the pulse decreased along the artery. When the input pressure wave was small the solution was more linear and the peak and foot of the wave travelled at approximately the same speed. When the input pressure wave was larger the peak travelled at a faster speed than the foot. When the stiffness of the artery was increased or the relaxed area was decreased, the wave propagated faster because the speed of sound of the system changed.

Numerical experiments showed that the computer code's behaviour corresponded to the behaviour that can be seen in CFD applications. When the time integration was done in a explicit manner, the solution became unstable. When the time integration was done in a implicit manner there was unwanted numerical diffusion of the wave. When the length of the time-step was decreased, the wave propagated faster. A decrease in the length of the increment results in a smoother shape. When the viscosity increased, the pulse was dampened. The propagation speed of the waves is dependant on the speed of sound, c, of the system, which in turn is dependant on A_0 and β.

When the input pressure wave is small the behaviour is linear. The peak of the wave propagates at approximately the same speed as the foot. When non-reflecting boundary conditions are implemented, the wave proceeds unhindered through the computational domain.

When the input pressure wave is large the behaviour becomes non-linear. The peak of the wave propagates faster than the foot. When non-reflecting boundary conditions are implemented, a small part of the wave is reflected at the outlet.

Discontinuities in the arteries causes reflection of the pressure waves. At branching points there is also a positive reflection of the pressure wave. A positive reflection occurs when the area suddenly decreases, the material becomes stiffer or at a branching point. When a positive reflection occurs the amplitude of the pressure wave increases. This increased pressure maximum may damage the artery.

Recommendations for future research include:

- An experimental setup should be built so that it would be possible to validate the results. Alternatively data from an MRI could be obtained to validate results. Another option is to use results from a 3D model to validate the results of the 1D model.
- Extending the model to include the heart, smaller arteries, capillaries and veins to form a closed loop model. At present any numerical errors can be 'pumped' out of the model. This will not be possible if the model is a closed loop.
- The boundary conditions should be modified so that it is useful for larger pressure waves that show non-linear behaviour.
- The model should be rewritten in a different programming language that solves faster.
- The computer code should be generalised so that it is possible to simulate any arterial configuration.

Bibliography

[1] Alastruey, J., 2006. Numerical modelling of pulse wave propagation in the cardiovascular system: development, validation and clinical applications. Ph.D. thesis, Departments of Bioengineering and Aeronautics, Imperial College London.

[2] Avolio, A. P., 1980. Multi-branched model of the human arterial system. Medical and Biological Engineering and Computing 18 (6), 709–718.

[3] Barnard, A. C. L., Hunt, W. A., Timlake, W. P., Varley, E., 1966. A theory of fluid flow in compliant tubes. Biophysical Journal 6 (6), 717–724.

[4] Brook, B. S., Falle, S., Pedley, T. J., 1999. Numerical solutions for unsteady gravity-driven flows in collapsible tubes: evolution and roll-wave instability of a steady state. Journal of Fluid Mechanics 396 (1), 223–256.

[5] Caro, C. G., Fitz-Gerald, J. M., Schroter, R. C., 1971. Atheroma and arterial wall shear observation, correlation and proposal of a shear dependent mass transfer mechanism for atherogenesis. Proceedings of the Royal Society of London.Series B.Biological Sciences 177 (1046), 109.

[6] Casson, N., 1959. Rheology of Disperse Systems. Pergamon Press, London.

[7] Eaton, J. W., 2009. GNU Octave 3.2.3.
URL `http://www.gnu.org/software/octave/`

[8] Formaggia, L., Lamponi, D., Quarteroni, A., 2003. One-dimensional models for blood flow in arteries. Journal of Engineering Mathematics 47 (3), 251–276.

[9] Formaggia, L., Nobile, F., Quarteroni, A., Veneziani, A., 1999. Multiscale modelling of the circulatory system: a preliminary analysis. Computing and Visualization in Science 2 (2), 75–83.

[10] Formaggia, L., Quarteroni, A., Veneziani, A., 2009. Cardiovascular Mathematics: Modeling and simulation of the circulatory system. Springer Verlag, Milano, Italy.

[11] Greyvenstein, G. P., 2002. An implicit method for the analysis of transient flows in pipe networks. International Journal for Numerical Methods in Engineering 53 (5), 1127–1143.

[12] Greyvenstein, G. P., Laurie, D. P., 1994. A segregated cfd approach to pipe network analysis. International Journal for Numerical Methods in Engineering 37 (21), 3685–3705.

[13] He, Y., Liu, H., Himeno, R., 2004. A one-dimensional thermo-fluid model of blood circulation in the human upper limb. International Journal of Heat and Mass Transfer 47 (12-13), 2735–2745.

[14] Huo, Y., Kassab, G. S., 2007. A hybrid one-dimensional/Womersley model of pulsatile blood flow in the entire coronary arterial tree. American Journal of Physiology-Heart and Circulatory Physiology 292 (6), 2623–2633.

[15] John, L. R., 2004. Forward electrical transmission line model of the human arterial system. Medical and Biological Engineering and Computing 42 (3), 312–321.

[16] Karamanoglu, M., O'Rourke, M. F., Avolio, A. P., Kelly, R. P., 1993. An analysis of the relationship between central aortic and peripheral upper limb pressure waves in man. European Heart Journal 14 (2), 160–167.

[17] Klein, S., 2010. Engineering Equation Solver (EES).
URL `http://www.fchart.com/ees/`

[18] Meyer, B. J., Meij, H. S., Meyer, A. C., 1994. Human physiology: Chemical, physical, and physiological principles. Juta (Kenwyn).

[19] Mukhopadhyay, S., Layek, G. C., 4/15 2011. Analysis of blood flow through a modelled artery with an aneurysm. Applied Mathematics and Computation 217 (16), 6792–6801.

[20] Mynard, J. P., Nithiarasu, P., 2008. A 1d arterial blood flow model incorporating ventricular pressure, aortic valve and regional coronary flow using the locally conservative Galerkin (LCG) method. Communications in Numerical Methods in Engineering 24 (5), 367–417.

[21] Nithiarasu, P., 2008. Special issue on biofluid dynamics. International Journal for Numerical Methods in Fluids 57 (5), 473–474.

[22] Olufsen, M. S., 1999. Structured tree outflow condition for blood flow in larger systemic arteries. American Journal of Physiology-Heart and Circulatory Physiology 276 (1), 257–268.

[23] Olufsen, M. S., Nadim, A., 2004. On deriving lumped models for blood flow and pressure in the systemic arteries. Mathematical Biosciences and Engineering 1 (1), 61–80.

[24] Olufsen, M. S., Peskin, C. S., Kim, W. Y., Pedersen, E. M., Nadim, A., Larsen, J., 2000. Numerical simulation and experimental validation of blood flow in arteries with structured-tree outflow conditions. Annals of Biomedical Engineering 28 (11), 1281–1299.

[25] Ottesen, J. T., Olufsen, M. S., Larsen, J. K., 2004. Applied mathematical models in human physiology. Society for Industrial Mathematics, Philadelphia.

[26] Patankar, S. V., Spalding, D. B., 1972. A calculation procedure for heat, mass and momentum transfer in three-dimensional parabolic flows. International Journal of Heat and Mass Transfer 15 (10), 1787–1806.

[27] Pontrelli, G., 1 2006. The role of the arterial prestress in blood flow dynamics. Medical Engineering & Physics 28 (1), 6–12.

[28] Quarteroni, A., Formaggia, L., 2004. Mathematical modelling and numerical simulation of the cardiovascular system. Handbook of numerical analysis 12, 3–127.

[29] Quarteroni, A., Tuveri, M., Veneziani, A., 2000. Computational vascular fluid dynamics: problems, models and methods. Computing and Visualization in Science 2 (4), 163–197.

[30] Quarteroni, A., Veneziani, A., Zunino, P., 2002. Mathematical and numerical modeling of solute dynamics in blood flow and arterial walls. SIAM journal on numerical analysis, 1488–1511.

[31] Raghu, R., Taylor, C. A., 2011. Verification of a one-dimensional finite element method for modeling blood flow in the cardiovascular system incorporating a viscoelastic wall model. Finite Elements in Analysis and Design 47, 586–592.

[32] Rappitsch, G., Perktold, K., Pernkopf, E., 1997. Numerical modelling of shear-dependent mass transfer in large arteries. International Journal for Numerical Methods in Fluids 25 (7), 847–857.

[33] Rhoades, R., 1996. Rhoades and Pflanzer (1996) Human physiology. Vol. 3. Saunders College Pub.(Fort Worth).

[34] Ricotta, J. J., Pagan, J., Xenos, M., Alemu, Y., Einav, S., Bluestein, D., 2008. Cardiovascular disease management: the need for better diagnostics. Medical and Biological Engineering and Computing 46 (11), 1059–1068.

[35] Ruan, W., Clark, M. E., Zhao, M., Curcio, A., 2003. A hyperbolic system of equations of blood flow in an arterial network. SIAM Journal on Applied Mathematics 64 (2), 637–667.

[36] Ruan, W., Clark, M. E., Zhao, M., Curcio, A., 7/15 2007. Global solution to a hyperbolic problem arising in the modeling of blood flow in circulatory systems. Journal of Mathematical Analysis and Applications 331 (2), 1068–1092.

[37] Sheng, C., Sarwal, S. N., Watts, K. C., Marble, A. E., 1995. Computational simulation of blood flow in human systemic circulation incorporating an external force field. Medical and Biological Engineering and Computing 33 (1), 8–17.

[38] Sherwin, S. J., Formaggia, L., Peiro, J., Franke, V., 2003. Computational modelling of 1d blood flow with variable mechanical properties and its application to the simulation of wave propagation in the human arterial system. International Journal for Numerical Methods in Fluids 43 (6-7), 673–700.

[39] Sherwin, S. J., Franke, V., Peiro, J., Parker, K., 2003. One-dimensional modelling of a vascular network in space-time variables. Journal of Engineering Mathematics 47 (3), 217–250.

[40] Smith, N. P., Pullan, A. J., Hunter, P. J., 2001. An anatomically based model of transient coronary blood flow in the heart. SIAM Journal on Applied Mathematics 62, 990–1018.

[41] Stedman, T. L., 1999. Stedman (1999) Stedman's medical dictionary, 27th Edition. Williams & Wilkins, Baltimore.

[42] Steele, B. N., Taylor, C. A., Wan, J., Ku, J. P., Hughes, T. J. R., 2001. In vivo validation of a one-dimensional finite element method for simulation-based medical planning for cardiovascular bypass surgery. In: Engineering in Medicine and Biology Society, 2001. Proceedings of the 23rd Annual International Conference of the IEEE. Vol. 1. IEEE, pp. 120–123 vol. 1.

[43] Taylor, C. A., Draney, M. T., 2004. Experimental and computational methods in cardiovascular fluid mechanics. Annual Reviews of Fluid Mechanics 36, 197–231.

[44] Taylor, C. A., Draney, M. T., Ku, J. P., Parker, D., Steele, B. N., Wang, K., Zarins, C. K., 1999. Predictive medicine: computational techniques in therapeutic decision-making. Computer Aided Surgery 4 (5), 231–247.

[45] Taylor, C. A., Hughes, T. J. R., Zarins, C. K., 1998. Finite element modeling of blood flow in arteries. Computer Methods in Applied Mechanics and Engineering 158 (1-2), 155–196.

[46] Thomas, C. G., Nithiarasu, P., 2008. An element-wise, locally conservative Galerkin (LCG) method for solving diffusion and convection-diffusion problems. International Journal for Numerical Methods in Engineering 73 (5), 642–664.

[47] Underwood, J. C. E., Cross, S. S., 2009. General and systematic pathology. Churchill Livingstone.

[48] Urquiza, S. A., Blanco, P. J., Venere, M. J., Feijoo, R. A., 2006. Multidimensional modelling for the carotid artery blood flow. Computer Methods in Applied Mechanics and Engineering 195 (33-36), 4002–4017.

[49] Versteeg, H. K., Malalasekera, W., 2007. An introduction to computational fluid dynamics: the finite volume method. Prentice Hall.

[50] Wan, J., Steele, B., Spicer, S. A., Strohband, S., Feijoo, G. R., Hughes, T. J. R., Taylor, C. A., 2002. A one-dimensional finite element method for simulation-based medical planning for cardiovascular disease. Computer Methods in Biomechanics and Biomedical Engineering 5 (3), 195–206.

[51] Wang, J. J., Parker, K. H., 4 2004. Wave propagation in a model of the arterial circulation. Journal of Biomechanics 37 (4), 457–470.

[52] Waters, S. L., Alastruey, J., Beard, D. A., Bovendeerd, P. H. M., Davies, P. F., Jayaraman, G., Jensen, O. E., J, L., Parker, K. H., Popel, A. S., Secomb, T. W., Siebes, M., Sherwin, S. J., Shipley, R. J., Smith, N. P., van de Vosse, F. N., 1 2011. Theoretical models for coronary vascular biomechanics: Progress & challenges. Progress in Biophysics and Molecular Biology 104 (1-3), 49–76.

[53] Womersley, J. R., 1957. Oscillatory flow in arteries: the constrained elastic tube as a model of arterial flow and pulse transmission. Physics in Medicine and Biology 2, 178–187.